NTNU

Norwegian University of
Science and Technology

Permeability Prediction from Acoustic Velocity

Hanna Skårdal Vølstad

Petroleum Geoscience and Engineering
Submission date: June 2016
Supervisor: Kenneth Duffaut, IPT

Norwegian University of Science and Technology
Department of Petroleum Engineering and Applied Geophysics

Abstract

Permeability is estimated in the middle Jurassic Garn Fm. in the Haltenbanken area in the Norwegian Sea by combining the Kozeny-Carman model for permeability estimation with Raymer's model for porosity estimation. The Kozeny-Carman model is derived for a tube-like pore-geometry and extended to yield for a granular media.

The porosity applied into the Kozeny-Carman model is estimated by Raymer's model from different sources of velocity data, such as fluid corrected sonic velocity, check-shots and seismic velocities.

The measured velocity and porosity data in the cleanest parts of the Garn Fm. follows the Raymer model, so the Raymer-relation is considered valid in this area. The scattering of the data around the Raymer-curve tends to plot more below than above the Raymer-line. This trend increase when the porosity decrease, leading to a gradual over-prediction of porosity. Hence, giving an overestimation in the permeability.

The permeability estimations are compared against log-derived permeabilities calibrated towards core measurements, referred to as core calibrated permeability. The permeability estimations show that porosity obtained from sonic velocity gives better permeability results than permeability estimates from seismic velocity derived porosities. However, when the seismic velocity is calibrated against check-shots and the effect of anisotropy is reduced to fit time-depth curves, the vertical seismic interval velocities in Garn are significantly improved, consequently providing better porosity and permeability estimates.

The results show that this model is able to translate velocity into estimates for porosity and permeability. The precision in the velocity is the most important factor in this analysis, so the challenge with applying seismic velocities is that the seismic signal are low frequent and affected by smoothing effects. Hence, the seismic velocity only perceive the slowly varying velocity trends as a response to lithology changes in the subsurface.

Sammendrag

Permeabilitet er predikert i Garn fm. fra midt-jura tiden på Haltenbanken i Norskehavet ved å kombinere Kozeny-Carmans modell for permeabilitetsestimering, og Raymers modell for porøsitetsestimering. Kozeny-Carman modellen er utledet for en rørlignende poregeometri og utvidet til å gjelde for et granulært materiale.

Porøsiteten som er brukt i Kozeny-Carman modellen er estimert fra Raymers modell fra ulike typer hastighetsdata, som fluid substituert sonisk hastighet, sjekk-skudd hastighet og seismisk hastighet.

Målte hastighets- og porøsitetsdata i de rene delene av Garn Fm. følger Raymer modellen, slik at modellen kan betraktes som en gyldig modell i dette området. Spredningen av data rundt Raymer-kurven har en tendens til å plotte mer på undersiden enn på oversiden av Raymer-linja, og denne trenden øker med minkende porøsitet. Dette fører til en økende grad av over-prediksjon av porøsitet når porøsiteten minker, noe som igjen fører til overestimering av permeabilitet.

Permeabilitetsberegningene sammenlignes med permeabilitet avledet fra brønnlogger kalibrert mot kjernemålinger, omtalt som kjernekalibrert permeabilitet. Permeabilitetsberegningene viser at porøsitet som er oppnådd fra sonisk hastighet gir bedre permeabilitetsresultater enn permeabilitet avledet fra porøsitet estimert fra seismiske hastigheter. Når imidlertid de seismiske hastighetene er kalibrert mot sjekk-skudd og effekten av anisotropi er redusert for å passe til tid-dyp-kurven, blir intervall-hastighetene i Garn betydelig forbedret, og gir bedre porøsitet- og permeabilitetsestimeringer.

Resultatene viser at denne modellen er i stand til å oversette hastighet til estimering av porøsitet og permeabilitet. Presisjonen i hastighet er den viktigste faktoren i denne analysen, så utfordringen ved å anvende seismiske hastigheter er at det seismiske signalet er lavfrekvent og påvirkes av glattingseffekter. Dette fører til at bare de lave og langsomt varierende hastighetstrendene, som er en respons til litologiendringer i undergrunnen, oppfattes av det seismiske signalet.

Acknowledgement

I thank my supervisor, Kenneth Duffaut, for extraordinary close and careful guidance throughout the work with this Master's thesis project. His involvement concerned the analytical method as well as help with code-writing in Matlab. He also performed extensive programming in order to extract velocity data from seismic 2D lines. I am thankful for the time he has spent on giving me valuable help, feedback and guidance.

Statoil have provided me with data that made this analysis possible, so for that I want to express my gratitude to the Åsgard team at Statoil Stjørdal. They have been involved during the whole process of this work, and made suggestions when problems arised as well as providing more data when requested. A special thank you to Jon Andre Haugen for interpolating the seismic velocities used in this analysis, Anca Langridge for uploading and sending the data, and last, but not least, I express my gratitude to Lill-Tove Wetjen Sigernes for coordinating and being the contact point throughout the work of this Master's thesis.

I acknowledge Schlumberger for providing the Petrel software and the Norwegian Petroleum Directorate for well data.

I give my thanks to Dicky Harishidayat who have assisted me in Petrel.

To my fellow students; thank you all for contributing to an encouraging and supportive learning environment in these 5 years at NTNU, and for all the fun we have experienced together.

Last, I thank Jonas Sørbel for patiently having relevant discussions with me, coming up with suggestions regarding the structure of this Master's thesis and for encouraging words when times were tough.

Table of Contents

List of Figures xi
List of Appendix Figures xiii
List of Tables xiii
1 Introduction 1
1.1 Structure of the Thesis 4
2 Background 5
3 Data and Study Area 6
4 Theory 9
4.1 The Kozeny-Carman equation 9
4.1.1 Step-by-step Derivation of the Kozeny-Carman Equation 11
4.2 Empirical Relations 14
4.2.1 Tortuosity-Porosity Relation 14
4.2.2 Raymer's Porosity-Velocity Relation 15
5 Method 19
5.1 Estimating the Clay Content 19
5.2 Estimating Brine and Matrix Velocities 21
5.2.1 Estimate Brine Velocity 21
5.2.2 Estimate Matrix Velocity 21
5.3 Total Porosity versus Effective Porosity 22
5.4 Percolation Threshold Porosity 23
5.5 Determine Grainsize and Cementation Factor 23
5.6 Calibrate Seismic Velocity 24
6 Ehrenberg's Work 27
7 Results 29
7.1 Testing the Validity of Raymer's Relationship 29
7.2 Blind Well Testing 32
7.3 Permeability Prediction on the Haltenbanken Dataset 36
7.4 Permeability Prediction from Seismic Velocities 38
7.5 Permeability Estimation along the Interpretation of the Garn Fm. 49

8 Discussion 55
8.1 Review of the Permeability Estimation Method 55
8.1.1 Raymer's Relationship 55
8.1.2 The Kozeny-Carman Relation 58
8.2 Sensitivity in the Models 59
8.2.1 Raymer's Model 59
8.2.2 Kozeny-Carman Model 62
8.3 Porosity and Permeability Estimations in the Test Well and on the Haltenbanken Dataset 66
8.4 Challenges Regarding the use of Seismic Velocities in the Permeability Prediction 67
9 Further Work 70
10 Conclusion 71
11 Nomenclature 72
12 Bibliography 75
Appendix A Empirical Relations for Density and Velocity for Brine and Water I
Appendix B Fluid Substitution II
Appendix C Porosity and Permeability Relations VII
Appendix D Seismic Velocities XI
Appendix E Derivative of the Kozeny-Carman Equation XXIII

List of Figures

Figure 1-1: Map showing the lateral extension of the Garn Fm. 3

Figure 3-1: Map showing the outline of the Haltenbanken area 6

Figure 4-1: The imagined pore-geometry for the derivation of the Kozeny-Carman relation. 13

Figure 5-1: Shale line and sand line defined by the maximum and minimum value on the gamma ray log respectively..... 20

Figure 5-2: Time-depth relationship provided by check-shots (blue) and seismic (red) in the location of well 5. 25

Figure 5-3: Time-depth relationship provided by check-shots (blue) and seismic (red) in the location of well 6. 26

Figure 6-1: Horizontal air permeability from routine core analysis versus porosity in Garn sandstones..... 28

Figure 7-1: Measured porosity versus measured velocity in the Garn Fm. on 5 different Haltenbanken fields. 29

Figure 7-2: Measured porosity versus measured velocity for the sand in the Garn Fm. that contain less than 10% clay. 31

Figure 7-3: Log overview of test well 17. 33

Figure 7-4: Measured porosity versus measured velocity for 100% saturated Garn Fm. in a test well. 34

Figure 7-5: Measured porosity versus Raymer-porosity..... 35

Figure 7-6: Effective porosity obtained from Raymer's relation versus predicted permability in test well 17. The lines represent the specific surface area lines provided by Ehrenberg. 36

Figure 7-7: Measured permeability versus modelled permeability in the Garn Fm. 37

Figure 7-8: Sonic log and seismic velocity profile in the well location of well 6..... 38

Figure 7-9: Sonic log and seismic velocity profile in the well location of well 6 zoomed in to the Garn interval. 39

Figure 7-10: Check-shot, calibrated velocity and un-calibrated velocity time-depth curves for well 5. 40

Figure 7-11: Check-shot, calibrated velocity and un-calibrated velocity time-depth curves for well 6. 41

Figure 7-12: Check-shot, calibrated velocity and un-calibrated velocity time-depth curves zoomed in for well 5..... 42

Figure 7-13: Check-shot, calibrated velocity and un-calibrated velocity time-depth curves zoomed in for well 6..... 43

Figure 7-14: The delta correction factor in the left pane is applied to the seismic profile in well 5, seen in red in the right pane. The right pane shows the sonic log, the original seismic

velocity profile and the calibrated seismic profile resulting from applying the delta factor to the red curve. 44

Figure 7-15: The delta correction factor in the left pane is applied to the seismic profile in well 6, seen in red in the right pane. The right pane shows the sonic log, the original seismic velocity profile and the calibrated seismic profile resulting from applying the delta factor to the red curve. 45

Figure 7-16: Estimated permeability in well 5 from porosity estimations from various acoustic velocities by Raymer's model. 46

Figure 7-17: Estimated permeability in well 6 from porosity estimations from various acoustic velocities by Raymer's model. 47

Figure 7-18: Comparison of the modelled permeability from various sources of acoustic velocity in the Garn Fm. in well 5, together with the core-calibrated permeability. 48

Figure 7-19: Comparison of the modelled permeability from various sources of acoustic velocity in the Garn Fm. in well 6, together with the core-calibrated permeability. 49

Figure 7-20: Reflectivity seismic along Line 3 in time, together with the well location of well 5 and 6 and the Garn interpretation. 50

Figure 7-21: Velocity model for Line 3, together with the well location of well 5 and 6 and the Garn interpretation. 51

Figure 7-22: Extracted P-wave velocity from the velocity model along the Garn interpretation in two-way-travel time. 52

Figure 7-23: Porosity modelled along the Garn interpretation in time by transforming extracted seismic velocities from the velocity model into porosity by Raymer's model. 53

Figure 7-24: The modelled permeability from the Raymer-Kozeny-Carman model along the time-interpretation of the Garn Fm. 54

Figure 8-1: Various velocity-porosity relations plotted for three different types of sandstone. 56

Figure 8-2: Raymer's relation for Garn sand containing less than 2% clay. 57

Figure 8-3: Sensitivity of matrix velocity in the estimated acoustic velocity from Raymer's relation. 60

Figure 8-4: Sensitivity of fluid velocity in the estimated acoustic velocity from Raymer's relation. 61

Figure 8-5: Estimated Raymer-velocity depend more on the fluid velocity when porosity increase. 62

Figure 8-6: Resulting change in permeability when grainsize is varying 63

Figure 8-7: Resulting change in permeability when tortuosity is varying 64

Figure 8-8: Resulting change in permeability when porosity is varying 65

Figure 8-9: Permeability along the time-interpretation of Garn 69

List of Appendix Figures

Figure Apx 1: Lithostatic stress, pore pressure and differential stress. III

Figure Apx 2: Estimated temperature gradient well 15. IV

Figure Apx 3: Sonic log and seismic velocity profile in the well location of well 6. XI

Figure Apx 4: Sonic log and seismic velocity profile in the well location of well 5, zoomed in to the Garn interval. XII

Figure Apx 5: Reflectivity seismic along Line 1 in time, together with the well location of well 6 and the Garn interpretation. XIII

Figure Apx 6: Velocity model for Line 1, together with the well location of well 6 and the Garn interpretation. XIV

Figure Apx 7: Extracted P-wave velocity from the velocity model along the Garn interpretation in time. XV

Figure Apx 8: Porosity modelled along the Garn interpretation in time by transforming extracted seismic velocities from the velocity model into porosity by Raymer's model. XVI

Figure Apx 9: The modelled permeability from the Raymer-Kozeny-Carman model along the time-interpretation of the Garn Fm. XVII

Figure Apx 10: Reflectivity seismic along Line 2 in time, together with the Garn interpretation. XVIII

Figure Apx 11: Velocity model for Line 2, together with the Garn interpretation. XIX

Figure Apx 12: Extracted P-wave velocity from the velocity model along the Garn interpretation in time. XX

Figure Apx 13: Porosity modelled along the Garn interpretation in time by transforming extracted seismic velocities from the velocity model into porosity by Raymer's model. XXI

Figure Apx 14: The modelled permeability from the Raymer-Kozeny-Carman model along the time-interpretation of the Garn Fm. XXII

List of Tables

Table 3-1: Well id and field id for the Haltenbanken wells. 7

Table 5-1: Values used for calculating matrix velocity in the Garn Fm. 22

Table 7-1: Matrix and brine velocities used to plot Raymer's function with no restriction to clay content and with a clay content restriction. 32

Table 7-2: Average interval velocity in Garn from check-shot data at top and bottom of Garn. 44

1 Introduction

Permeability is a measure of a material's capacity of allowing fluids to pass through it without changing the structure of the medium or displace its parts. In the context of hydrocarbon production, the material is usually a sedimentary rock and the fluid is either oil, gas or water (North, 1985; Rubino, Velis, & Holliger, 2012)

Accurate knowledge of the permeability parameter is essential for hydrocarbon production, reservoir management and development. This knowledge contributes to estimate production rates and optimize drainage strategies, involving locating good drainage points for well placements and injection strategies for the reservoir (Ahmed, Crary, & Coates, 1991; Walderhaug, Eliassen, & Aase, 2012).

Permeability of a geologic formation is known to be very difficult to estimate. Normally, three major permeability measurement techniques are used by the industry; wireline-log analysis, laboratory testing on core samples and well testing. In lack of any of these, as the methods require that wells have been drilled, permeability can be derived from 3D seismic data or be derived from pore models (Grude, Dvorkin, & Landrø, 2015). The disadvantage of relating permeability to porosity is that rock fabric and pore geometry affects permeability and porosity differently. For example, the permeability depend not only on the size of the pores but also the shape and geometry of the pores (North, 1985).

When permeability is obtained from wireline-log measurements, empirical correlations of permeability with porosity and intergranular surface area is applied. The first equation that relates measurable rock properties with permeability was proposed in 1927 by Josef Kozeny and later, in 1937, P. C. Carman modified the relation ((Kozeny, 1927); (Carman, 1937)). Their relation is used in this Master's thesis study to estimate the permeability in a sandstone formation in the Norwegian Sea.

Nelson (1994) describes the importance of the Kozeny-Carman relationship:

"Most models that relate the permeability to a pore dimension are derived, either in spirit or in rigor from the Kozeny-Carman relationship which recognizes explicitly the dependence of permeability on grain size squared".

According to Dvorkin (2009), the Kozeny-Carman equation relates the permability to porosity and grain size as

$$k \sim d^2 \, \varphi^3 \qquad (1)$$

Where d is the grain diameter and φ is the porosity.

In this analysis, the permeability is calculated from the Kozeny-Carman equation with porosity modelled from velocity by Raymer's empirical relation. Porosity-estimates from sonic velocities, check-shot velocities and seismic velocities are used in the Raymer model for porosity estimation. Each velocity provides a porosity estimate that are applied into the Kozeny-Carman model for permeability estimation.

This method involves investigating whether or not seismic velocities are able to monitor slow-varying porosity-changes in the subsurface, and if the Kozeny-Carman model can extract information about permeability from the estimated porosity.

The empirical Raymer relation used for porosity estimation needs to be validated in the area where the permeability prediction is carried out. The area is Haltenbanken in the Norwegian Sea within the middle Jurassic Garn Fm. The verification of Raymer's model is done from well data from 15 Haltenbanken wells.

The Haltenbanken area is of high relevance as it is an important petroleum province, and the Garn Fm. is one of the principal hydrocarbon reservoirs in this area (Ehrenberg, 1990; Lundberg, 2011). The depositional interpretation of the sandstones in the Garn Fm. is a wave-dominated shoreface system with marine mud-dominated sediments deposited towards north and south (NPD, 2014). It is considered a good candidate for this permeability estimation analysis. Figure 1-1 shows the depth and lateral extension of the Garn Fm.

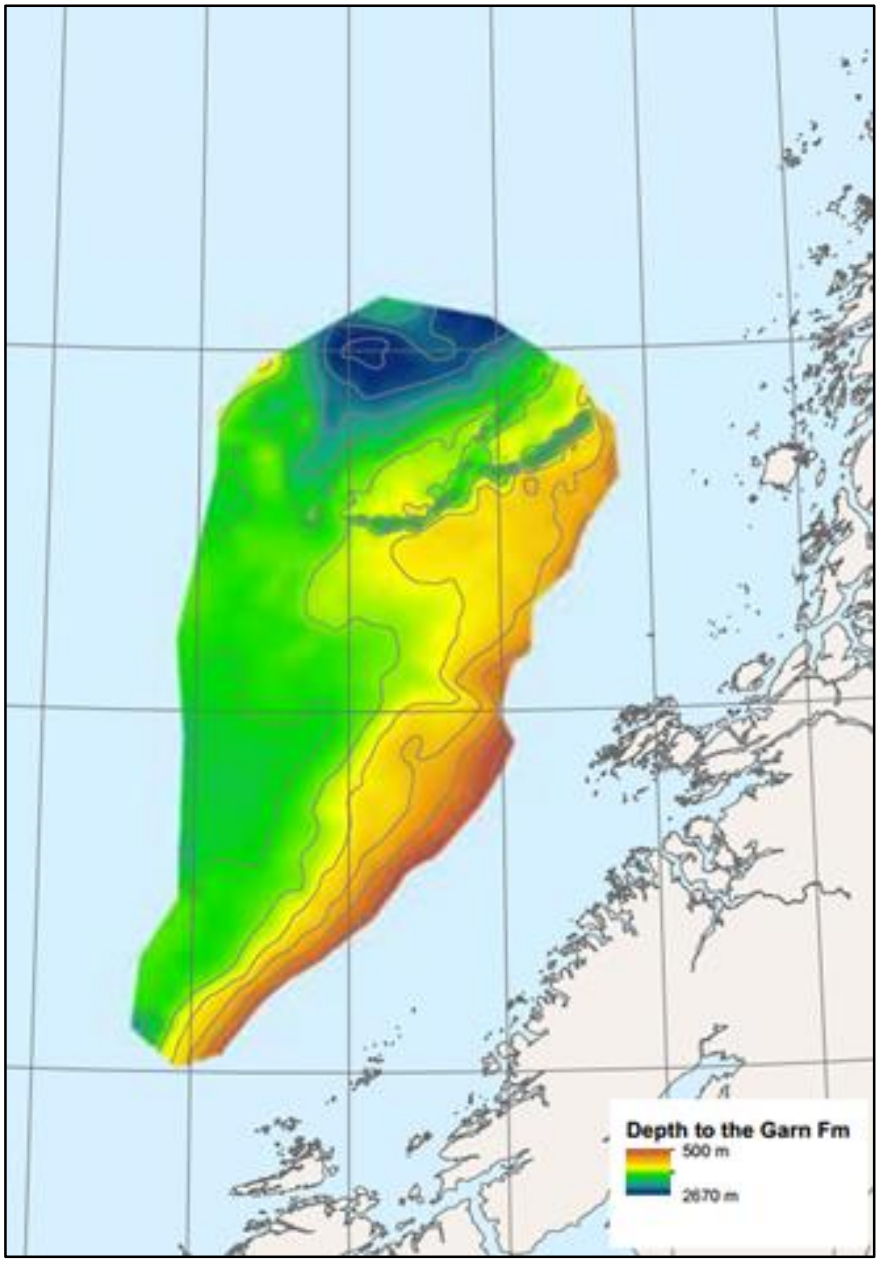

Figure 1-1: Map showing the lateral extension of the Garn Fm. (NPD, 2014)

1.1 Structure of the Thesis

The organization of this thesis are as follows:

- Chapter 2 introduces the importance of permeability in the petroleum industry and the leading methods for permeability prediction.
- Chapter 3 establishes the area where this analysis is carried out.
- Chapter 4 provides theory of the models and empirical relations applied in this study.
- Chapter 5 addresses the methodology, which involves establishing necessary parameters such as grainsize and cementation factor, and describes a series of small calculations necessary to model permeability from this method. These calculations involves clay volume estimation from gamma ray log, introducing a percolation porosity into the model, reduce the estimated total porosity to effective porosity and calibrate seismic velocity profiles in two well locations.
- Chapter 6 describes an analysis performed by Ehrenberg (1990) relevant for comparing the permeability results of this work.
- Chapter 7 presents the results from this study. This involves checking the validity of the Raymer porosity-velocity relationship on the 15 Haltenbanken wells, and applying the Raymer model on a "test well" and estimate the permeability. The permeability prediction is also carried out on porosities estimated from check-shot velocity and seismic velocity in two well locations. The seismic velocities are calibrated against check-shot data before applied the permeability modelling. Last, the permeability prediction along the time-interpretation of the Garn Fm. across a 2D seismic line is showed.
- Chapter 8 gives a discussion of the results, and investigates the sensitivities of different parameters within the Raymer model and Kozeny-Carman model.
- Chapter 9 comes with a suggestion to further work.
- Chapter 10 concludes this Master's thesis work.

2 Background

Porosity, permeability and relative hydrocarbon saturation are essential parameters in the evaluation of a petroleum reservoir. A precise prediction of these parameters are important for correctly estimating the hydrocarbons in place and key factors in reservoir management for enhanced hydrocarbon production. Optimization of well placement, selection of cost effective production strategies and waste disposal strategies (i.e. storage of CO_2 or radioactive waste) are all factors affected by these parameters (Ahmed et al., 1991).

In the petroleum industry the unit for permeability is darcy ($1\ Darcy = 0.9869 \times 10^{-12}\ m^2$) and it represents $1\ cm^3$ of fluid with viscosity of $1\ cp$ flowing through a $1\ cm^2$ cross-sectional area of rock in 1 second under a pressure gradient of $1\ atm$ per $1\ cm$ of length in the direction of flow. The permeability is an intrinsic rock property, which is called absolute permeability when the rock is 100% saturated with one fluid phase (Ahmed et al., 1991).

The three major permeability measurement techniques are wireline-log analysis, laboratory testing on core samples and well testing.

Permeability predictions from log measurement can provide level-by-level permeability values, whereas for example well-test permeability measure the flow provided by permeability when the contributing interval is known, but lacks level-by-level resolution. If more than one fluid phase is produced, the calculated permeability from well tests may not describe the formation permeability accurately, and the measured value is the effective permeability (which is the permeability of a specific fluid when the rock is saturated with multiple fluid phases) rather than the absolute permeability (North, 1985).

An acceptable value for permeability can be obtained experimentally from core samples tested in the laboratory or from well logs. The coring operation is however a very costly process, which may lead to not having sufficient cores to examine. Besides, the core may not bear any significant production characteristics of the formation because of inhomogeneity effects in the rock volume.

In this thesis, the Kozeny-Carman model estimates permeability with porosities estimated by Raymer's model from acoustic velocity data.

3 Data and Study Area

The permeability estimation in this analysis is performed in the clean parts of the Garn Fm. on Haltenbanken in the Norwegian Sea. Haltenbanken is located on the Mid-Norwegian continental shelf, between the Trøndelag platform in the east and the Vøring-Møre basins in the west (Storvoll, Bjørlykke, & Mondol, 2005). Figure 3-1 shows the location of the Haltenbanken area.

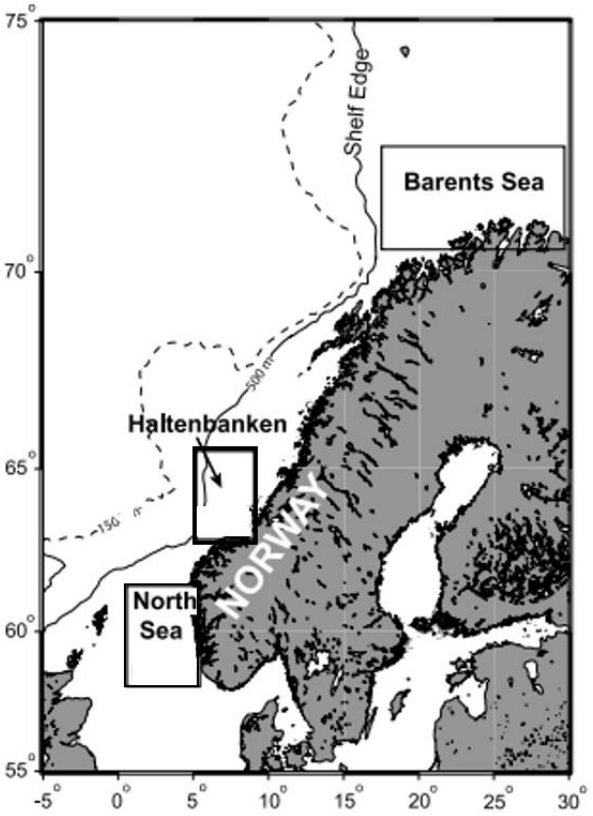

Figure 3-1: Map showing the outline of the Haltenbanken area, where all the wells used in this study are located (Storvoll et al., 2005).

The fields on Haltenbaken are Draugen, Heidrun, Njord, Norne (this field is north of the real Haltenbanken), Kristin and Åsgard (which includes the fields Midgard, Smørbukk and Smørbukk Sør).

15 wells from five Haltenbanken fields make up the original database for this analysis. The wells are differently spread amongst each of the 5 fields due to available wells, and also the necessity of choosing wells that provides good porosity spreading in the Garn Fm.

Each well have a number from 1-15 and the table below shows which field (1-5) each well belong to.

Table 3-1: Well id and field id for the Haltenbanken wells.

Well	Field
1	1
2	1
3	1
4	1
5	2
6	2
7	2
8	2
9	2
10	3
11	3
12	3
13	3
14	4
15	5

The well log data from this well database is used to verify Raymer's relation and to estimate the permeability.

All the log data applied in the porosity and permeability estimation is corrected for fluid effects. In most wells, the fluid substitution had already been done and fluid corrected logs are available. However, it is necessary to do a fluid substitution within the Garn Fm. in the other wells, and the procedure is explained in Appendix B.

4 Theory

4.1 The Kozeny-Carman equation

One problem when predicting permeability from measurable rock properties is to select a proper model relating the measured properties to permeability.

The first approaches focusing on relating permeability to measurable rock properties, were based on the study of flow through thin tubes.

Poiseuille (1840) studied the flow of liquids in very thin glass tubes in the context of physiology, but his result can be used if it is accepted that the set of thin tubes is analogue to a sandstone. The result of Poiseuille's work suggests that permeability should be a function of pore throat diameter. For sand without clay or other minerals between the sand grains the pore throat diameter should be related to grain size, grain shape and the type of packing (Poiseuille, 1840).

Darcy (1856) performed experiments on the vertical downward flow of water through sand packs which resulted in what we know as Darcy's law.

Dary's law was expressed in familiar terms as (Hubbert, 1956)

$$Q = \kappa\, A\, \frac{h_1 - h_2}{l} \qquad (2)$$

Where Q is the fluid flow (volume per unit time) passing vertically downward through the cross section A of sand with thickness l, h_1 and h_2 are the heights above a standard reference elevation of water in equivalent water manometers terminated above and below the sand respectively, and κ is a factor of proportionality that includes the effect of permeability.

Kozeny (1927) made the next outstanding contribution to the problem of permeability after Darcy's work.

Walderhaug et al. (2012) summarizes Kozeny's work:

"Kozeny considered the flow of an incompressible fluid through a porous medium when inertial forces can be disregarded, and solved the Navier-Stokes equations for a set of channels passing through a cross section normal to the direction of flow when there is no tangential component of the flow velocity in the cross section normal to the flow channels"

For flow through a system of regularly packed spherical grains with diameter, d, and porosity, φ, Kozeny (1927) arrived at the following expression for the average speed of flow, v, through the porous medium:

$$v = \frac{\gamma I}{\mu} c \frac{L}{l} \frac{\varphi^3 d^2}{36(1-\varphi)^2} \tag{3}$$

Where γ is the fluid density multiplied by the gravitational acceleration, μ is the viscosity, I is the gradient in hydraulic head along the flow path, c is a dimensionless shape factor determined by the cross sections of the pores, with a value of about 0.5.

The assumption is that each flow path is a twisted, tortuous and independent path from one end of the sample to the other.

This gives rise to the definition of the parameter tortuosity, defined as

$$\tau = \frac{l}{L} \tag{4}$$

Where L and l are the lengths of the theoretical straight flow path and the real curved flow path around the grains respectively.

By equating the expression for linear flow rate, given by Equation (3), with the expression for linear flow rate from Darcy's law, one arrives at the Kozeny equation for permeability.

$$k = c \frac{\varphi^3 d^2}{36(1-\varphi)^2 \tau^2} \tag{5}$$

4.1.1 Step-by-step Derivation of the Kozeny-Carman Equation

An alternative way of deriving the Kozeny-Carman equation is based on combining an equation for total volume flux through a circular pipe and Darcy's law (Mavko, Mukerji, & Dvorkin, 2009).

The total volume flux through a cylindrical pipe of length l and a circular cross-section of radius R is given by Poiseuille's equation:

$$Q = -\frac{\pi R^4}{8\mu}\frac{\Delta P}{l} \tag{6}$$

Where ΔP is the pressure head along the length of the pipe and μ is the dynamic viscosity of the fluid. The flow rate within the tube is assumed low enough for the flow to be laminar rather than turbulent.

Darcy's law can be expressed slightly different than in Equation (2), as

$$Q = -k\,\frac{A}{\mu}\frac{\Delta P}{L} \tag{7}$$

Where k is the permeability parameter and L is the theoretical straight flow path ($L \leq l$)

By combining Equation (6) and (7) the permeability are expressed as:

$$k = \frac{\pi R^4}{8 A \tau} \tag{8}$$

Total porosity is the volume of the pores in the sample divided by the total bulk volume of the cylindrical sample.

$$\varphi = \frac{V_{pore}}{V_{bulk}} = \frac{\pi R^2 l}{AL} = \frac{\pi R^2}{A}\,\tau \tag{9}$$

Where R is the pore radius and l is the length of the continuous pore-path which the fluid pass through.

This expression for porosity is used to rewrite Equation (8) so it becomes

$$k = \frac{\pi R^2}{A}\tau\frac{R^2}{8\tau^2} = \frac{\varphi R^2}{8\tau^2} \tag{10}$$

The specific surface area is the pore surface area divided by the sample volume (Mavko et al., 2009).

$$S = \frac{2\pi Rl}{AL} = \frac{2\pi R}{A}\tau \tag{11}$$

Where R is the pore radius. Equation (11) can be written as a function of porosity as

$$S = \frac{\pi R^2 \tau}{A}\frac{2}{R} = \frac{2\varphi}{R} \tag{12}$$

This expression for specific surface area is rewritten with respect to R and becomes

$$R = \frac{2\varphi}{S} \tag{13}$$

The expression for R above can be inserted into Equation (8) and the permeability of a block is expressed by the general properties φ and S, and gives the Kozeny-Carman equation.

$$k = \frac{\varphi}{8\tau^2}\left(\frac{2\varphi}{S}\right)^2 = \frac{\varphi^3}{2\tau^2 S^2} \tag{14}$$

Behind this derivation lies the approximation that the porous system within a sand pack or sandstone is analogue to a set of parallel thin tubes or pipes. The figure below illustrates this tube-like pore geometry with one such pore path (note that the dimension of the pore path is heavily expanded compared to the sample).

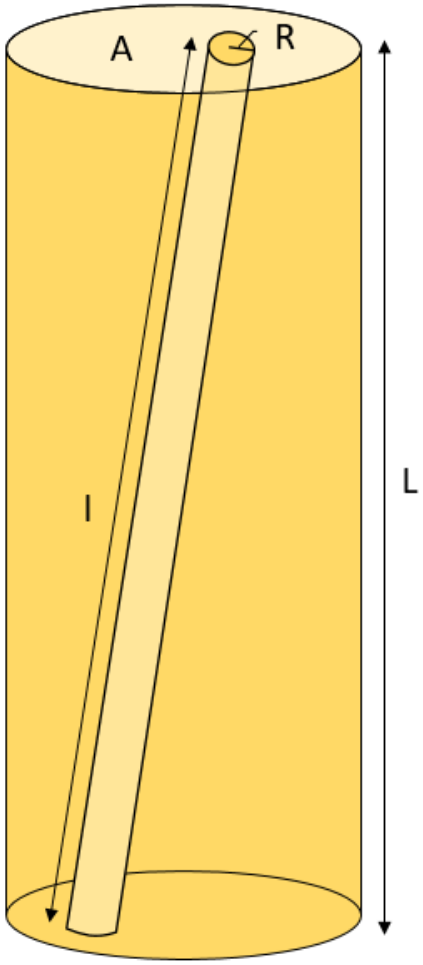

Figure 4-1: The imagined pore-geometry for the derivation of the Kozeny-Carman relation is that the pore-system in a sandstone is analogue to a set of parallel, thin tubes going through the sample.

It is common to extend the Kozeny-Carman relation for a circular pipe to consider a packing of identical spherical grains of diameter d. Although this granular porespace geometry is not consistent with the pipe-like geometry, it is common to use the original Kozeny–Carman functional form and believe that the tortuosity factor adjust for the twisted path.

The specific surface area for a rock with spherical grains can be written as a function of porosity:

$$S = \frac{3(1-\varphi)}{R} \tag{15}$$

By inserting Equation (15) into Equation (14) and replacing the grain radius with the grain diameter ($d = 2R$), the Kozeny-Carman equation can be written as

$$k = \frac{\varphi^3 \, d^2}{72(1-\varphi)^2\tau^2} \tag{16}$$

This form of the Kozeny-Carman equation is applied in this Master's thesis analysis.

4.2 Empirical Relations

As mentioned, the objective of this study is to combine empirical models with the Kozeny-Carman model, so that the porosity applied in the permeability calculation is a function of velocity.

The empirical relations are presented in the following chapter.

4.2.1 Tortuosity-Porosity Relation

Grude et al. (2015) applies Archie's (1942) relation between the formation factor, F, and porosity. The formation factor is defined as the ratio between water saturated sandstone conductivity and bulk water conductivity, and Archie (1942) found that it could be expressed as

$$F = a\varphi^{-m} \tag{17}$$

Where a is the tortuosity factor, assumed to be 1, and m is usually called the cementation factor. It depends on shape, type and size of the grains, shape and size of the pore throats and the size and number of dead-end pores in the rock (Salem & Chilingarian, 1999).

Wyllie and Spangler (1952) developed a different relation for expressing the formation factor

$$F = \frac{\tau}{\varphi} \tag{18}$$

Grude et al. (2015) exploits these two relations for the formation factor to express the tortuosity in terms of porosity and cementation factor as showed below

$$\tau = \varphi^{1-m} \tag{19}$$

This relation replaces the tortuosity in the Kozeny-Carman equation, and Equation (16) becomes

$$k = \frac{\varphi^3 \, d^2}{72(1-\varphi)^2(\varphi^{1-m})^2} \tag{20}$$

4.2.2 Raymer's Porosity-Velocity Relation

The sonic log was the first log measurement permitting evaluation of the formation porosity independent of the fluid saturation. Today, several more logging tools permits porosity related measurements, such as the density-log and neutron-log. As for most of well logging measurements, the sonic log does not measure the parameter it is associated with directly (which for the sonic-log is porosity). What the sonic log measure is the time required for a sound wave to travel a given distance in a formation. The measured acoustic velocity, also referred to as transit time, must be translated to porosity, thus the porosity is not a direct measurement. Various equations, based on experimental data, theoretical developments, or a combination of the two, have been proposed for performing the operation going from transit time to porosity (Raymer, Hunt, & Gardner, 1980).

A common equation, often referred to as Wyllie time-average, relates porosity and velocity through a weighted time average (Wyllie, Gregory, & Gardner, 1956)

$$\frac{1}{v_p} = \frac{\varphi}{v_{fl}} + \frac{1-\varphi}{v_{ma}} \tag{21}$$

Where v_p, v_{fl} and v_{ma} are the P-wave acoustic velocity for a saturated rock, the velocity of the saturating pore fluid and the rock matrix velocity, respectively. The Wyllie time-average equation assumes that the total transit time for a wave to pass through a media is the sum of the time it travels in the mineral material and the time the wave travels in the pore fluid.

Raymer et al. (1980) points out some shortcomings of the Wyllie time-average equation. I. e., at low porosities (less than, say, 15%) sonic transit time does not increase with increased porosity quite as rapidly as predicted by the time-average equation. Another problem associated with transforming sonic transit time to porosity is related to uncertainties in the matrix velocity.

The problems related to the use of the Wyllie time-average led Raymer et al. (1980) to propose a new and improved empirical transit time-to-porosity transform for consolidated sandstones. The relation is based on numerous comparisons of transit time versus porosity observed over many years of log interpretative experience, and will for simplicity be referred to as Raymer's relation or Raymer's model throughout this report. The relation is given by

$$v_p[km/s] = (1-\varphi)^2\, v_{ma} + \varphi v_{fl} \qquad \varphi < 37\ \% \tag{22}$$

$$\frac{1}{\rho {v_p}^2} = \frac{\varphi}{\rho_{fl}\, v_{fl}^2} + \frac{1-\varphi}{\rho_{ma} v_{ma}^2} \qquad \varphi > 47\ \% \tag{23}$$

Only Equation (22) is considered in this report, as a porosity cut-off are set at 37%.

The assumptions and limitations that are required to use the Raymer relation are:

- Isotropic rock
- The rock-composing minerals have the same velocity
- The rock is saturated with fluid
- The model is empirical
- The effective pressure (the pressure carried by the rock frame) should be high enough to reach "thermal velocities". This velocity is reached when the velocity-increase with depth appear to level off. Here, the crack-like pore space is closed due to the increase of pressure as a result of increasing depth, and is usually around 30 MPa.
- The relation work best for consolidated low-to-medium porosity and high porosity cemented sandstones.
- The relation should not be used for unconsolidated sandstones.

Rewriting Equation (22) with respect to porosity gives

$$\varphi = \frac{2v_{ma} - v_{fl} - \sqrt{4v_{ma}(v_p - v_{fl}) + v_{fl}^2}}{2v_{ma}} \quad (24)$$

Note that the porosity provided by the Raymer equation is the total porosity, as the velocity will see both dead-end pores and isolated pores.

The expression above provides porosity as a function of velocity. v_p is the measured acoustic velocity, and can be various types of velocity (such as sonic velocities, check-shot velocities and seismic velocities, which are used in this study).

However, before the velocity derived Raymer-porosities are applied in the Kozeny-Carman model, some adjustments are done to the estimated porosity. The methodology chapter coming next explains these steps.

5 Method

The following sections explains the steps performed to arrive at the point where the permeability can be estimated from the Kozeny-Carman model. These steps involve:

- Estimate the clay content. A clay content restriction is put on the Garn Fm., so that the permeability can be calculated in the clean parts of the Garn Fm. only.
- Estimate the matrix and fluid velocities in order to apply Raymer's relationship to predict the porosity.
- Adjust the porosity obtained from Raymer's relation to become the effective porosity, not the total porosity.
- A percolation threshold porosity is introduced in the Kozeny-Carman equation.
- Establish the values for grain size and cementation factor necessary to apply the Kozeny-Carman model.
- Investigate the seismic velocity profiles in two well locations.
- Investigate seismic 2D lines and the interpretation of the Garn Fm.

5.1 Estimating the Clay Content

Since the permeability prediction ought to be performed in clean sands, it is necessary to apply a restriction on the clay content within the Garn Fm.

The shale volume obtained from the gamma ray log is used to estimate the clay volume. Since the log derived shale volume includes silt, the clay volume will be somewhat overestimated.

The gamma ray value for shale can vary enormously, but the value for pure shale tend to be constant. Therefore, the maximum average gamma ray value is considered to represent 100% shale, and this line is called the shale line. The lowest average gamma ray value represent the sand line (100% sand) (Rider, 2000).

Figure 5-1 shows the two baselines (shale line and sand line) together with the gamma ray log as an illustration.

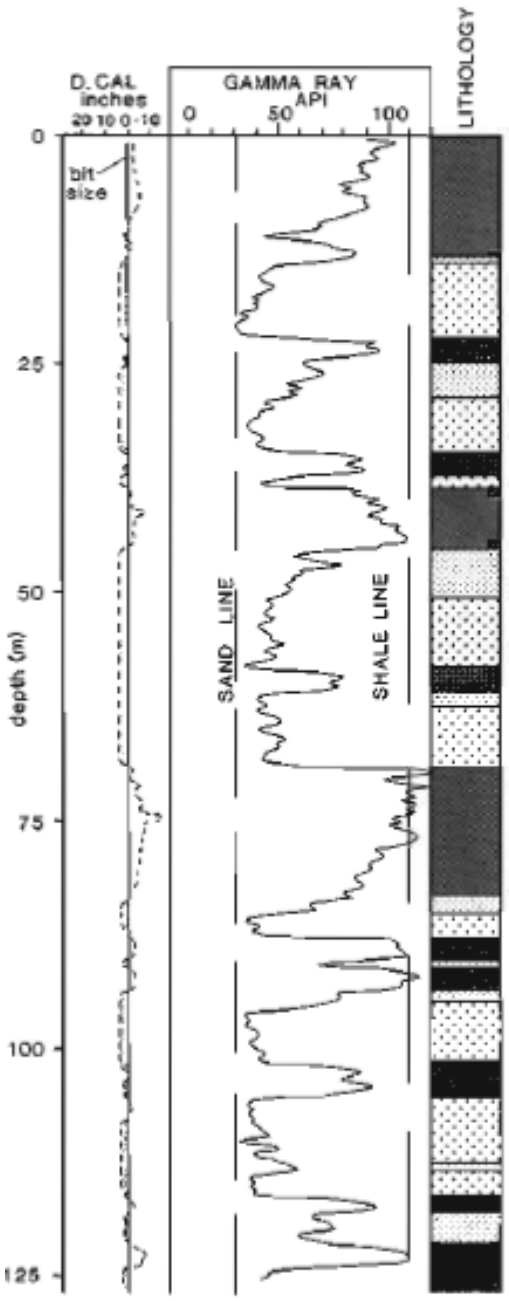

Figure 5-1: Shale line and sand line defined by the maximum and minimum value on the gamma ray log respectively (Rider, 2000).

From the shale line, sand line and the gamma ray log readings, the clay volume is calculated from the following equation.

$$V_{cl} = \frac{GR\ value\ (log) - GR\ (min)}{GR\ (\max) - GR\ (min)} \qquad (25)$$

Where V_{cl} is the clay content in percent, $GR\ (max)$ is the line representing 100% shale (shale line) and $GR\ (min)$ represent 0% shale (sand line).

The calculated clay volume is actually the shale volume, so it includes the silt volume. Although the estimated clay volume is not very accurate, it tends to give an upper limit of the clay volume. The volumetric clay content is used to find the points within the Garn Fm. that is sufficiently clean for the permeability estimation to be carried out, and to reduce the total Raymer-porosity to become the effective Raymer-porosity, by assuming that the pores within the clay are isolated.

5.2 Estimating Brine and Matrix Velocities

5.2.1 Estimate Brine Velocity

The Raymer model requires the matrix velocity and the fluid velocity to calculate the porosity. In this analysis, the permability is calculated in fluid corrected samples, so all the samples are fluid substituted with 100% brine. Therefore, the fluid velocity is the brine velocity.

The density and velocity of brine is a function of pore pressure, temperature and salinity (Batzle & Wang, 1992). See Appendix A for Batzle and Wang's empirical relations for the estimation of velocity and density for brine and pure water.

The average brine velocity within the Garn Fm. is applied to be the brine velocity in the whole Garn interval in each well. That means that the brine velocity is constant in the whole Garn interval for each well.

The brine velocity did not change much from Garn Fm. in one well to the next. It is generally a little above 1.6 km/sec, which is reasonable.

5.2.2 Estimate Matrix Velocity

The matrix velocity is assumed to be a weighted average of the time the wave travels through the different material composing the matrix, which are assumed to be sand and clay. By using a time average equation the matrix velocity becomes

$$v_{ma} = \frac{V_{sand}}{1-\varphi} \times v_{sand} + \frac{V_{cl}}{1-\varphi} \times v_{cl} \qquad (26)$$

Where v_{sand} and v_{cl} are the velocities in the sand part of the matrix and the clay part respectively. V_{sand} and V_{cl} are the sand volume and clay volume respectively.

The velocity for each material is calculated by the following equation

$$v = \sqrt{\frac{K + \frac{4}{3} G}{\rho}} \tag{27}$$

Where K is the bulk modulus, G is the shear modulus and ρ is the density of the material the velocity is calculated for. Table 5-1 shows the values for these parameters.

Table 5-1: Values used for calculating matrix velocity in the Garn Fm. Numbers are taken from Avseth et al. (Avseth, Mukerji, Mavko, & Dvorkin, 2010).

Elastic modulus	Sandstone	Clay
Bulk modulus, K	37 GPa	33 GPa
Shear modulus, G	45 GPa	9 GPa
Density, ρ	2.65 g/cm^3	2.65 g/cm^3

5.3 Total Porosity versus Effective Porosity

The porosity produced by Raymer's relation is the total porosity. Since P-wave velocity includes isolated and dead-end pores not contributing to the permeability, it is more convenient to reduce the total Raymer-porosity to effective Raymer-porosity before using it into the Kozeny-Carman model.

By assuming that the porosity in the clay volume only contributes to total porosity, the effective porosity is the remaining when the clay-porosity is subtracted from the total porosity.

By using the clay volume obtained from the gamma ray log, the effective porosity is calculated from

$$\varphi_{eff} = \varphi_{tot}(1 - V_{cl}) \tag{28}$$

Where φ_{tot} is the porosity obtained from Raymer's relation, as given in Equation (24) and V_{cl} is the clay volume derived from the gamma ray log.

5.4 Percolation Threshold Porosity

A problem with relating permeability to porosity with the Kozeny-Carman relation, is that it appear to fail at low porosities because the permeability decrease more rapidly than porosity with decreasing porosity.

By including a percolation threshold porosity into the Kozeny-Carman relation, the derived third-power dependence on porosity can be retained for an extended range. Also, previous work show that introduction of a percolation porosity significantly improve the predicted permeability (Mavko & Nur, 1997) .

Experiments suggests that the percolation porosity is between 1 and 3%, depending on the mechanism of porosity reduction. The percolation effect is incorporated in the Kozeny-Carman equation by replacing φ with $\varphi - \varphi_c$, where φ_c is a critical porosity which needs to be overcome for the porosity to give a contribution to the permeability (Mavko & Nur, 1997).

In this analysis, the threshold porosity is set to 2%.

With a percolation threshold porosity introduced, the Kozeny-Carman equation becomes:

$$k = \frac{(\varphi - \varphi_c)^3 \, d^2}{72(1 - \varphi + \varphi_c)^2((\varphi - \varphi_c)^{1-m})^2} \tag{29}$$

Note that φ refers to the effective Raymer-porosity.

5.5 Determine Grainsize and Cementation Factor

The grain diameter is necessary in order to apply the Kozeny-Carman model. Panda and Lake (1994) modified the Kozeny-Carman equation to express the single phase permeability in terms of the particle size distribution (psd) statistics and the bulk physical properties, which are the porosity and tortuosity. They modified the Kozeny-Carman equation for a medium with spherical grains with a range of particle diameters that have an arbitrary psd.

They arrived at the following modification of the Kozeny-Carman equation:

$$k = \frac{\bar{d}^2 \varphi^3}{72(1 - \varphi)^2} \left[\frac{(\gamma \, C_d^3 + 3 \, C_d^2 + 1)^2}{(1 + C_d^2)^2} \right] \tag{30}$$

Where C_d is the coefficient of variation of the psd (standard deviation, σ, divided on the mean grainsize, $\bar{d}$) and γ is the skewness (a measure of the asymmetry of a probability distribution).

For a homogeneous medium, the term in brackets in Equation (30) becomes zero, and else it can be seen as a correction to the permeability calculated by the original Kozeny-Carman equation.

In most Garn zones within the wells used in this permeability prediction, the grainsize is not available, and so is the grainsize distribution.

The lithology and depositional environment in the Garn Fm. is believed to be consistent with a grainsize classified as medium sized sand, which is classified to range from 0.25-0.5 mm on Wentworth's (1922) size scale. A constant grain diameter of 0.37 mm is applied in the permeability estimation.

The last parameter that needs to be discussed before the permeability estimation can be carried out is the cementation factor. The cementation factor, m, indicates a reduction in the number and size of pore openings. The cementation factor vary from one sample to another as well as between different formations and different mediums. According to Wyllie and Rose (1950), the cementation factor can in theory become infinity but in practice, it lies between 1.3 and 3 (Wyllie & Rose, 1950).

For most consolidated sandstones, the cementation factor is 2 (Rider, 2000). The cementation factor is kept at this value throughout this analysis.

5.6 Calibrate Seismic Velocity

Two seismic velocity profiles in the locations of well 5 and 6 from the Haltenbanken dataset need calibration before the seismic acoustic velocities are used in the Raymer model for porosity estimation. The seismic velocity profiles are modified so that the seismic time-depth curve correlate with the check-shots. Figure 5-2 and Figure 5-3 show the time-depth curve obtained from the check-shots and the seismic before any calibration is done to the seismic velocities for well 5 and 6 respectively. Before receiving the seismic velocities, the data have been calibrated towards the check-shots already, but additional calibration is possible and may improve the velocities.

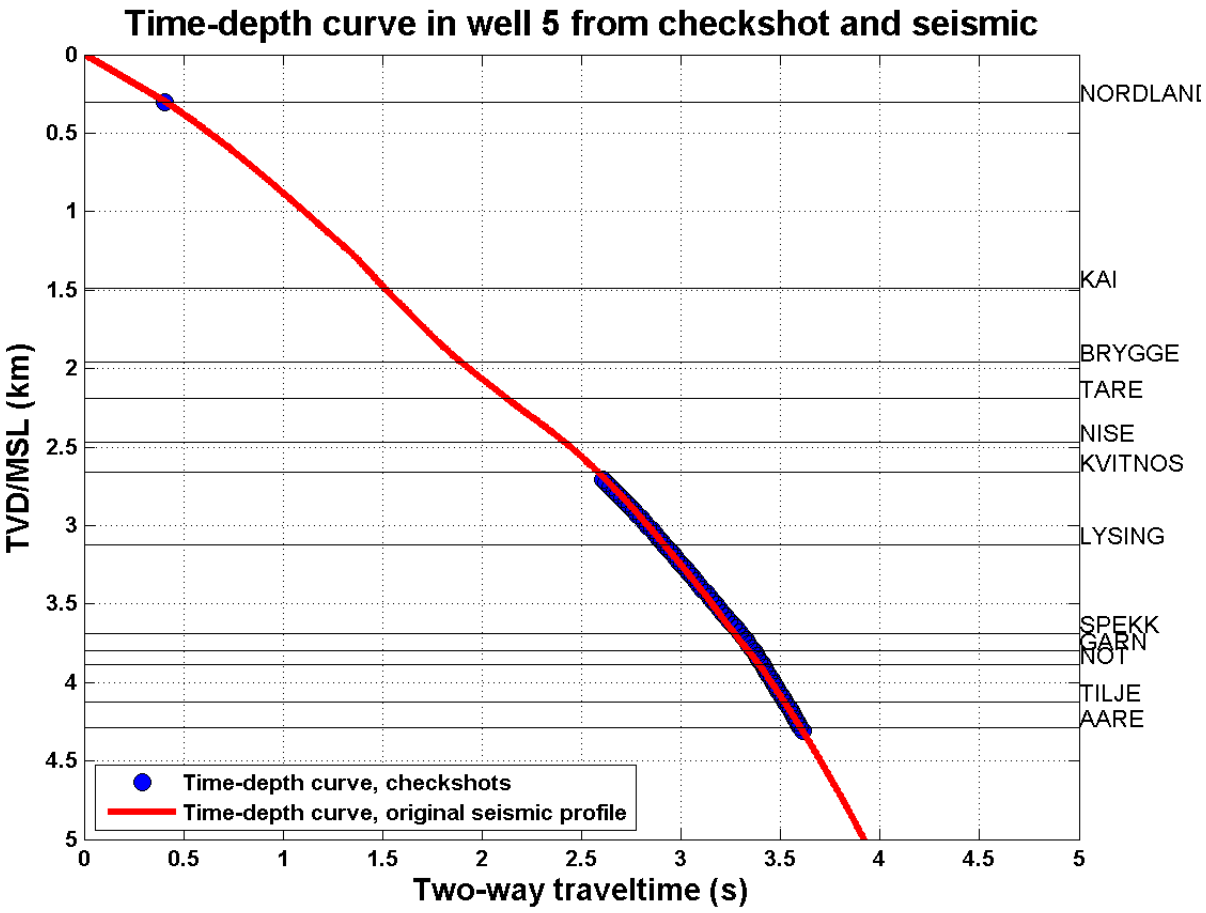

Figure 5-2: Time-depth relationship provided by check-shots (blue) and seismic (red) in the location of well 5.

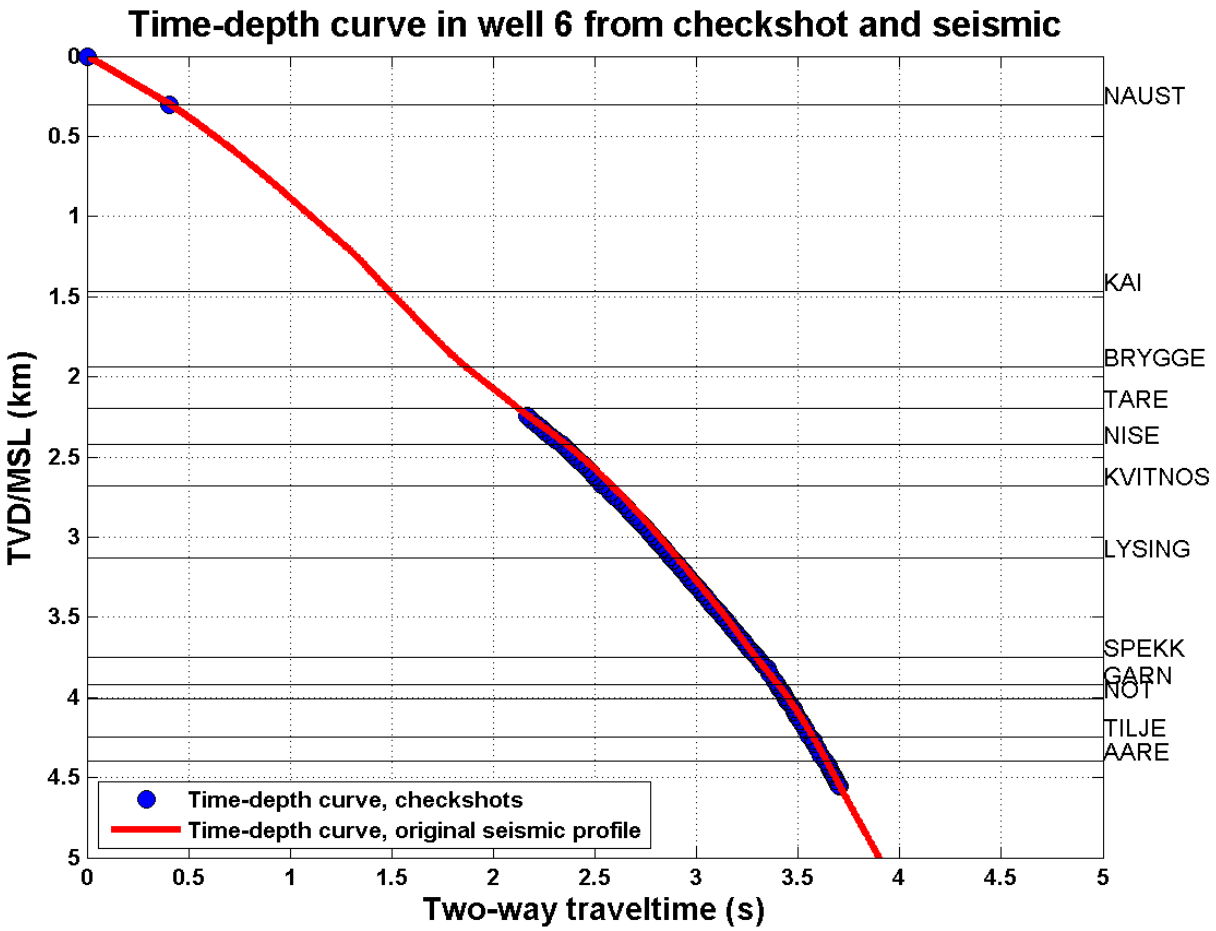

Figure 5-3: Time-depth relationship provided by check-shots (blue) and seismic (red) in the location of well 6.

Though the correlation between the time-depth curves above are quite good, it is improved by introducing a delta correction factor. The correction factor focuses on reducing the anisotropy effects above the Garn Fm., causing the Garn velocities to be mapped to the wrong depth when depth migrated.

The seismic velocity profiles are modified by dividing the velocity in a given interval with $\sqrt{1+2\delta}$ where δ is one of Thomson's parameters for a VTI medium (vertical symmetry axis) (Mavko et al., 2009).

The interval velocity at different intervals is then obtained from the original NMO (normal-move-out) velocity from the equation

$$v_{int} = \frac{v_{NMO}}{\sqrt{1+2\partial}} \qquad (31)$$

Different delta factors are applied for different intervals, resulting in calibrated seismic velocity profiles and seismic time-depth relationships that correlates better with the check-shot time-depth curves for the two wells respectively.

6 Ehrenberg's Work

Ehrenberg (1990) performed a study that is important for this analysis, since it also involves permeability prediction in the Garn Fm. on Haltenbanken by using the Kozeny-Carman relation. He plotted porosity versus permeability for 26 Haltenbanken wells (some of his wells are the same as used in this analysis). However, he applied a slightly different variety of the Kozeny-Carman equation, given as

$$k = \frac{\varphi^3}{5\,S^2(1-\varphi)^2} \tag{32}$$

When comparing this variety of the Kozeny-Carman equation to Equation (16) (which is the variety of the Kozeny-Carman equation applied in this work) it is clear that $1/5\ S^2$ corresponds to $d/72\ \tau^2$.

Ehrenberg assumes cubic packing of spheres of uniform diameter, which gives a specific surface area of

$$S = \frac{6}{d} \tag{33}$$

This is a different definition of the specific surface area than used here (see Equation (15)), but his results from plotting the porosity and permeability in the Garn Fm. from Equation (32) correlates to a specific surface area of 200 to 400, as showed in the figure below.

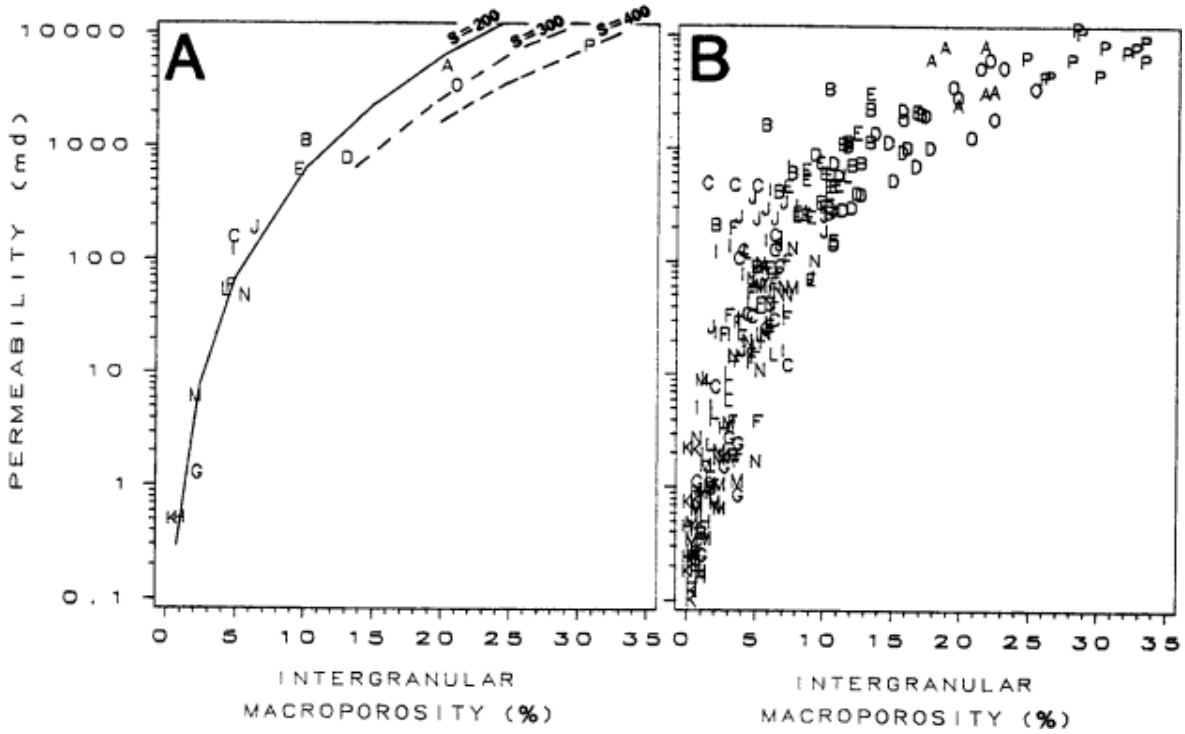

Figure 6-1: Horizontal air permeability from routine core analysis versus porosity in Garn sandstones. (A) Average specific surface area for each well. (B) Individual analysis (Ehrenberg, 1990).

The letters in the plot above refers to the wells Ehrenberg applied in his work, see Table 1 in (Ehrenberg, 1990).

This plot is a good reference for the permeability predicted in this study, as it tells us that the permeability in Garn, according to Ehrenberg, should be within the lines of a specific surface area varying between 200 cm^2/cm^3 and 400 cm^2/cm^3. These lines is plotted together with the estimated permeability as a way of comparing the predicted permeability with Ehrenberg's result. It should be noted that only a few wells are included in both analysis, but since the Garn Fm. is analysed in both studies it is reasonable to compare the results from this analysis with Ehrenberg's anyway.

7 Results

This chapter consists of five parts

- Test the validity of Raymer's model in the Garn Fm. on Haltenbanken
- Estimate the permeability in a "blind/test well" by using sonic velocities
- Estimate the permeability from check-shot velocity derived porosity
- Estimate the permeability from calibrated seismic velocity derived porosities in two well locations
- Model the permeability across the Garn Fm. along seismic 2D lines.

7.1 Testing the Validity of Raymer's Relationship

The measured porosity and velocity in the Garn Fm. are plotted together with Raymer's relation in Figure 7-1, and the colours indicate the field number. All the samples are corrected for fluid effects, so the fluid saturation is 100% brine.

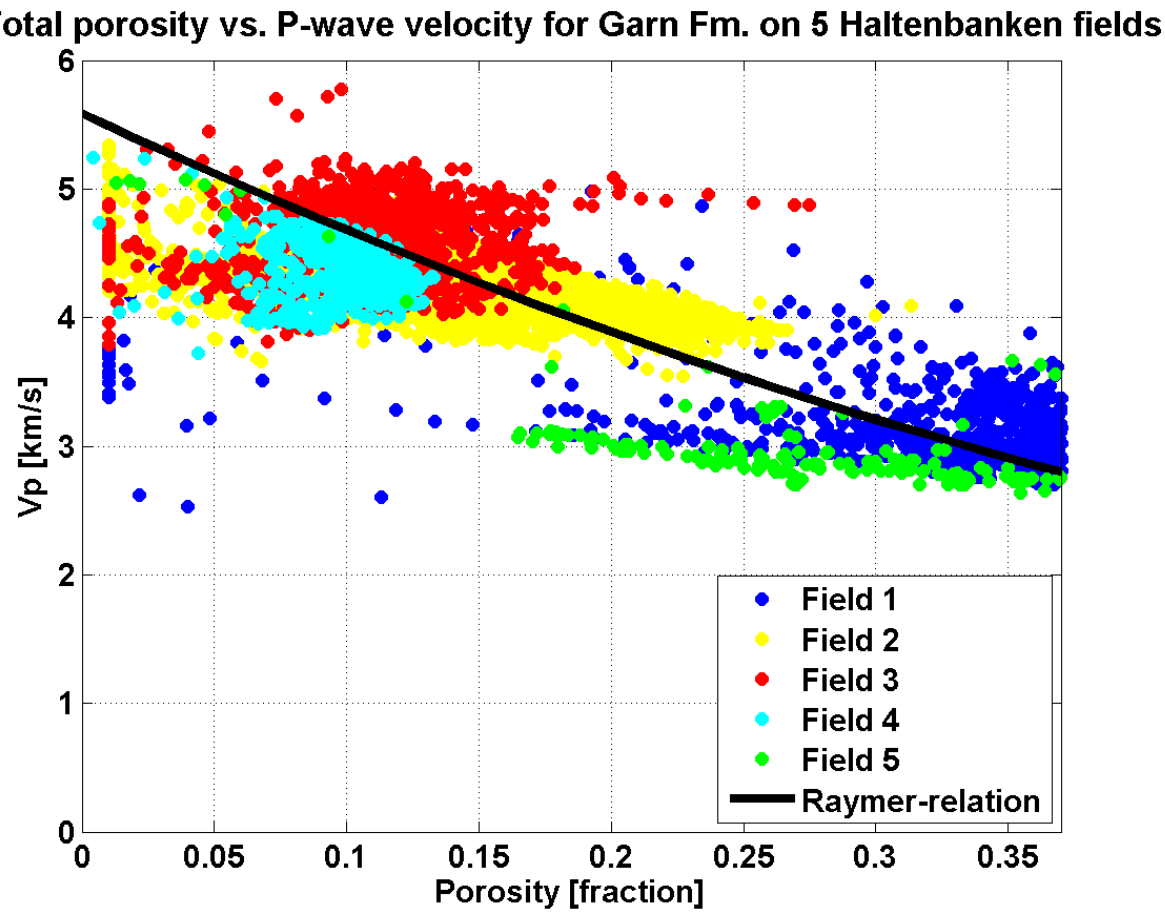

Figure 7-1: Measured porosity versus measured velocity in the Garn Fm. on 5 different Haltenbanken fields. The black line shows Raymer's relation between velocity and porosity.

Some of the wells had a porosity log available, which is a log modelled from various parameters by a petrophysicist, and not a direct measurement. However, not all the wells had such a porosity log available so the porosity in the Garn Fm. in these wells are calculated from the density log by the equation

$$\varphi = \frac{\rho_{ma} - \rho}{\rho_{ma} - \rho_{fl}} \tag{34}$$

Where ρ_{ma} is the matrix density, which is the density of clay and sand, both assumed to be $2.65\ g/cm^3$, ρ is the bulk density (the value measured by the density tool) and ρ_{fl} is the density of fluid in the pores, which is brine because of the fluid substitution. The fluid density is calculated from Batzle & Wang's empirical equations (Appendix A).

The density porosity and the modelled porosity are both referred to as measured porosity in this report.

The black line shows Raymer's relation of velocity as a function of porosity, as given in Equation (22). This line shows where Raymer's function models the velocity for a given porosity when the matrix and brine velocity are constant.

Figure 7-1 has extensive scattering around the black Raymer-curve. A restriction to the clay content allowed in the Garn sand reduces the scattering. Only the Garn points containing less than 10% clay are plotted in Figure 7-2, and there is less scattering around the Raymer curve in this figure compared to Figure 7-1.

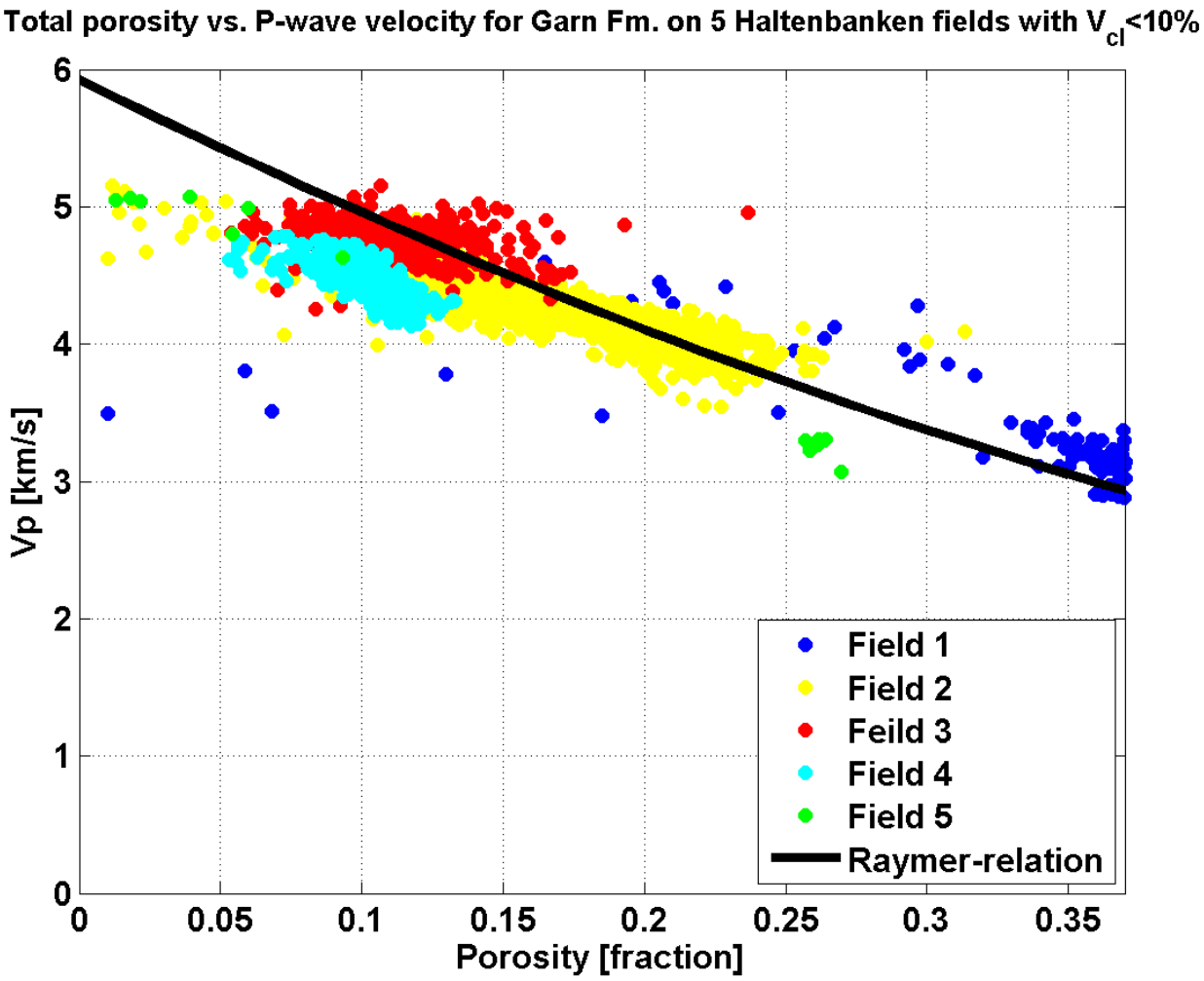

Figure 7-2: Measured porosity versus measured velocity for the sand in the Garn Fm. that contain less than 10% clay.

There is still a fair range in porosity in this figure, but fewer points in the porosity range from 0.25 to 0.33. If the clay-volume restriction is put even lower, the porosity range would not be satisfying.

The matrix velocity and brine velocity are necessary in order to plot the black Raymer-curve (see Equation (22)). These values are found by taking the average of the matrix velocity and brine velocity for the relevant points in the Garn Fm. in all the wells.

The table below shows the average matrix and fluid velocities used to plot the Raymer-line when there is no restriction regarding the clay content (Figure 7-1), and when the clay-volume cut-off is 10% (Figure 7-2).

Table 7-1: Matrix and brine velocities used to plot Raymer's function with no restriction to clay content and with a clay content restriction.

	Matrix velocity	Fluid velocity
All Garn points, no clay content restriction	5.58 km/s	1.57 km/s
Garn points containing less than 10% clay content	5.92 km/s	1.56 km/s

The black Raymer-line in the figures above are not adjusted individually to fit Garn in each well, because the Garn Fm. is considered as a whole to obtain a large porosity range. However, the matrix and brine velocity values should be estimated only from the points plotted in the respective figure.

7.2 Blind Well Testing

When it is verified that the velocity-porosity measurements in the Garn Fm. on Haltenbanken follows the trend given by Raymer's equation, a "blind" well or test well, that is not included in the previous dataset, is tested to see if it, too, follows the Raymer-trend.

Three blind wells are tested but only one is suitable for presenting, since the other two had problems such as only one porosity value throughout the Garn interval or did not have appropriate log readings. The test well that is presented is named well 17.

Figure 7-3 show a log overview of well 17.

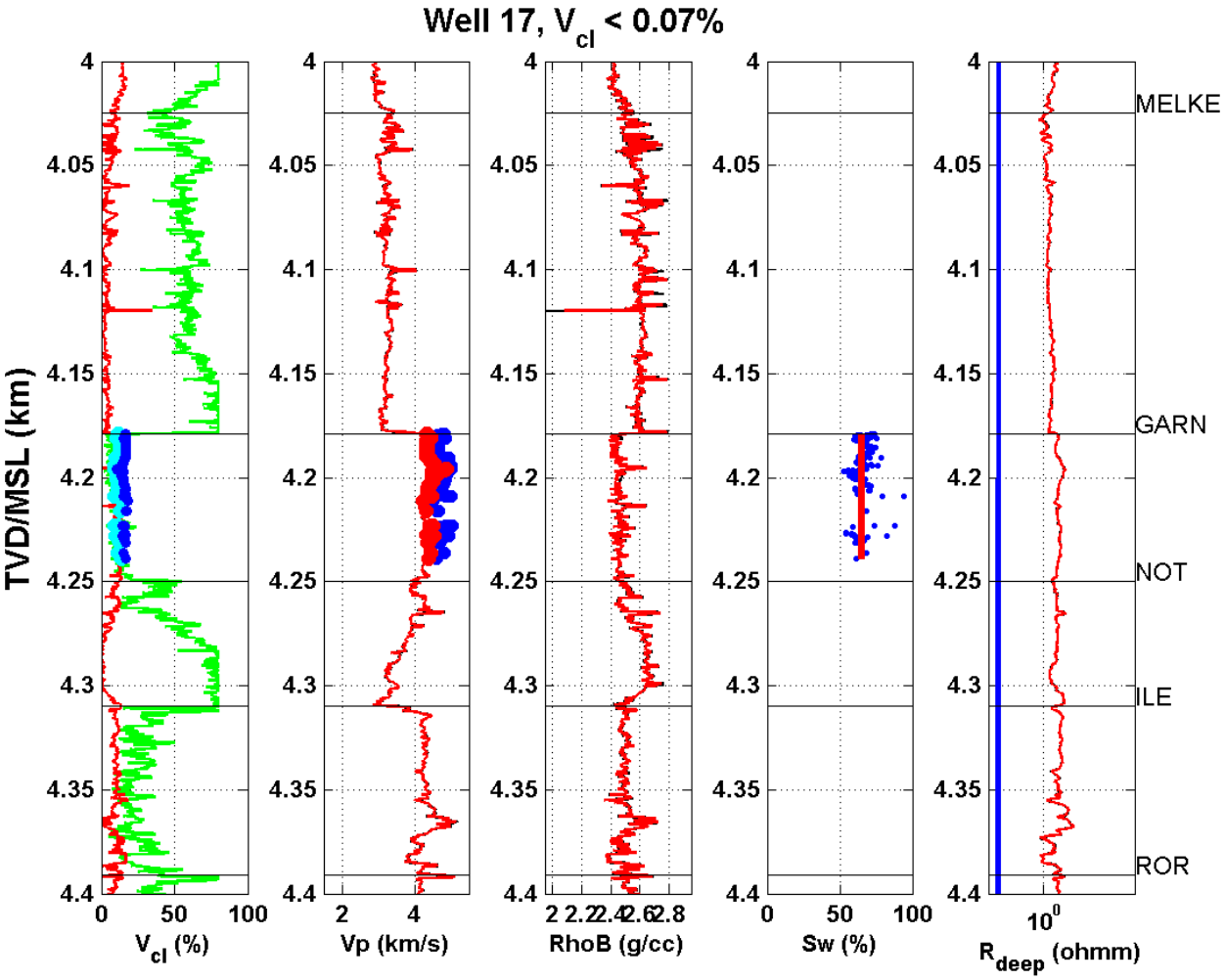

Figure 7-3: Log overview of test well 17.

In the first pane, the green and red logs are the estimated clay content and the porosity respectively. The cyan points are the measured porosity and the blue points are the Raymer-porosity, calculated from the sonic log by applying Raymer's equation.

The red points in the second pane show the fluid corrected sonic log in Garn, and the blue points are the Raymer-velocity obtained by transforming the measured porosity into velocity through Raymer's relation.

Figure 7-4 below plots the Raymer-line together with the measured velocity and porosity in this test well.

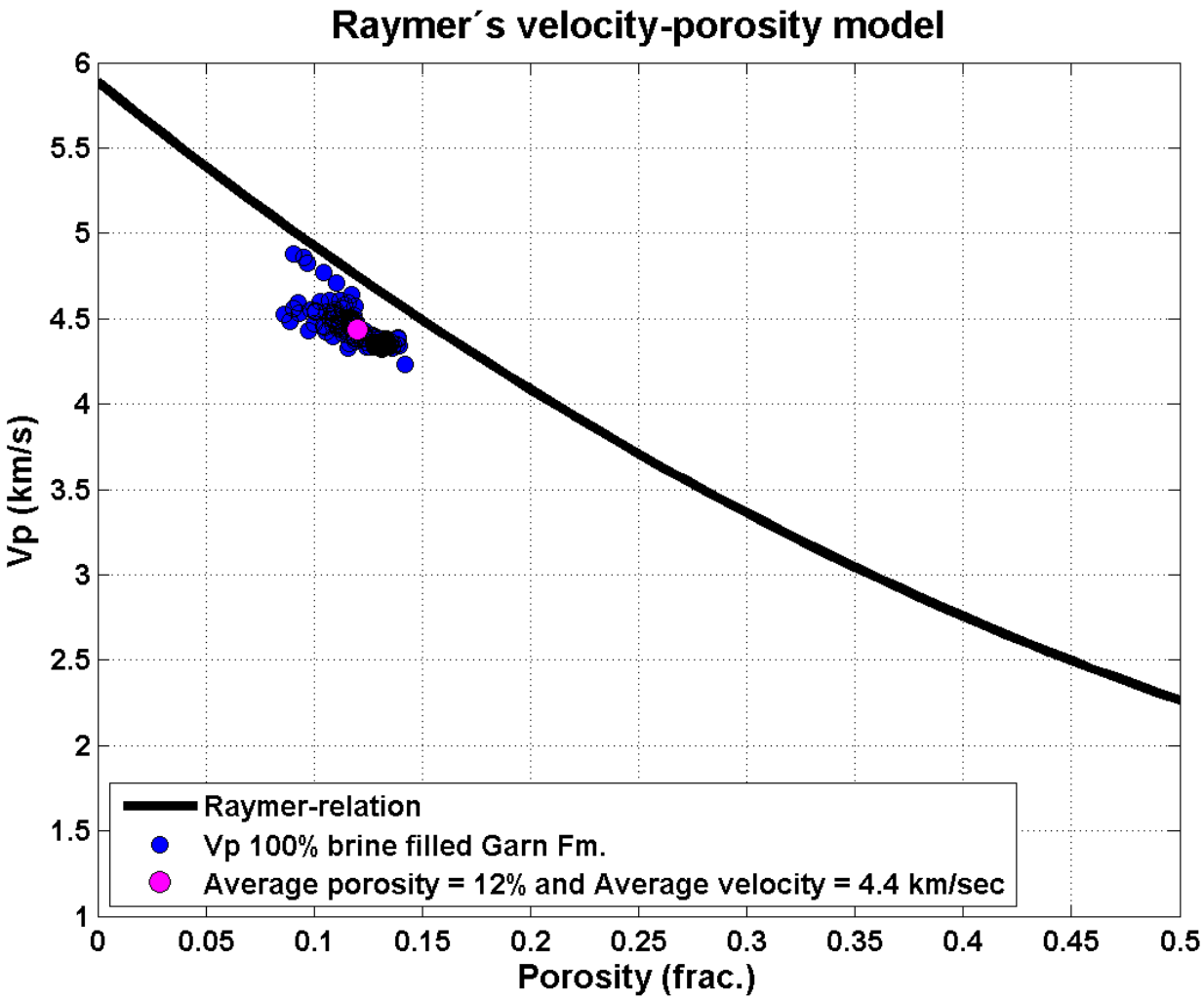

Figure 7-4: Measured porosity versus measured velocity for 100% saturated Garn Fm. in a test well.

Figure 7-5 shows the measured porosity and the resulting Raymer-porosity calculated from the fluid corrected sonic log readings.

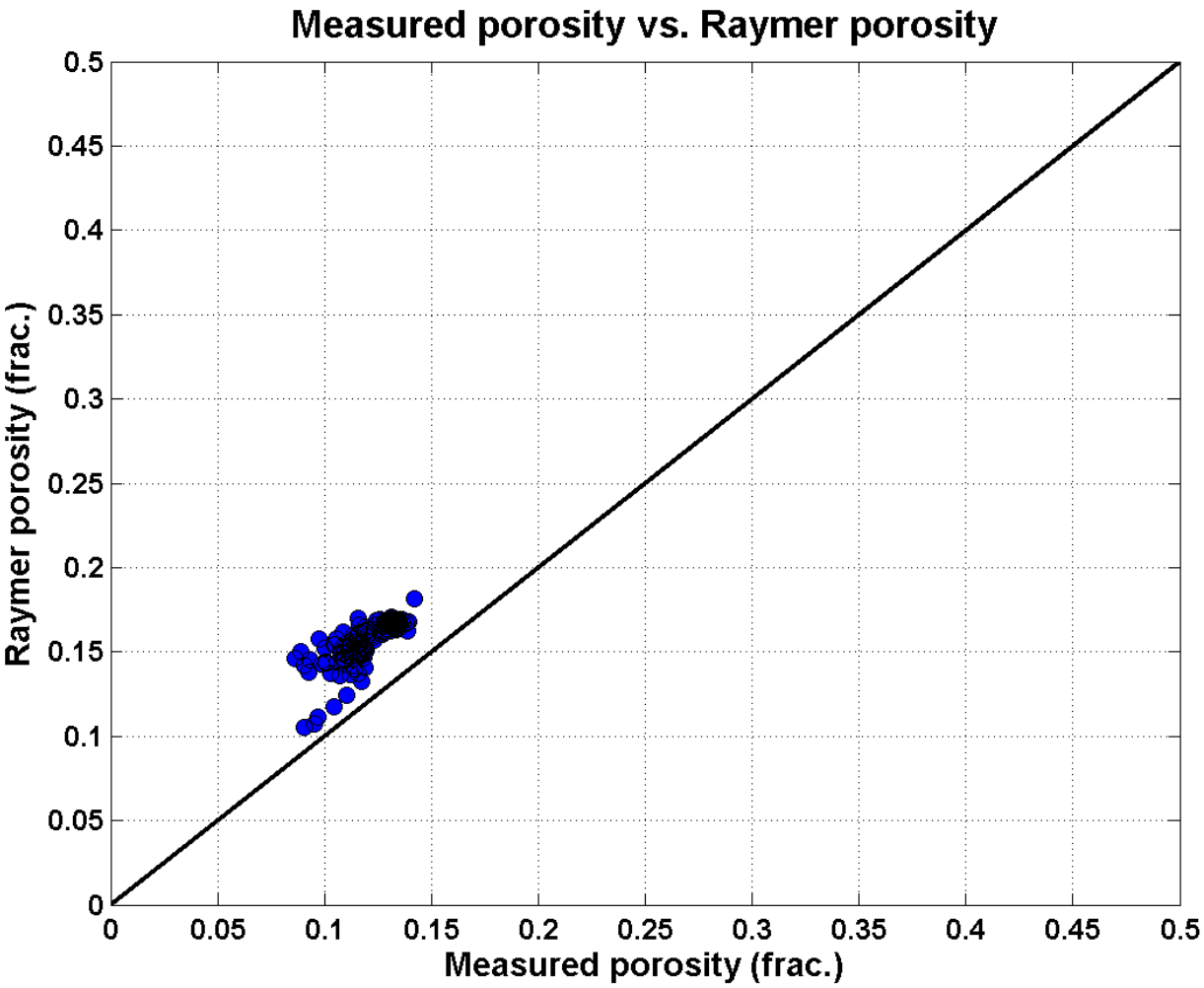

Figure 7-5: Measured porosity versus Raymer-porosity

With the porosity estimated from Raymer's relation, the permeability is calculated by Kozeny-Carman's equation, Equation (29).

The estimated permability in test well 17 is showed in Figure 7-6 below.

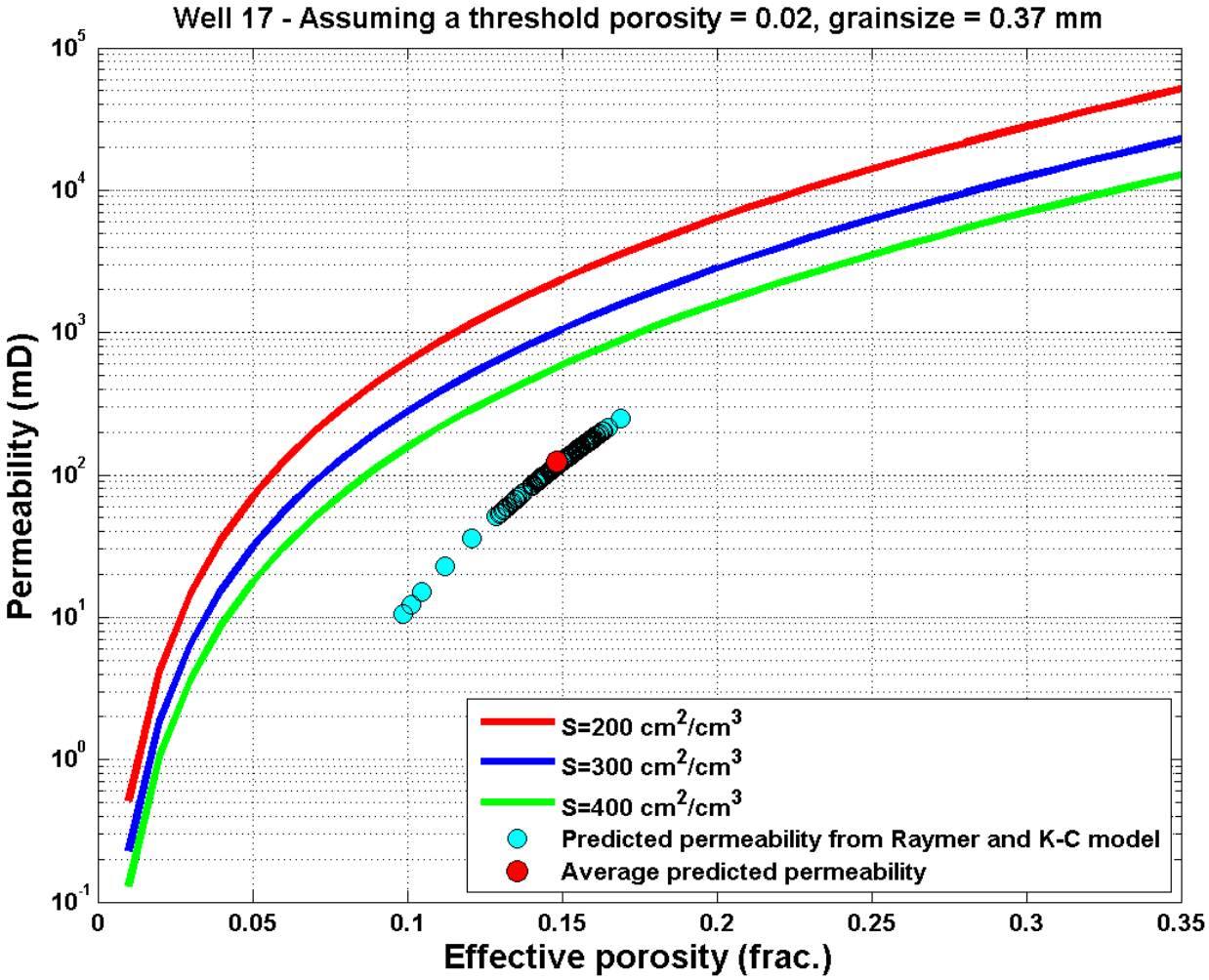

Figure 7-6: Effective porosity obtained from Raymer's relation versus predicted permability in test well 17. The lines represent the specific surface area lines provided by Ehrenberg.

7.3 Permeability Prediction on the Haltenbanken Dataset

The permeability is also estimated on the Haltenbanken dataset. The wells 1-13 (except well 10) have core-calibrated permeability logs available, which is suited for comparison with the modelled permeability. The core-calibrated permeability is considered the closest to measured permeability of the data available in this analysis.

The core calibrated permeability values are obtained from predictive models, such as the Kozeny-Carman model. Well logs are employed to model the permeability by using a suited permeability model (see Appendix C for a review of different porosity-permeability models), and compared to permeability measurements performed on cores in the laboratory. By comparing the modelled and lab-measured permeability, the best-suited model is found, and it

is adjusted to match with the coarsely sampled measured core-permeability. When the empirical model is established, the permeability is calculated by using the well log readings into the model. This is a much more detailed permeability model than the Raymer-Kozeny-Carman model because it is calibrated towards real measured permeability values, and thus referred to as core-calibrated permeability.

Figure 7-7 shows the core calibrated permeability and the modelled permeability from the Raymer-Kozeny-Carman model.

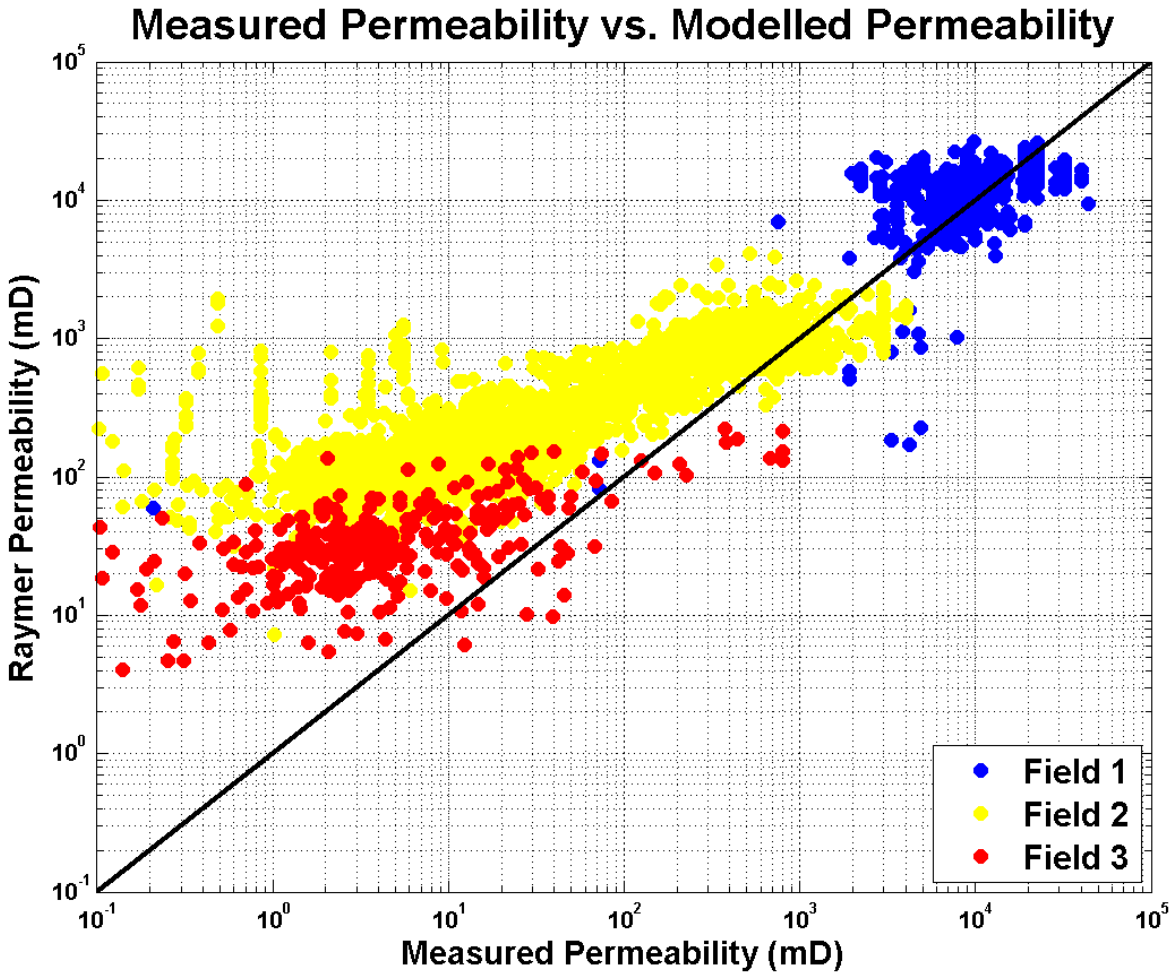

Figure 7-7: Measured permeability versus modelled permeability in the Garn Fm.

7.4 Permeability Prediction from Seismic Velocities

As this method models the permability by transforming a measured acoustic velocity into porosity, and applying this porosity in a permeability-porosity model, it is possible to estimate the permeability from check-shots and seismic velocities. An important task in the analysis is checking whether permability changes are observable by transforming seismic velocities into porosity, and use the modelled porosities in the Kozeny-Carman model.

Seismic velocity profiles are extracted in the locations of well 5 and 6 from the Haltenbanken dataset. These two profiles are calibrated with the focus of removing anisotropy effects in the overburden, causing the Garn velocities to be at the wrong depth when depth migrated . By comparing the original seismic profile with the sonic log it seems that the seismic velocity observes the largest velocity trends given in the sonic log, as seen in the figure below for well 6.

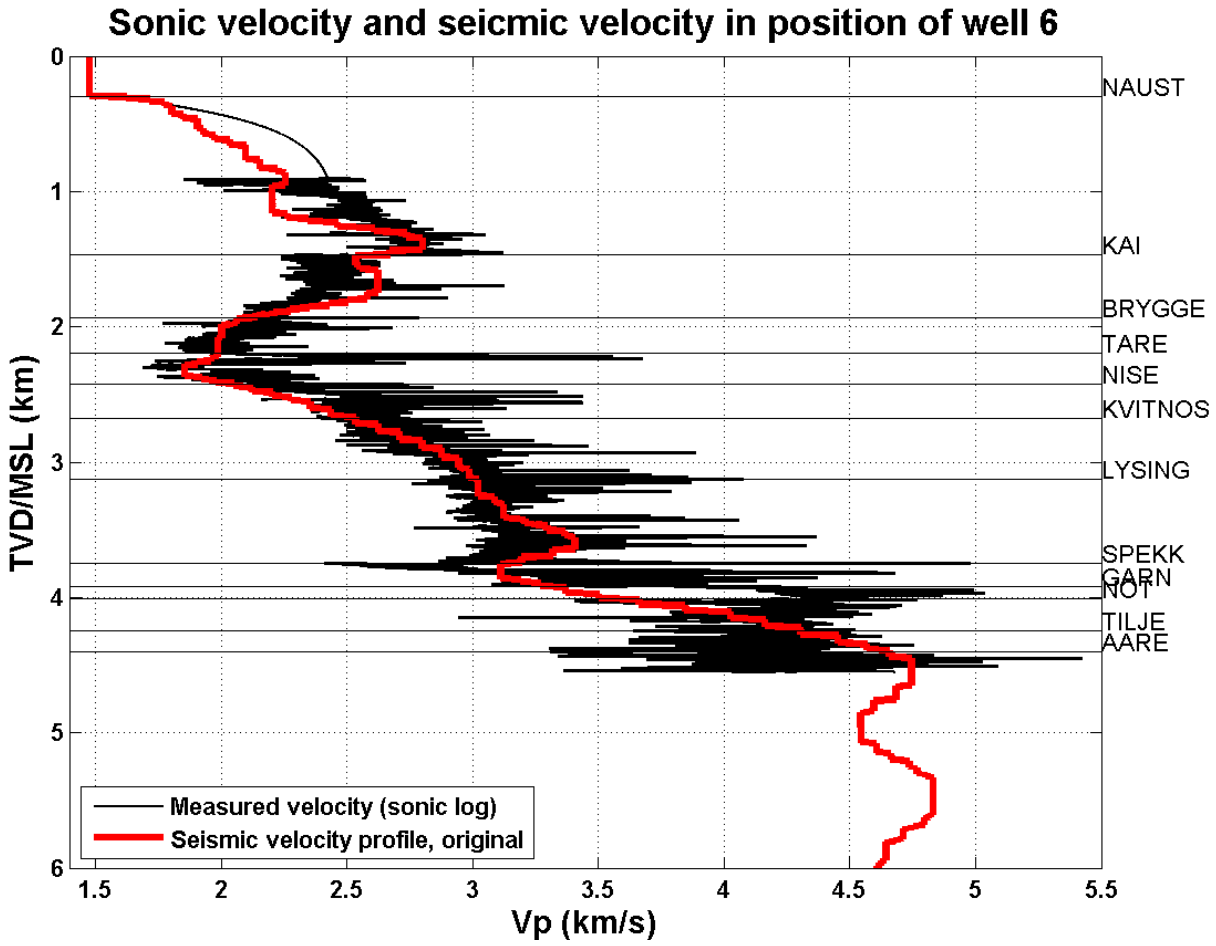

Figure 7-8: Sonic log and seismic velocity profile in the well location of well 6.

However, when investigating the Garn interval closer, it is clear that the seismic velocity differ extensively from the sonic log within the Garn Fm. (but note that the seismic velocity profile and sonic log are not calibrated against each other, so they do not have the same time-depth relationship).

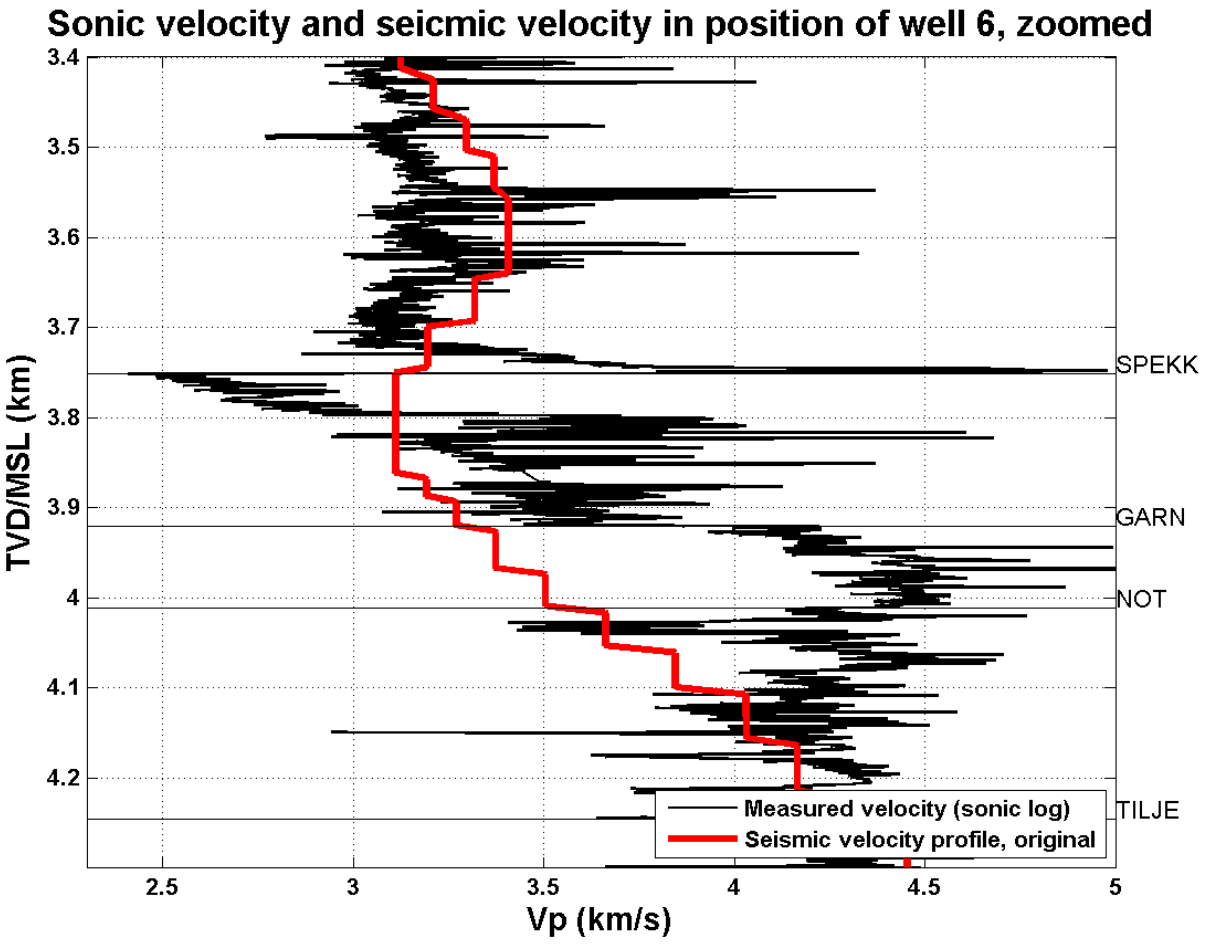

Figure 7-9: Sonic log and seismic velocity profile in the well location of well 6 zoomed in to the Garn interval.

The calibrated interval velocity is obtained by using Equation (31) where the NMO-velocity is the original seismic velocity. Because of the delta factor applied to the velocity in different intervals, the seismic time-depth curve is calibrated to fit better with the check-shot data.

Figure 7-10 and Figure 7-11 show the calibrated time-depth curve in green when a delta factor is applied to the seismic velocities for well 5 and 6 respectively. The red curves are the seismic velocity time-depth curve before the calibration.

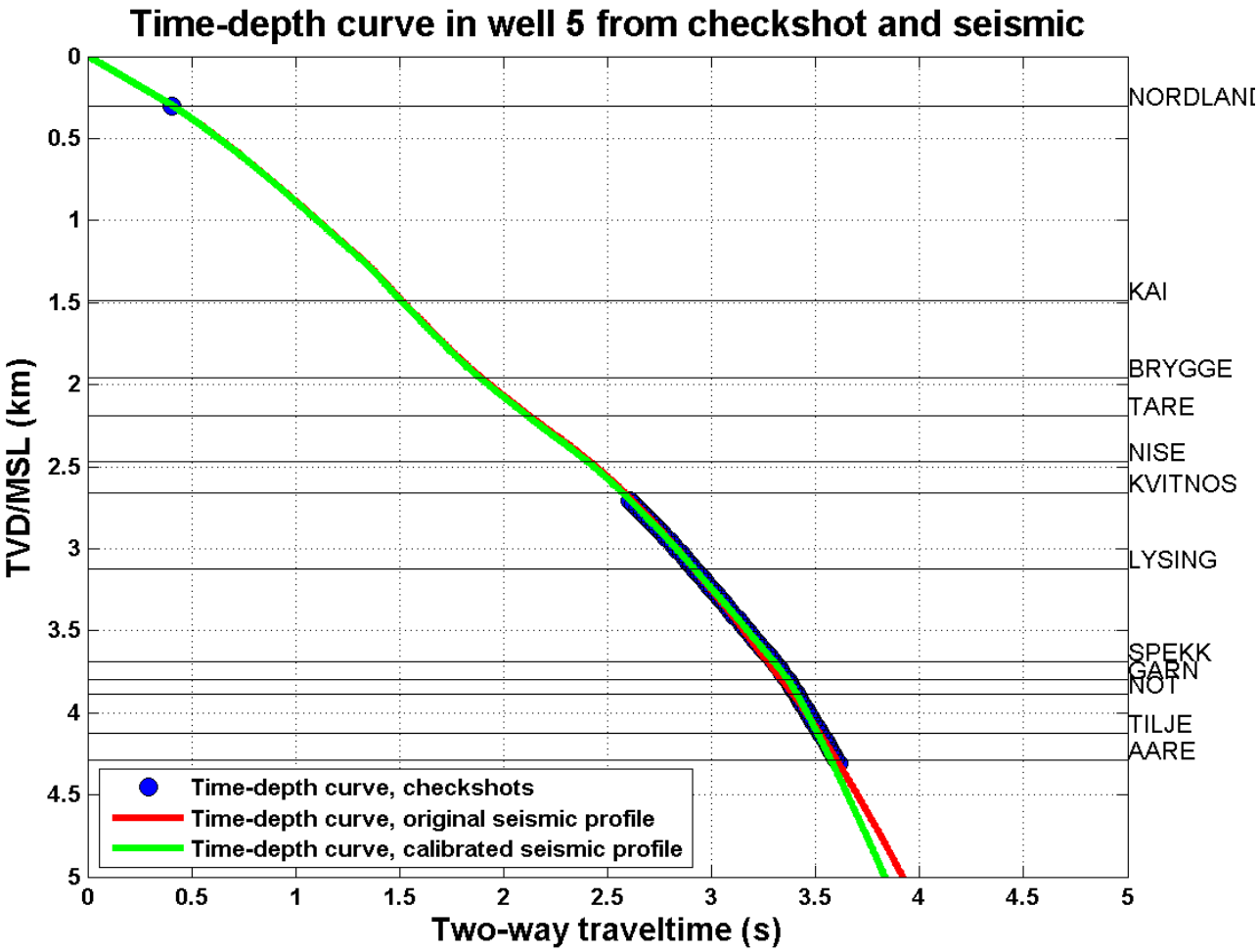

Figure 7-10: Check-shot, calibrated velocity and un-calibrated velocity time-depth curves for well 5.

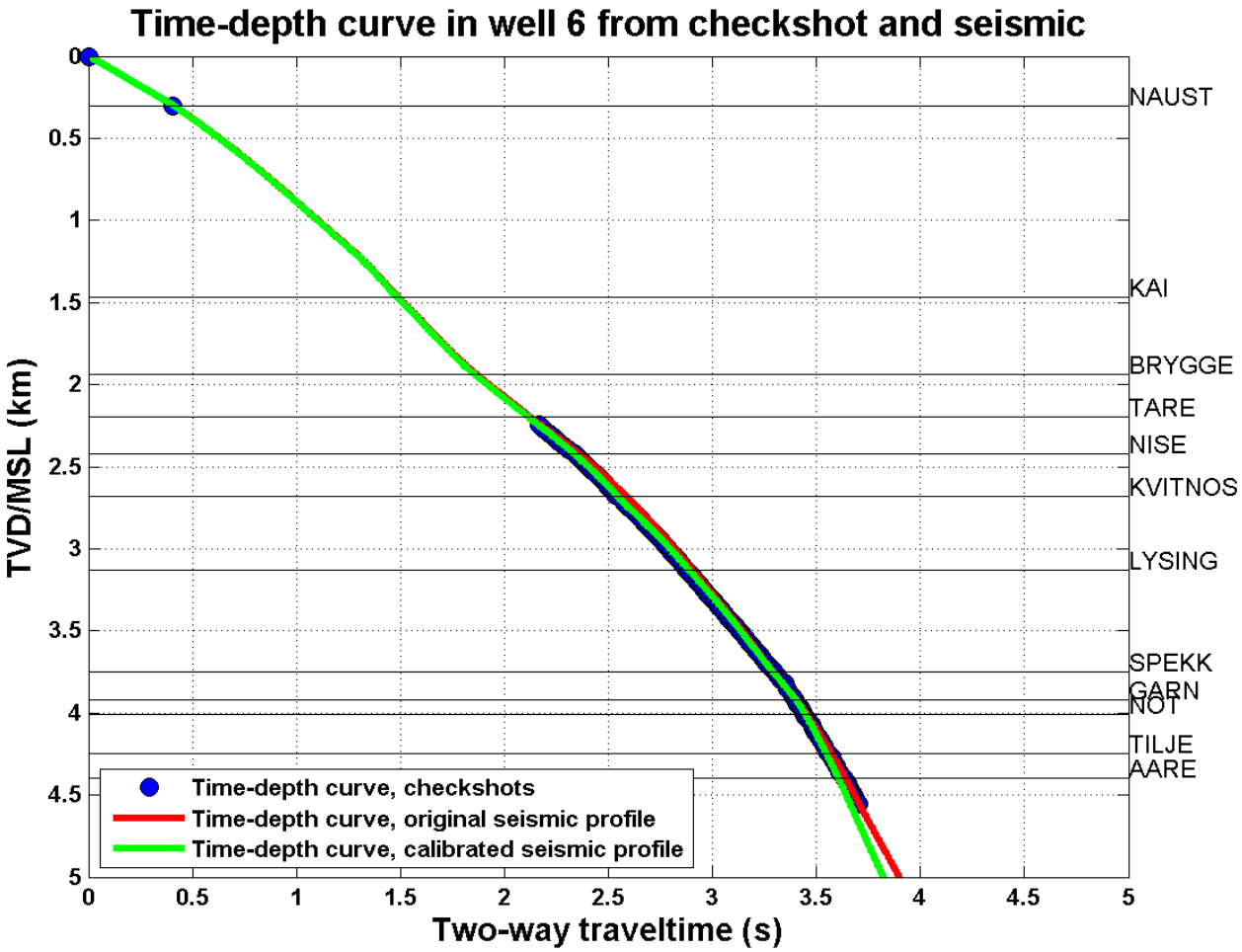

Figure 7-11: Check-shot, calibrated velocity and un-calibrated velocity time-depth curves for well 6.

The green and red curves in the figures above seem not to differ very much. However, by zooming closer to the Garn zone it becomes very clear that the time-depth curve is modified quite extensively within this interval to match better with the check-shot data. Figure 7-12 and Figure 7-13 compare the calibrated seismic and the un-calibrated seismic time-depth curves against check-shot data in the Garn Fm. for these two wells.

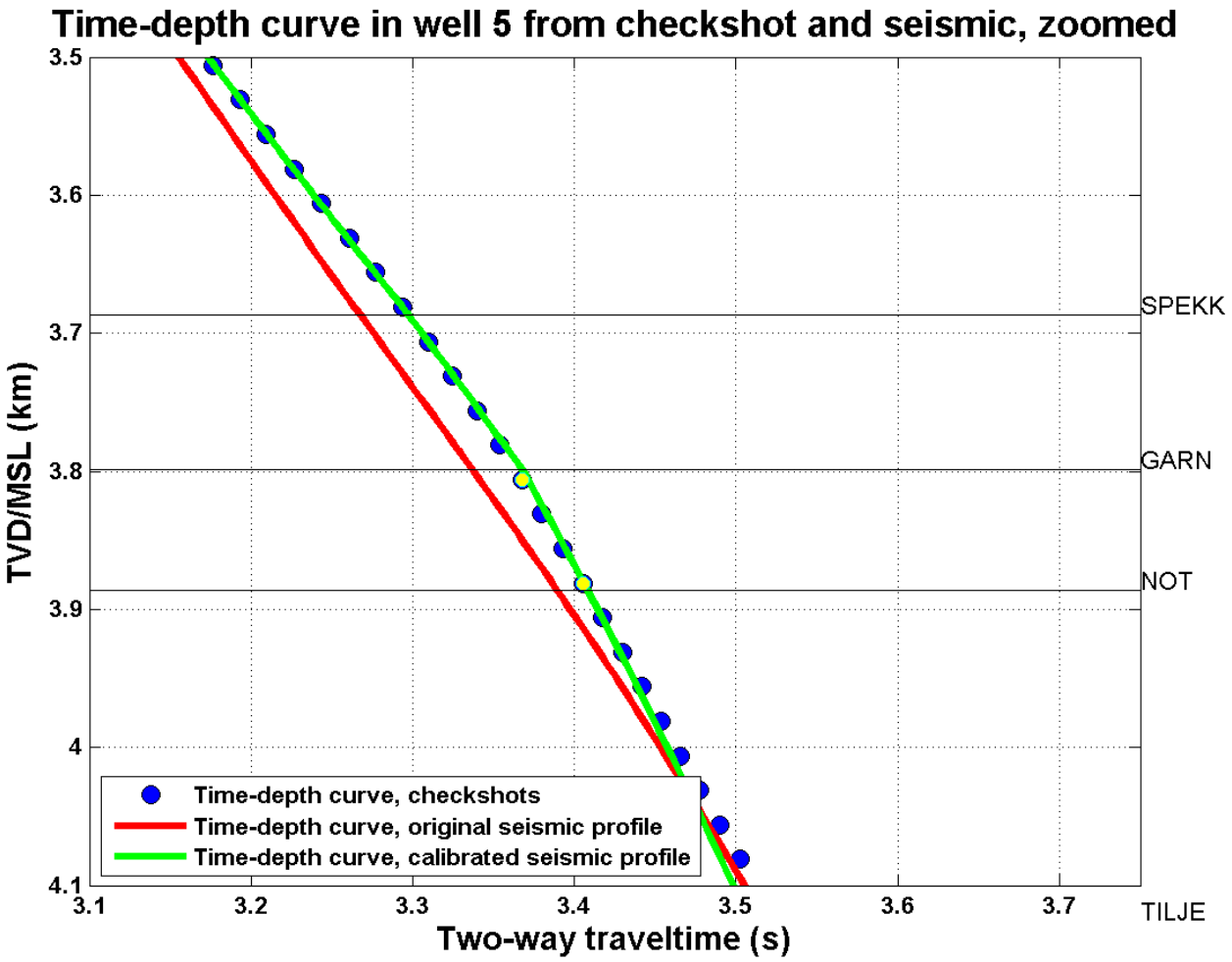

Figure 7-12: Check-shot, calibrated velocity and un-calibrated velocity time-depth curves zoomed in for well 5.

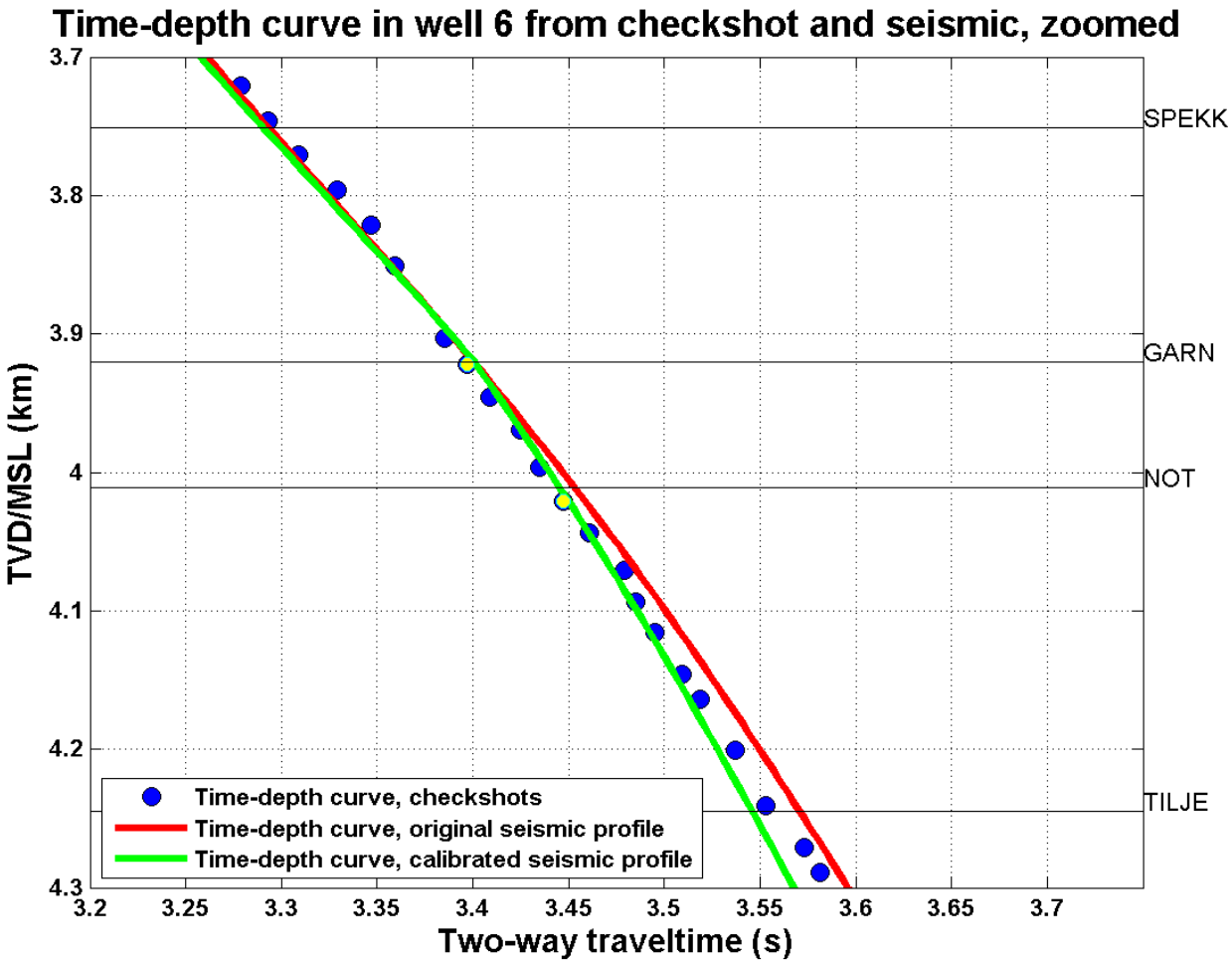

Figure 7-13: Check-shot, calibrated velocity and un-calibrated velocity time-depth curves zoomed in for well 6.

The yellow points highlighted in Figure 7-12 and Figure 7-13 show the check-shot points at top and bottom (approximately) of the Garn Fm. These points are used to calculate the average interval velocity in the Garn Fm. in both wells from the simple equation

$$v_{int} = \frac{\Delta z}{\Delta t/2} \qquad (35)$$

Where Δz is the thickness of the Garn Fm. and Δt is the two-way-travel time for the wave to pass through the Garn interval, and thus needs to be divided by 2 in the equation. The average interval velocity within Garn at these two well locations from checks-shots, are given in the table below.

Table 7-2: Average interval velocity in Garn from check-shot data at top and bottom of Garn.

	Well 5	Well 6
Average interval velocity form check-shot data	4 km/s	3.96 km/s

Figure 7-14 and Figure 7-15 show the delta factor applied to the original seismic velocity profile and the resulting seismic velocity profile after the calibration for well 5 and 6 respectively.

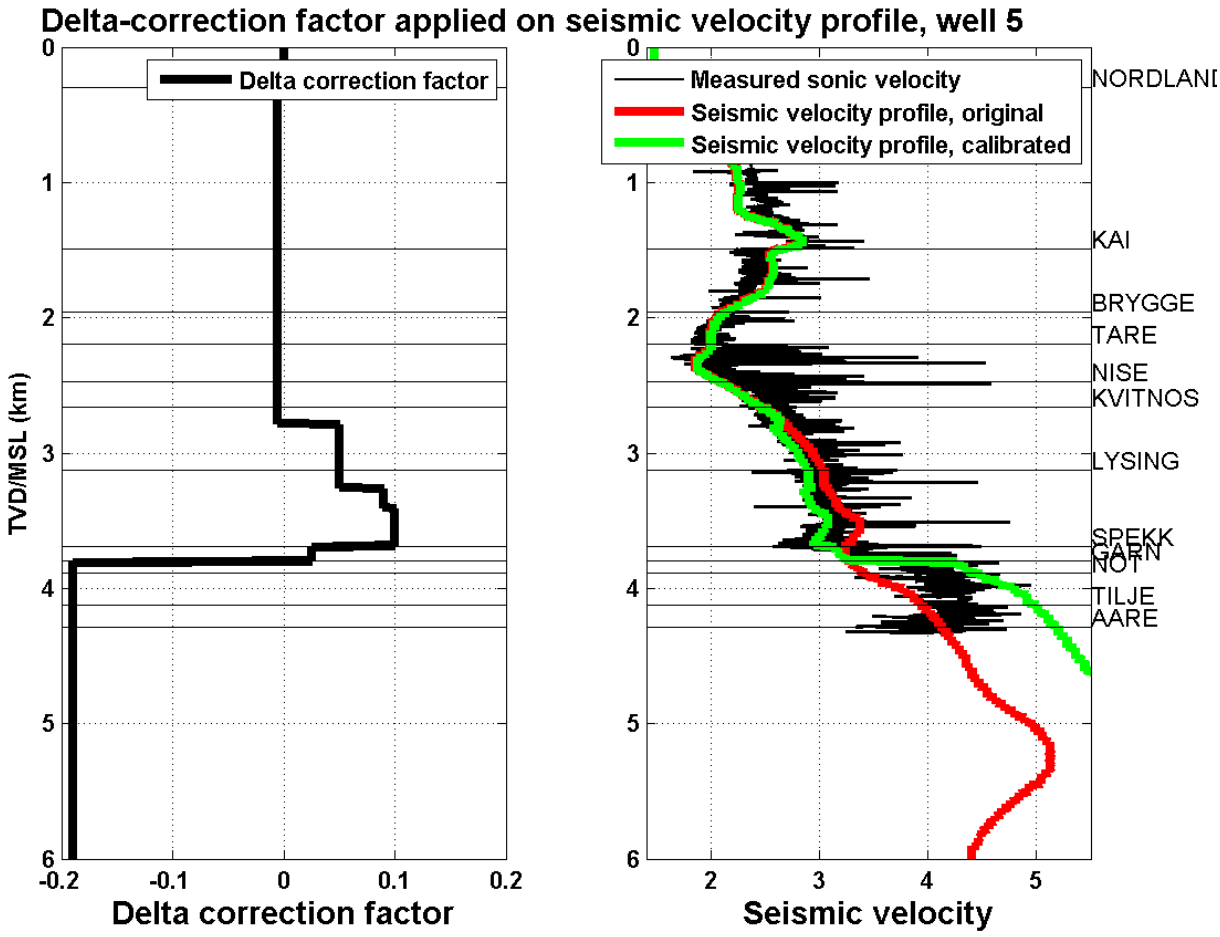

Figure 7-14: The delta correction factor in the left pane is applied to the seismic profile in well 5, seen in red in the right pane. The right pane shows the sonic log, the original seismic velocity profile and the calibrated seismic profile resulting from applying the delta factor to the red curve.

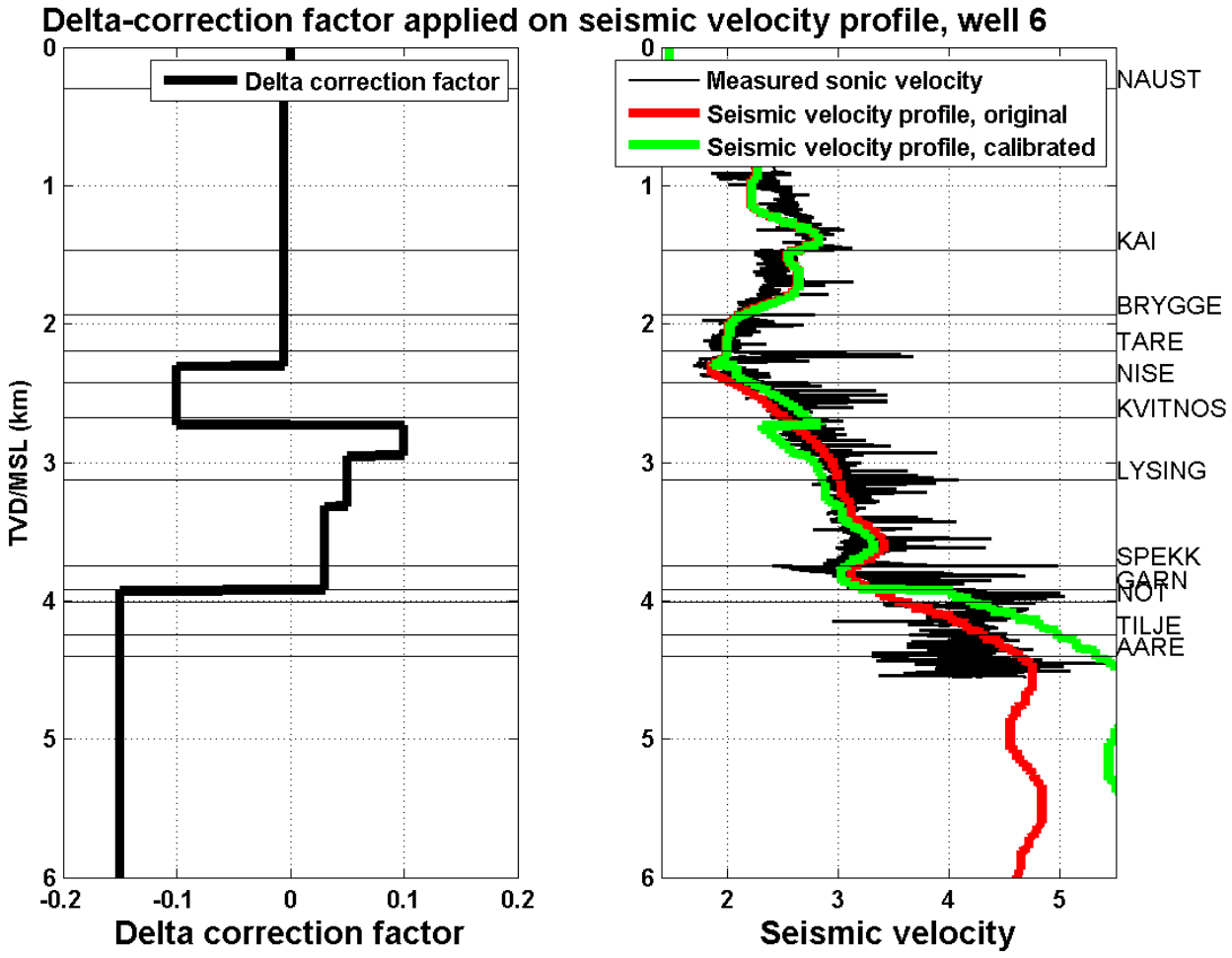

Figure 7-15: The delta correction factor in the left pane is applied to the seismic profile in well 6, seen in red in the right pane. The right pane shows the sonic log, the original seismic velocity profile and the calibrated seismic profile resulting from applying the delta factor to the red curve.

The delta factor is found by testing different values and see how the seismic time-depth curve fit with the check-shots. Note that a positive delta factor decrease the velocity and squeeze the velocity profile. This leads to higher velocities in Garn.

The permeability estimation from the calibrated seismic velocities are done by transforming the velocity curve into porosity by Raymer's model. The calibrated seismic velocity is believed to be more representable for the Garn-velocities than the uncalibrated seismic velocity, given by the red curve because this is much affected by anisotropy in the overburden and thus depth migrated erroneously. The calibrated velocities in well 5 and 6 are adjusted so that the anisotropy effects are reduced.

The result of the permeability estimation by using porosity estimated from un-calibrated seismic velocity, calibrated seismic velocity and check-shot interval velocity respectively are seen in Figure 7-16 and Figure 7-17 for well 5 and 6 respectively. The permeability estimated from sonic velocity derived porosity and the core-calibrated permeability is also included in the figures.

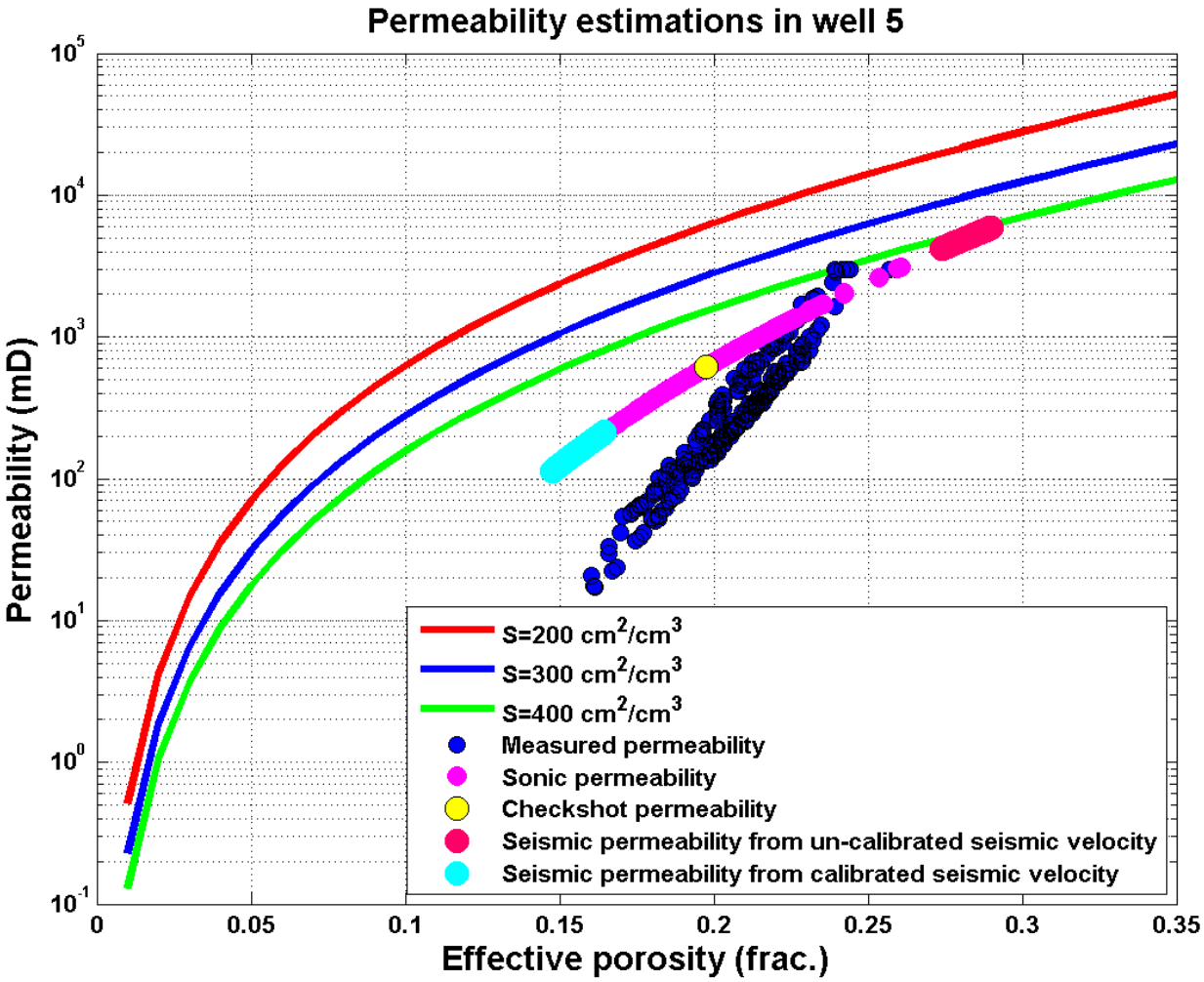

Figure 7-16: Estimated permeability in well 5 from porosity estimations from various acoustic velocities by Raymer's model. The red, blue and green curves are the specific surface area which Ehrenberg estimated the Garn permeability to be inside.

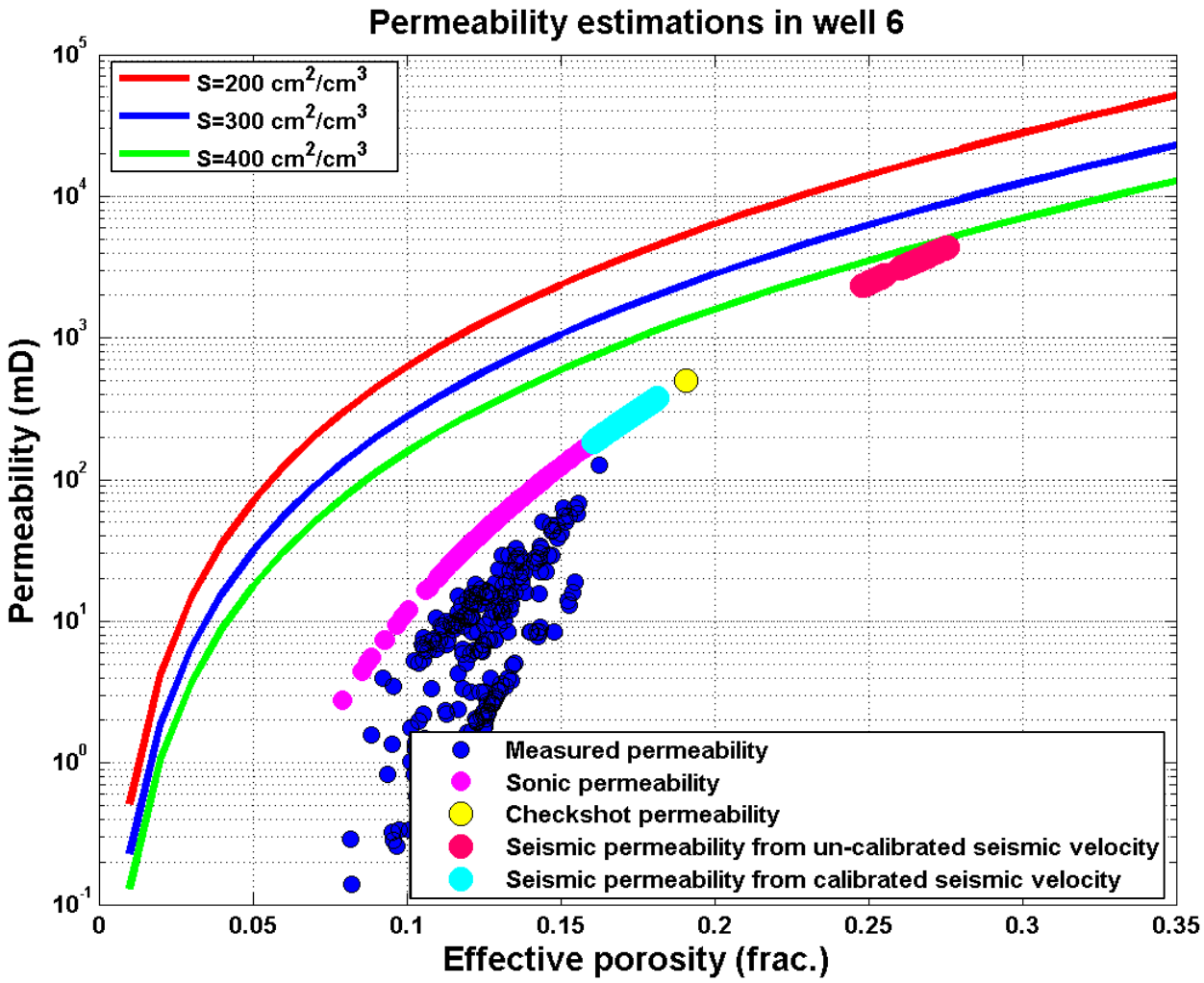

Figure 7-17: Estimated permeability in well 6 from porosity estimations from various acoustic velocities by Raymer's model. The red, blue and green curves are the specific surface area which Ehrenberg estimated the Garn permeability to be inside.

The permability is modelled from porosities derived from sonic velocity, check-shot velocity and seismic velocity (calibrated and un-calibrated). In Figure 7-18 and Figure 7-19 these permeabilities are plotted as logs for comparison within Garn for well 5 and 6 respectively, together with the core-calibrated permeability.

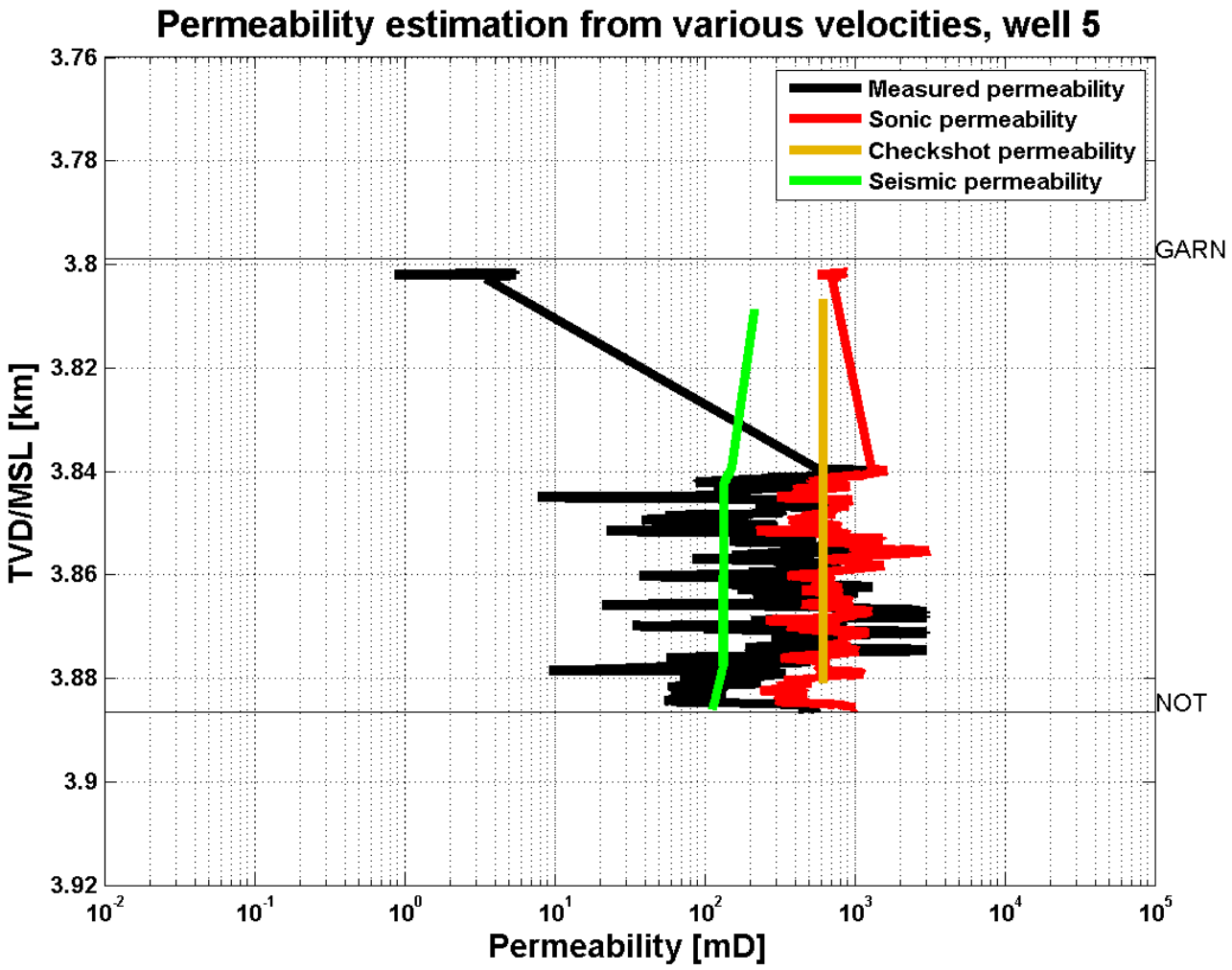

Figure 7-18: Comparison of the modelled permeability from various sources of acoustic velocity in the Garn Fm. in well 5, together with the core-calibrated permeability.

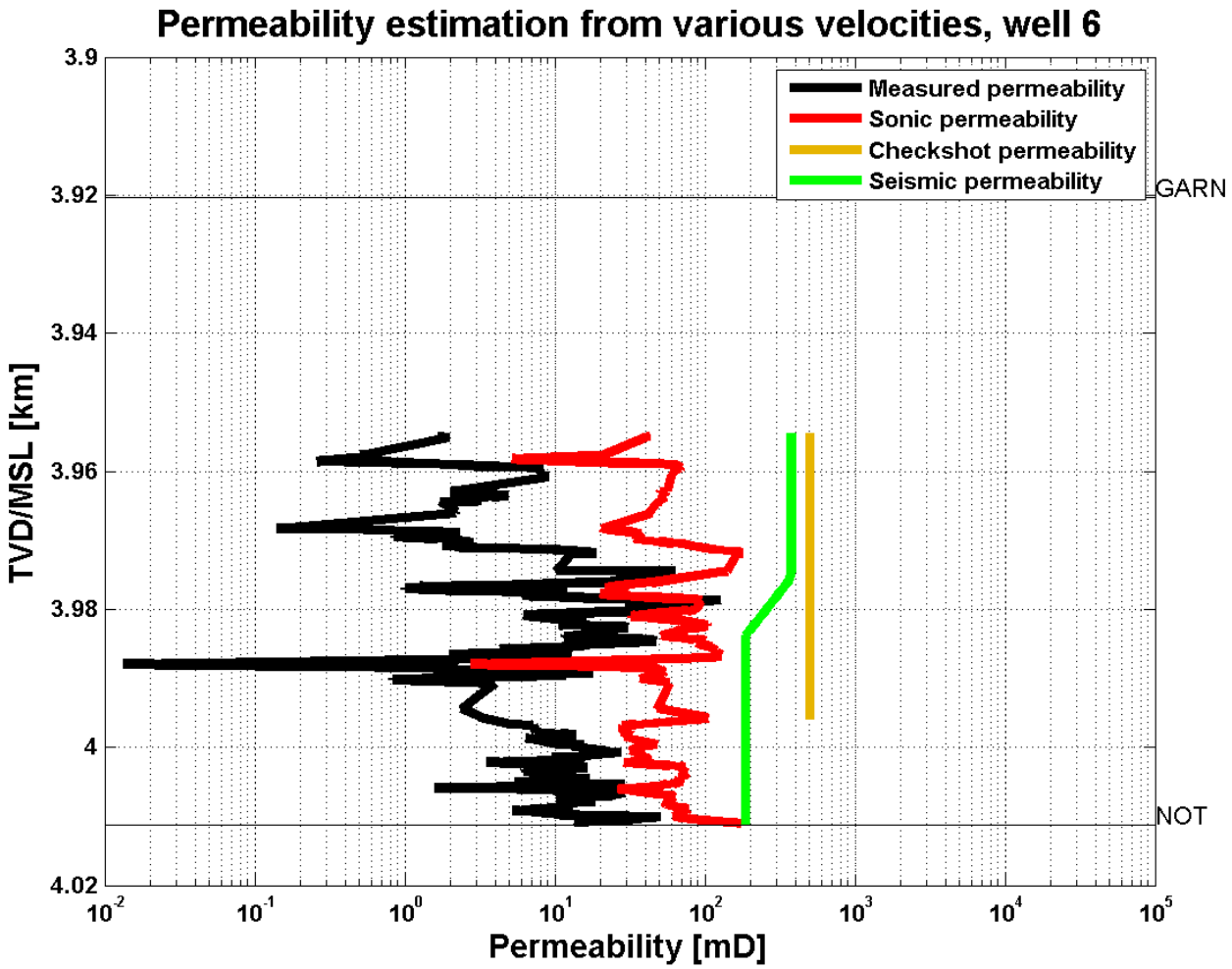

Figure 7-19: Comparison of the modelled permeability from various sources of acoustic velocity in the Garn Fm. in well 6, together with the core-calibrated permeability.

7.5 Permeability Estimation along the Interpretation of the Garn Fm.

The permeability is modelled along the time-interpretation of the Garn Fm. across 2D seismic lines. Three seismic lines are available, but only the permeability along Line 3 is showed in this section.

Figure 7-20 shows the reflectivity seismic section for Line 3 in two-way-travel time together with the well locations of well 5 and 6 and the Garn interpretation.

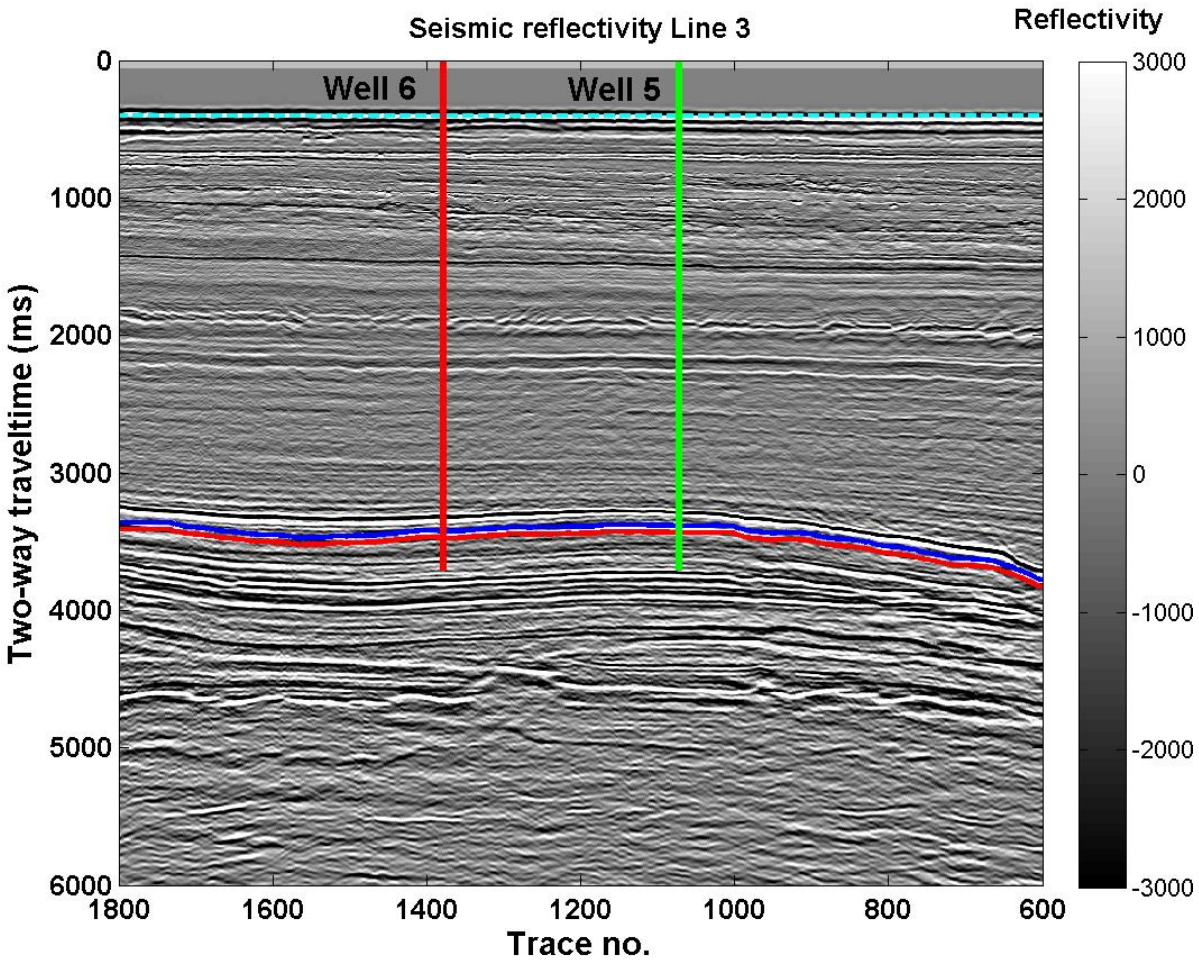

Figure 7-20: Reflectivity seismic along Line 3 in time, together with the well location of well 5 and 6 and the Garn interpretation.

To model the permeability along the Garn horizon by the Raymer-Kozeny-Carman model, the seismic velocities needs to be exported out of the velocity model, and transformed to porosity by Raymer's model.

Figure 7-21 show the velocity model for the whole seismic section along Line 3 in two-way-travel time with the Garn interpretation and the well locations of well 5 and 6.

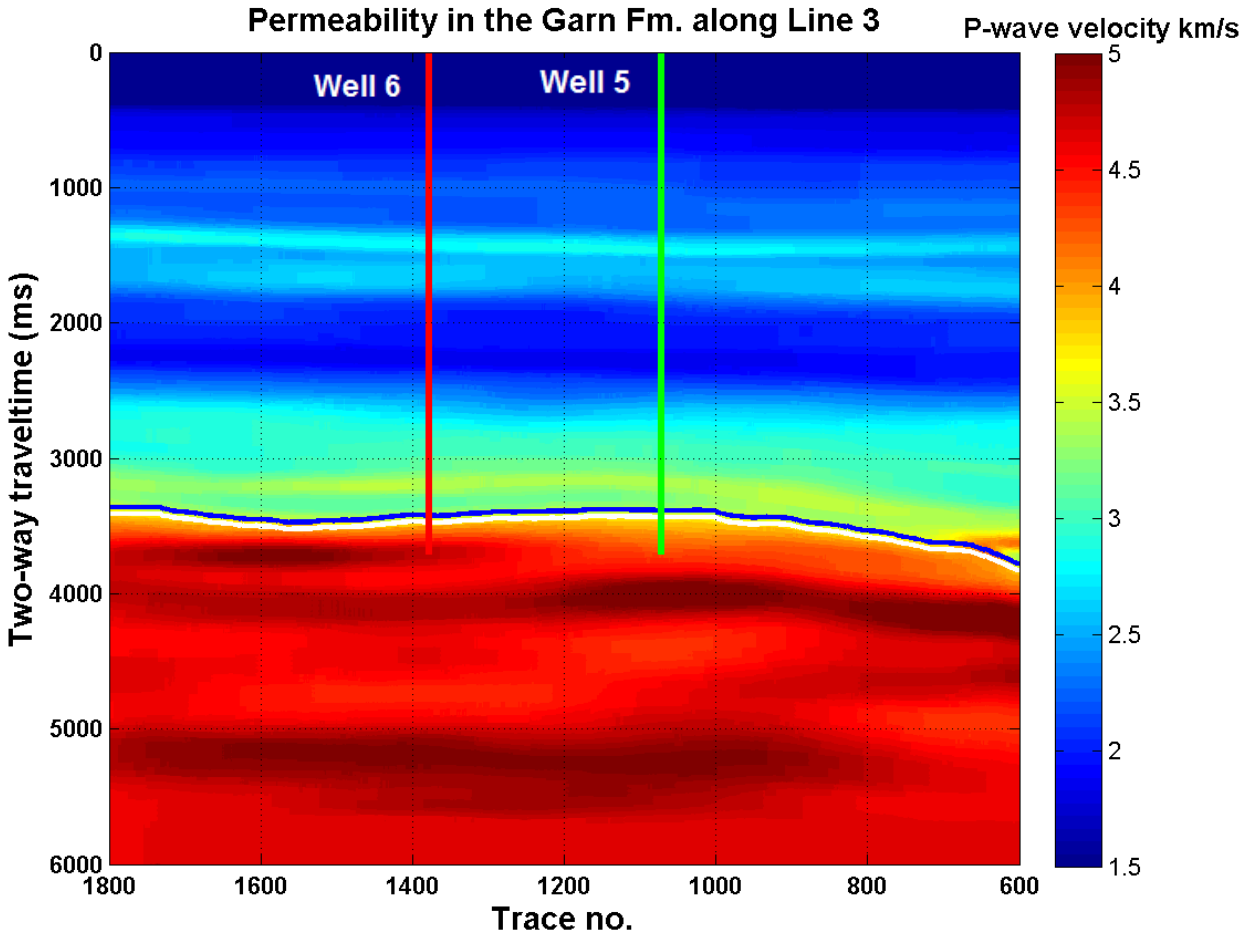

Figure 7-21: Velocity model for Line 3, together with the well location of well 5 and 6 and the Garn interpretation.

The extracted average velocity is showed in Figure 7-22.

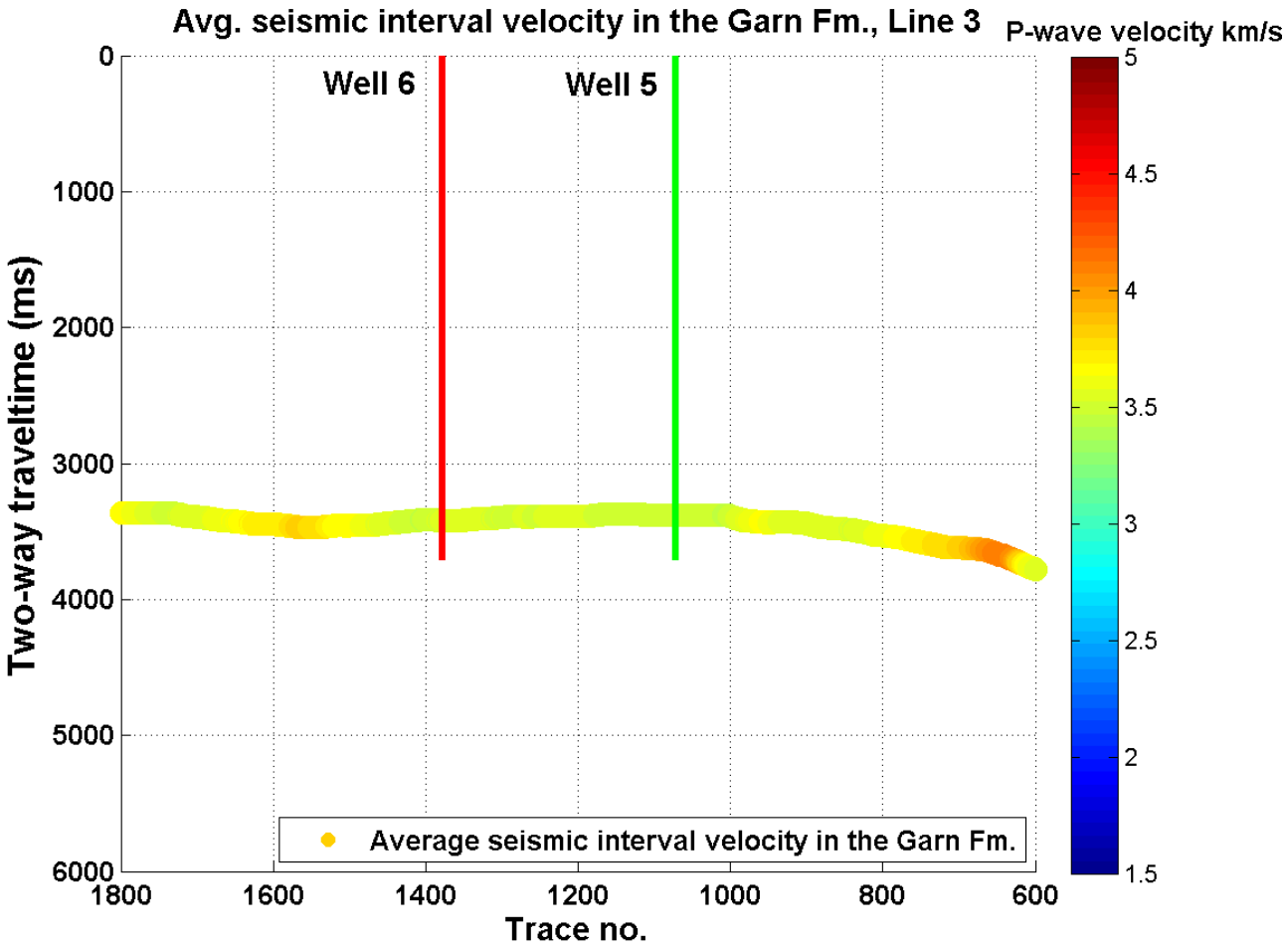

Figure 7-22: Extracted P-wave velocity from the velocity model along the Garn interpretation in two-way-travel time.

The extracted velocity is used to model porosity from Raymer's model. Figure 7-23 shows the modelled porosity.

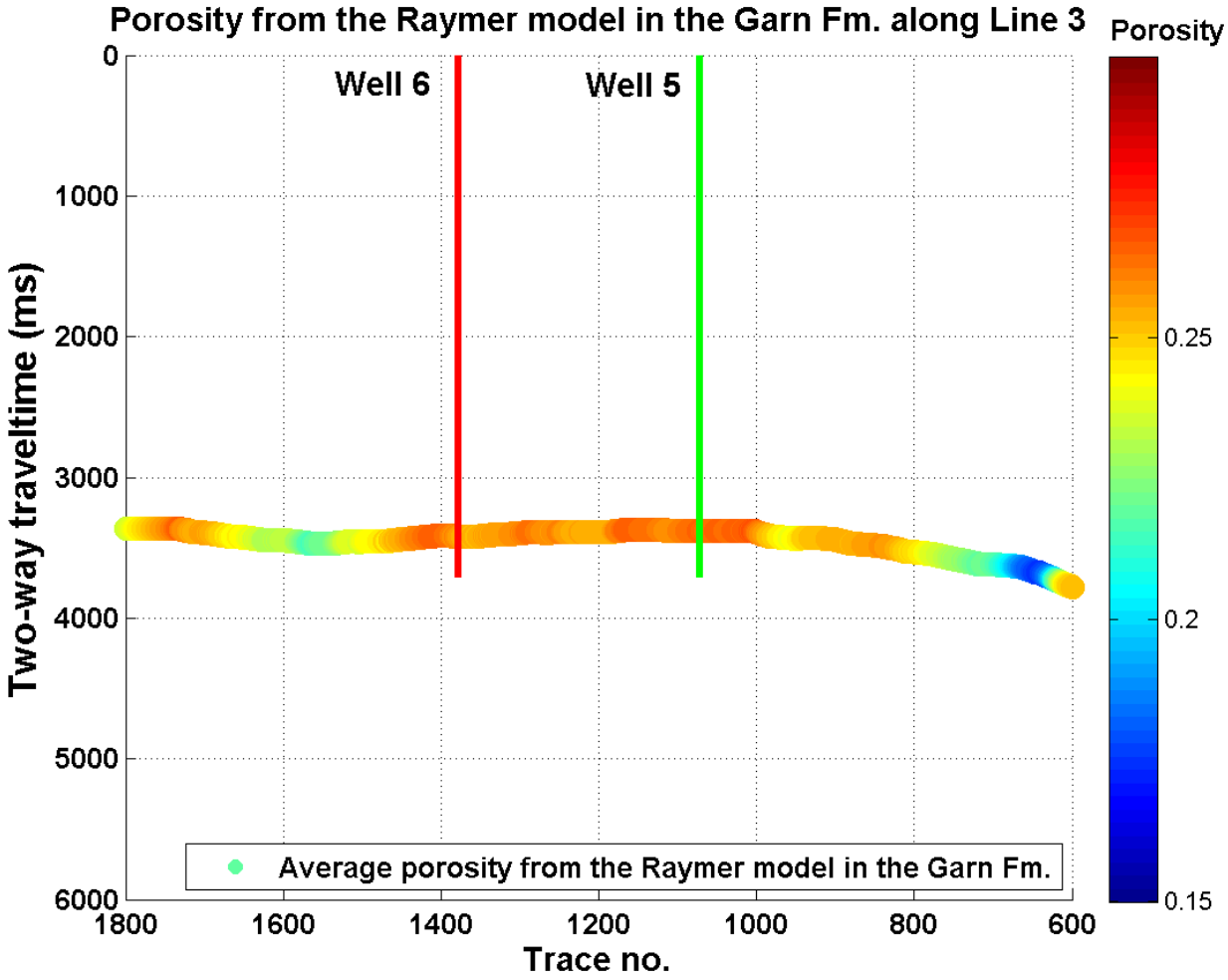

Figure 7-23: Porosity modelled along the Garn interpretation in time by transforming extracted seismic velocities from the velocity model into porosity by Raymer's model.

The estimated porosity is used in the Kozeny-Carman model for permeability modelling along the Garn interpretation. Figure 7-24 shows the resulting modelled permeability along the Garn interpretation in two-way-travel time.

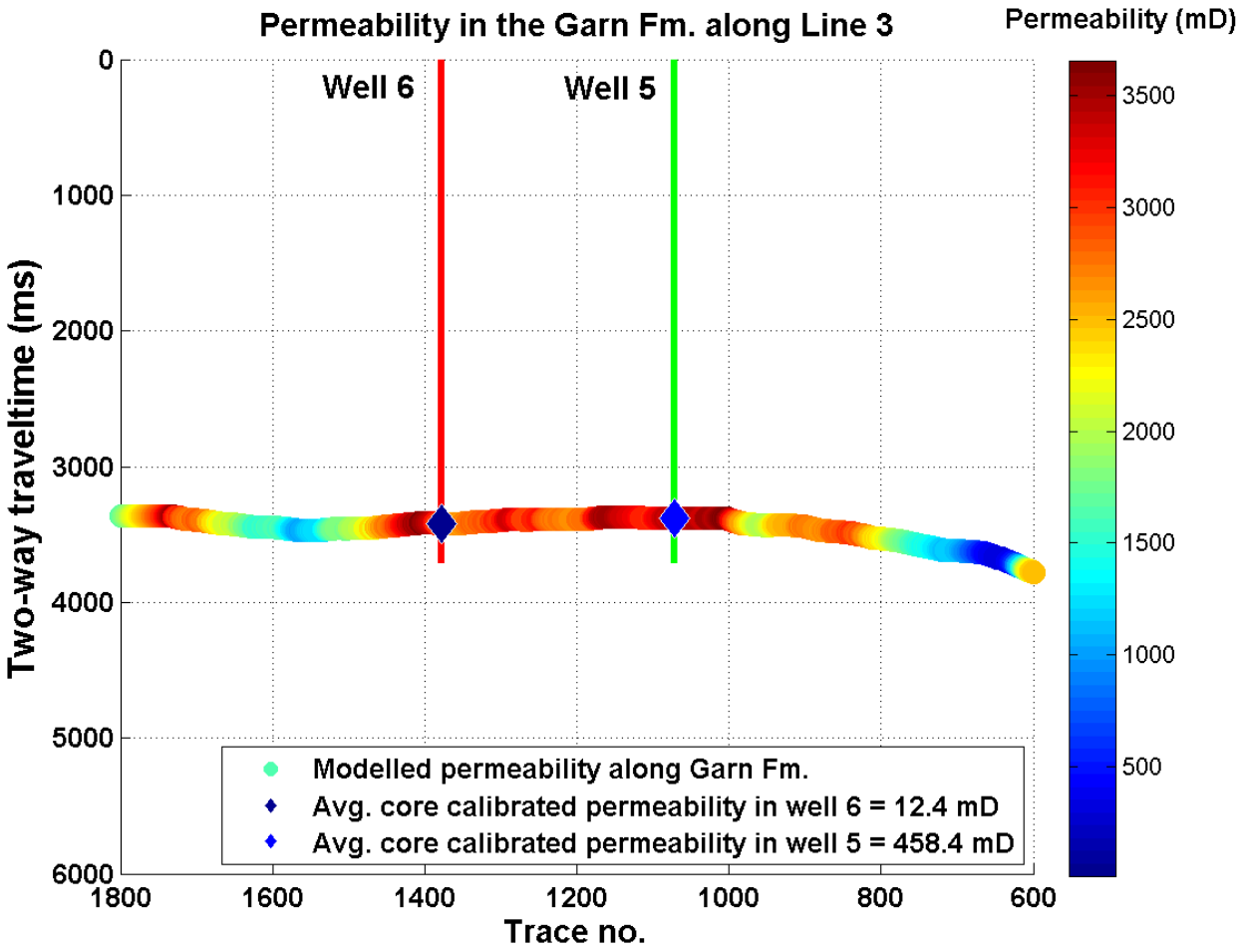

Figure 7-24: The modelled permeability from the Raymer-Kozeny-Carman model along the time-interpretation of the Garn Fm.

The reflectivity seismic and velocity models for Line 1 and Line 2 can be seen in in Appendix D, together with the figures for Line 1 and Line 2 corresponding to Figure 7-22-Figure 7-24.

8 Discussion

8.1 Review of the Permeability Estimation Method

Two important factors determine how well this method for permeability prediction are:

1. How accurate is the porosity obtained from Raymer's model?
2. How good is the Kozeny-Carman model for permeability estimation from measurable rock properties?

8.1.1 Raymer's Relationship

Expressions that relate velocity to porosity and pore fluid are important deliverables within rock physics, and so several expressions exist for this matter. The oldest and maybe most popular expression is the Wyllie time average, given in Equation (21). This equation is simple and convenient, but the experimental data is summarized in a deceptive way, since it is no physical reason for the total travel time to be the sum of the travel times in the individual components.

Dvorkin et al. (1998) discuss if it is necessary to abandon such non-physical time-average equations or equally simple traditional empirical relations, such as Raymer's relation in favour of rigorous physics oriented models. These take the internal structure of the rock into account. In his analysis, Dvorkin et al. tested traditional velocity-porosity models on three sandstone datasets. The results showed that the Raymer velocity-porosity relation are reliable for consolidated and cemented sandstones in the porosity interval from zero to 35%. The Wyllie time average is less accurate. These results are showed in the figure below.

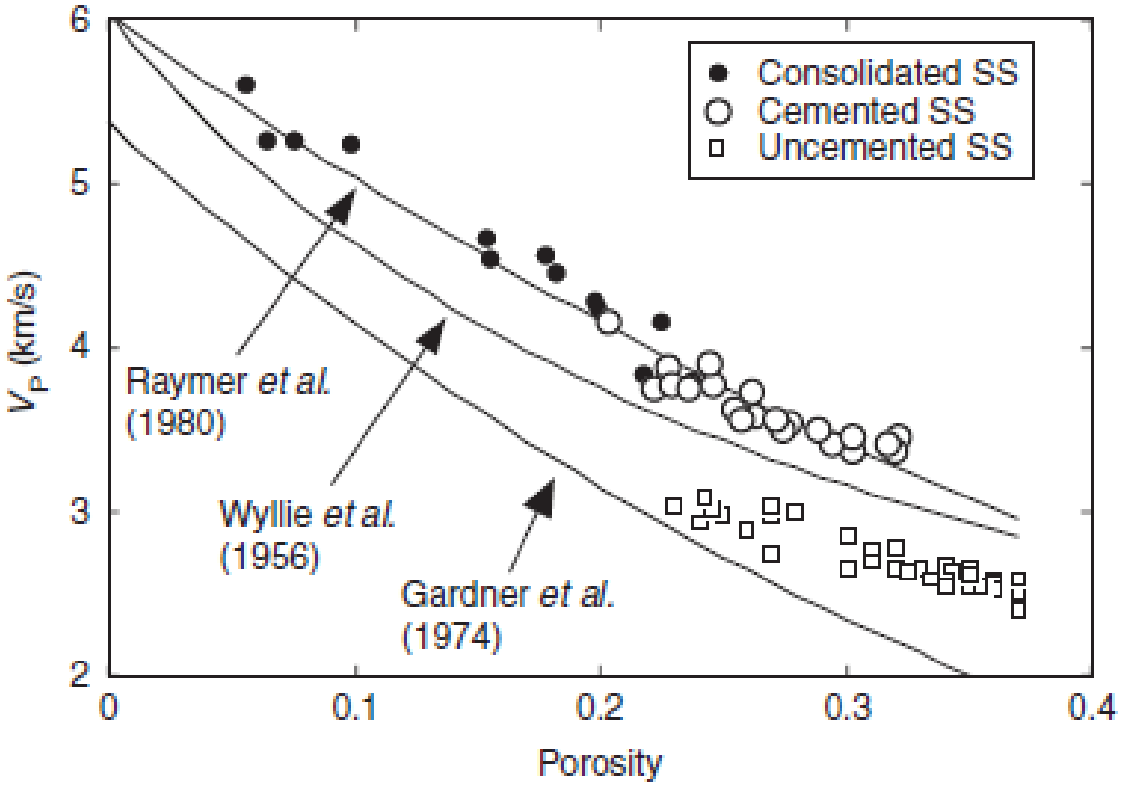

Figure 8-1: Various velocity-porosity relations plotted for three different types of sandstone. (Mavko et al., 2009)

Based on these results, Raymer's relation is a good model for porosity estimation in the Garn Fm., as it is a sandstone with the preferred characterises (cemented and consolidated). As mentioned earlier, the Raymer model is based on assumptions and have limitations. For example, the rock is assumed isotropic. The Garn Fm. contains mud and clay, so this assumption is not completely fulfilled. However, it can be argued that the Garn Fm. can be considered close to isotropic since a clay-content restriction is applied to the formation.

The well data from the Haltenbanken dataset verifies that the measured velocity and porosity follows the Raymer trend quite well, especially when only the clean parts of the Garn Fm. are plotted. However, there is still quite extensive scattering around the Raymer line even though the volumetric clay content cut-off is set to 10%. It might be that this clay-content cut-off is not sufficiently low and that it should rather be set to, say 2%.

Figure 8-2 show the dataset containing sands with a volumetric clay content of less than 2%. The Garn points follow the Raymer line quite well, but the porosity range only to approximately 25%, which is not ideal for this analysis, as it is better to verify the Raymer relation for a large porosity range.

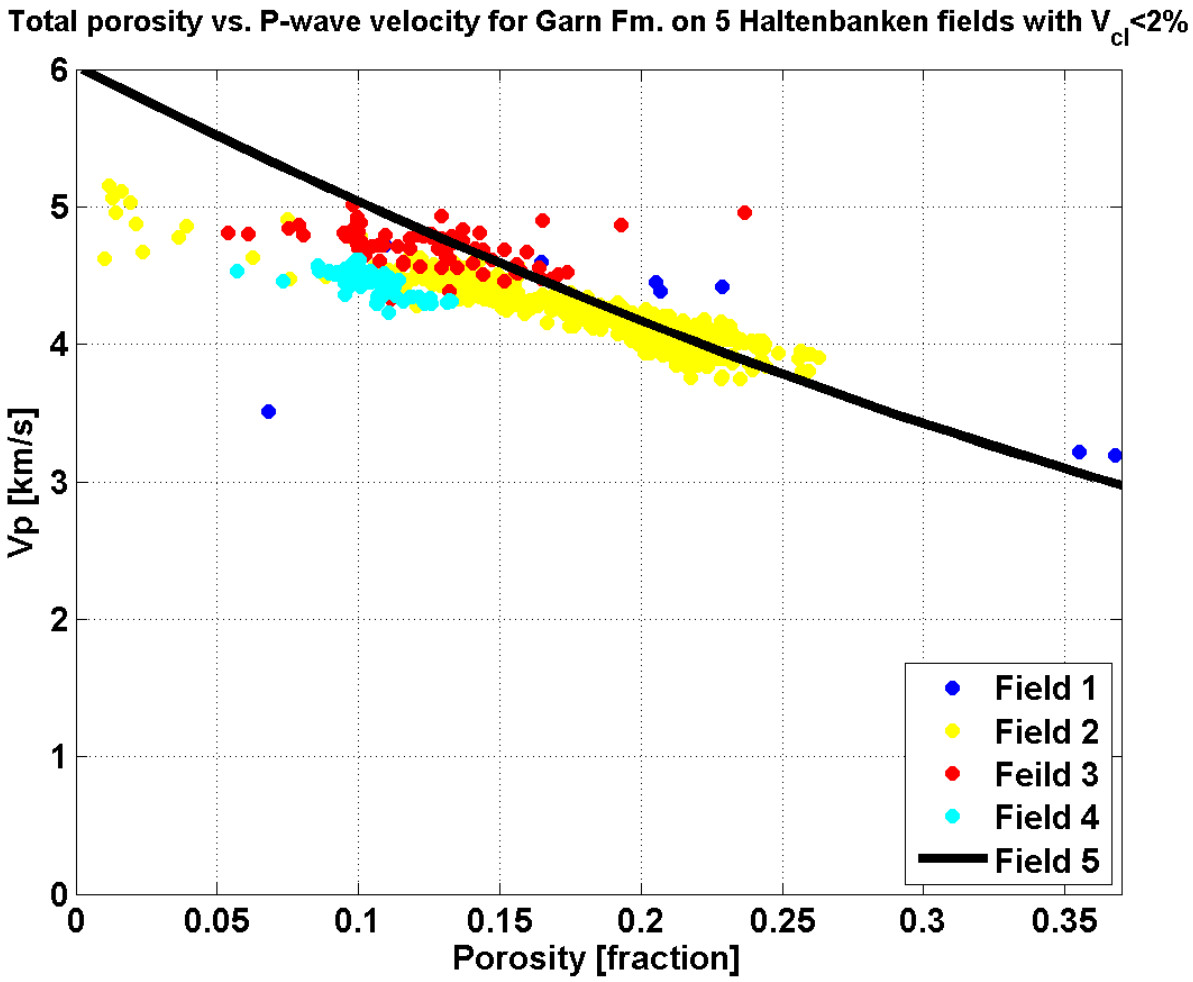

Figure 8-2: Raymer's relation for Garn sand containing less than 2% clay.

Though the velocity-porosity points in the Garn Fm. at Haltenbanken show good correspondence with the Raymer-line, it is still some scattering around the Raymer-curve, even when the clay-content cut-off is as low as 2%.

The scattered points tend to plot more below than above the Raymer-line, and this trend increase when the porosity decrease. This leads to an increasing over-prediction of porosity as porosity decrease. The percolation threshold porosity focuses to decrease this effect.

The estimated porosity from Raymer's relation depends not only on the measured acoustic velocity, but also on the matrix and fluid velocity. The resulting change in estimated porosity because of change in these parameters are discussed in Chapter 8.2.1

8.1.2 The Kozeny-Carman Relation

Dvorkin (2009) points at two inconsistencies or problems in the Kozeny-Carman equation when the grainsize is kept constant.

First, the Kozeny-Carman equation is derived for a solid medium with a set of parallel tubes representing the pore-system rather than a granular medium. A common extension of the Kozeny-Carman relation for a circular pipe is to consider a packing of identical spherical grains with diameter d. Although this granular pore-space geometry is not consistent with the pipe-like geometry, it is common to use the original Kozeny-Carman functional form on this geometry, as given in Equation (10). This allows a direct estimate of the specific surface area in terms of the porosity, and the Kozeny-Carman relation results in Equation (16). This extension breaks with its own assumptions, but it is believed that the tortuosity factor will adjust for this extension since it will become larger when the flow path get more tortuous.

Second, Dvorkin (2009) indicates that if grain size is used, it is not obvious that it does not change with varying porosity. This assumption, indicating that the porosity is not changing with changing grain diameter is not strictly valid. However, it can be argued that porosity is independent of grainsize when the rock is perfectly sorted and have spherical grains (Lippard, 2014) . In practice, however, porosity is dependent on grainsize since the rock never will have grains with equal size and shape. Experience usually show that decreasing grainsize give increasing porosity, since the degree of sorting will be less.

8.2 Sensitivity in the Models

In this chapter, the parameters in the Raymer model and the Kozeny-Carman model are investigated. The sensitivity analysis is quite simple as it considers the parameters in the models independently.

8.2.1 Raymer's Model

Raymer's relation can estimate porosity from acoustic measured velocity, and velocity from measured porosity, when the matrix and fluid velocities are known.

The sensitivity to change in the matrix and fluid velocities on the resulting estimated velocity, is investigated by checking how estimated velocity changes when matrix velocity and fluid velocity are varied for a given porosity.

The scattered points in Figure 8-3 show how the estimated velocity respond to changing the matrix velocity from 5.2-6.05 km/s for a given porosity of 15%, when the fluid velocity is constant at 1.5 km/s.

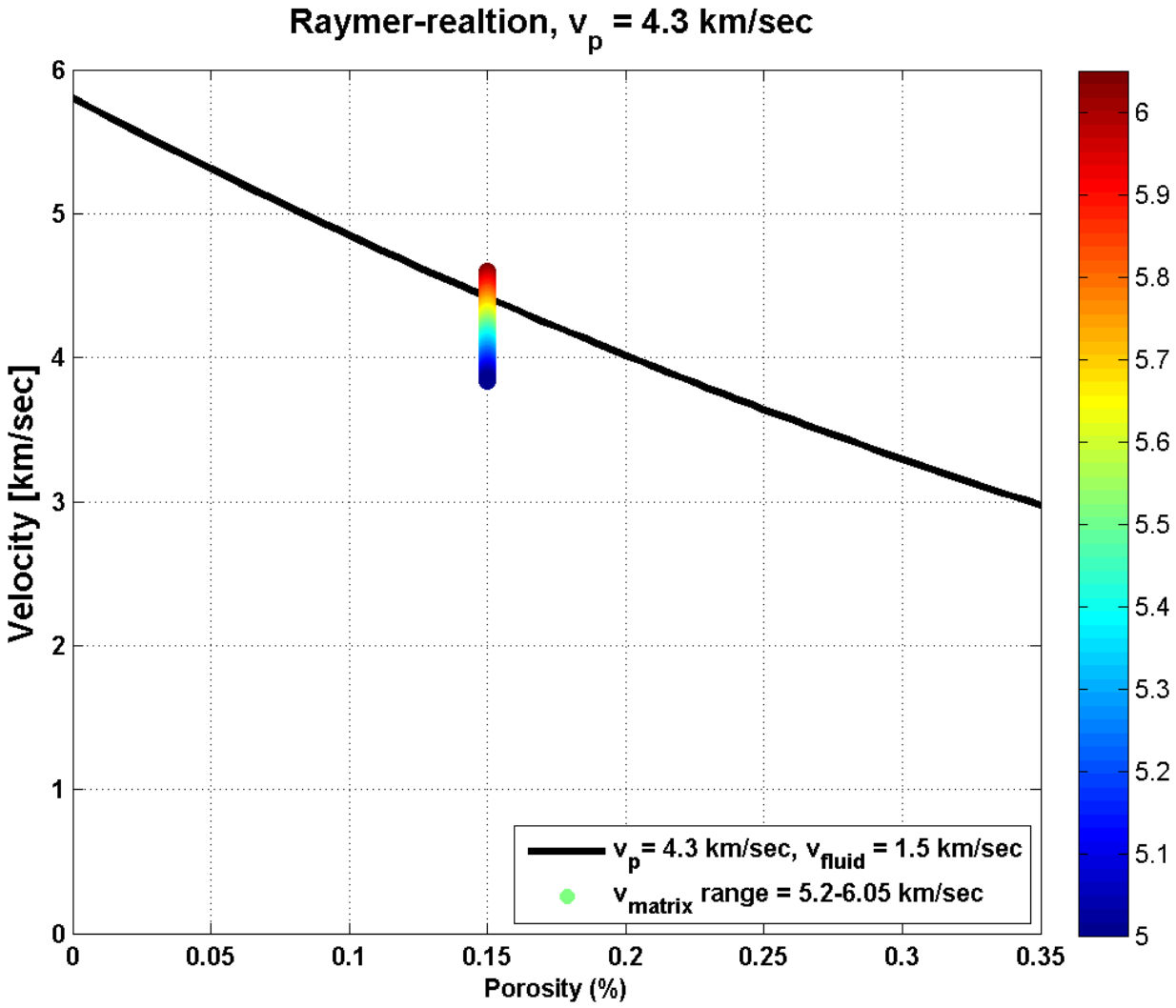

Figure 8-3: Sensitivity of matrix velocity in the estimated acoustic velocity from Raymer's relation.

The change in estimated acoustic velocity is found by derivation of the Raymer-relation with respect to matrix velocity, and adding the resulting change in acoustic velocity, as a response to the matrix changing, to a reference value. The reference value is set to 4.3 km/s.

The black line shows the acoustic velocity as a function of porosity, matrix and fluid velocities when the matrix velocity is 5.8 km/s and the fluid velocity is 1.5 km/s.

The estimated acoustic velocity seems rather sensitive to change in matrix velocity, as seen in the figure above. The span in the estimated acoustic velocity is quite extensive for a given porosity when the fluid velocity is constant.

Figure 8-4 show the sensitivity to the fluid velocity in the resulting estimated velocity, when the matrix velocity are constant and the fluid velocity ranges from 0.6 km/s-1.6 km/s for a

given porosity. The sensitivity is found the same way as above, however the derivation of the Raymer relation is done with respect to fluid velocity.

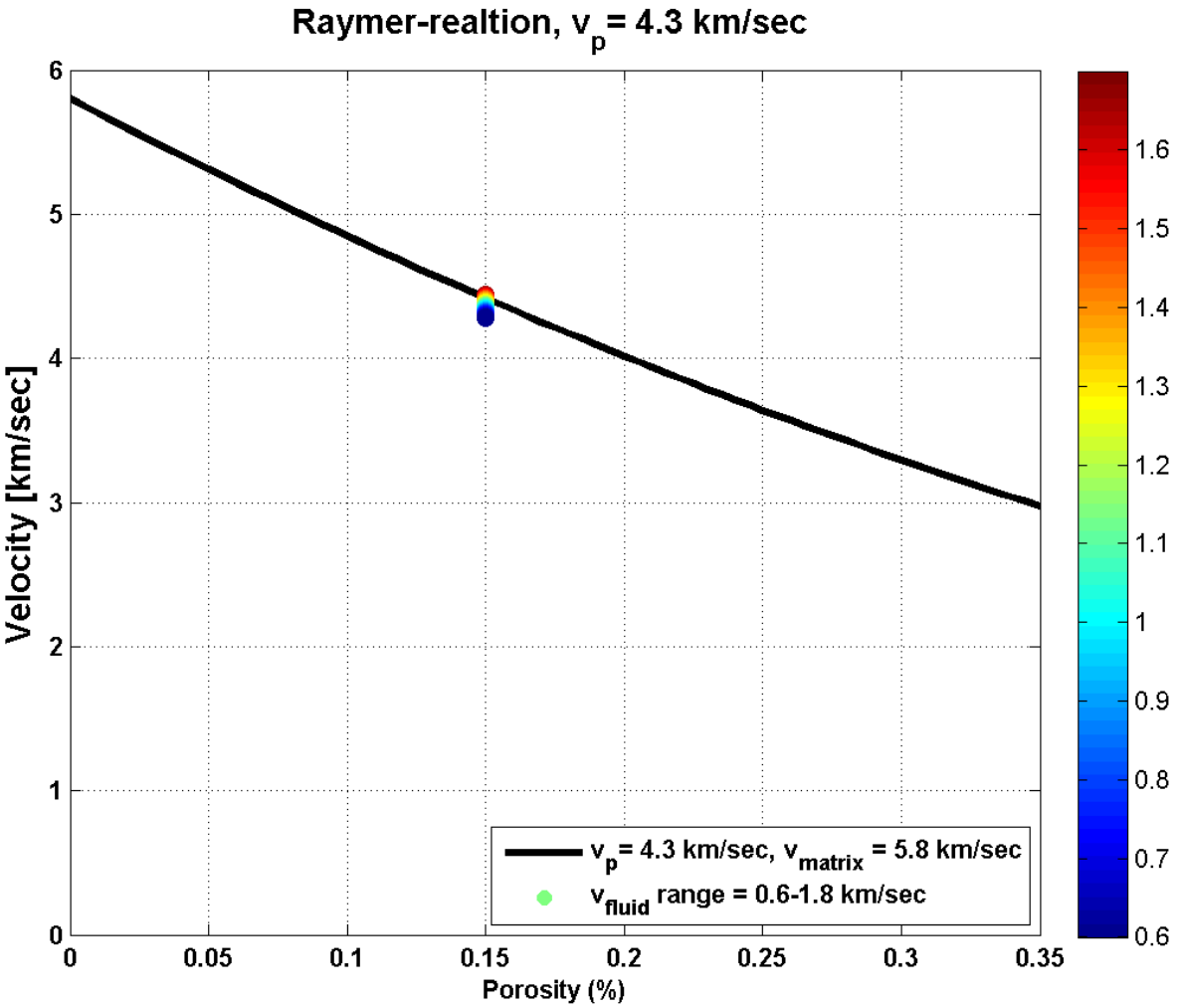

Figure 8-4: Sensitivity of fluid velocity in the estimated acoustic velocity from Raymer's relation.

The estimated Raymer-velocity show low sensitivity to this parameter when it is investigated independently from the other parameters. However, if the porosity increases, a larger fraction of the total bulk volume will be fluid so the estimated velocity's dependence on fluid velocity will increase, as seen in Figure 8-5.

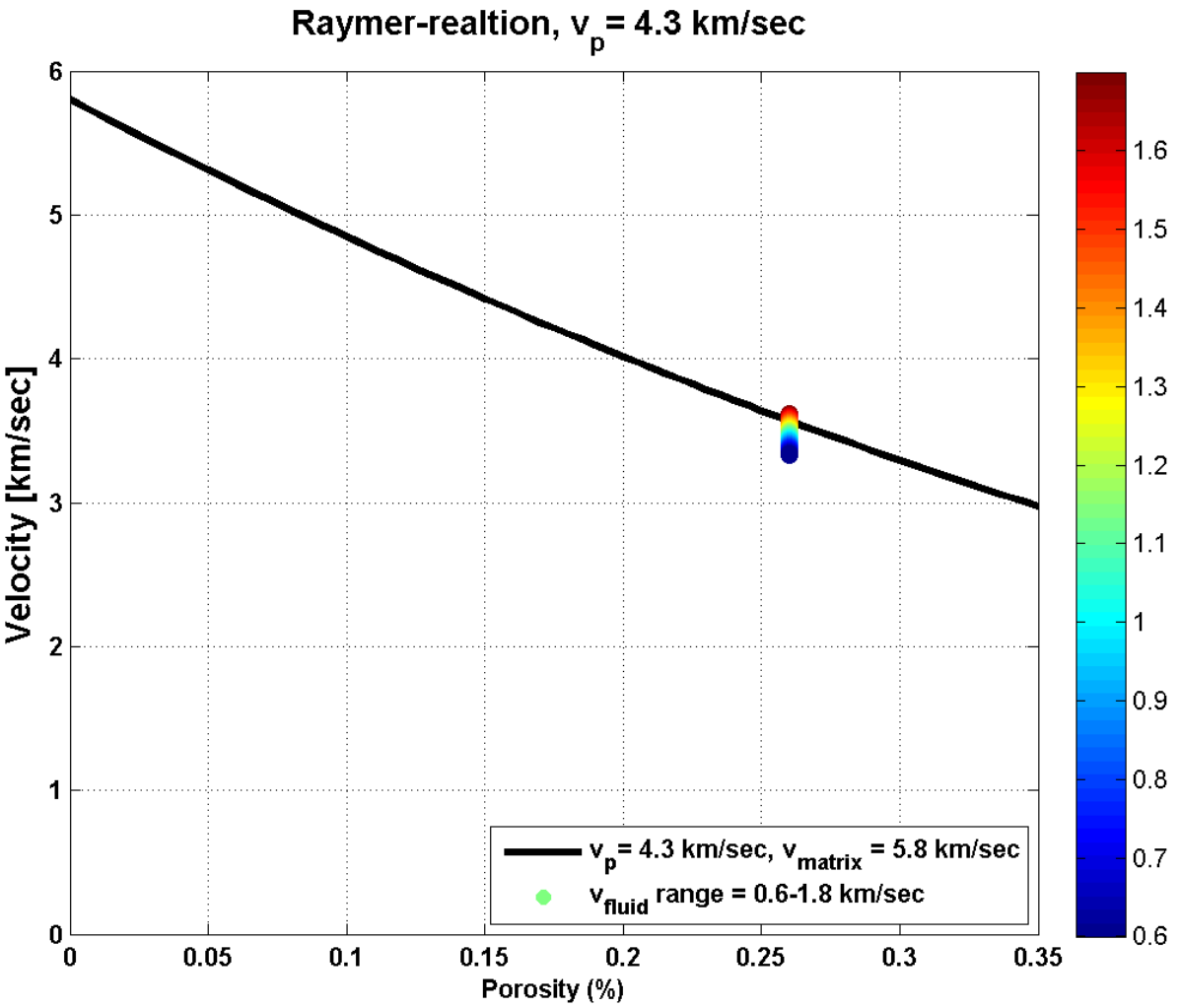

Figure 8-5: Estimated Raymer-velocity depend more on the fluid velocity when porosity increase.

8.2.2 Kozeny-Carman Model

Derivation of the Kozeny-Carman equation with respect to grainsize, tortuosity and porosity, describes the resulting change in permeability because of change in grainsize, tortuosity and porosity respectively.

Figure 8-6 and Figure 8-7 below show the change in permeability because of change in grainsize and tortuosity respectively. The red line shows the Kozeny-Carman relation as a function of porosity when the grainsize is 0.37 mm and tortuosity is 6. The sensitivity to grainsize and tortuosity are investigated for a given porosity value of 15%, as the figures show.

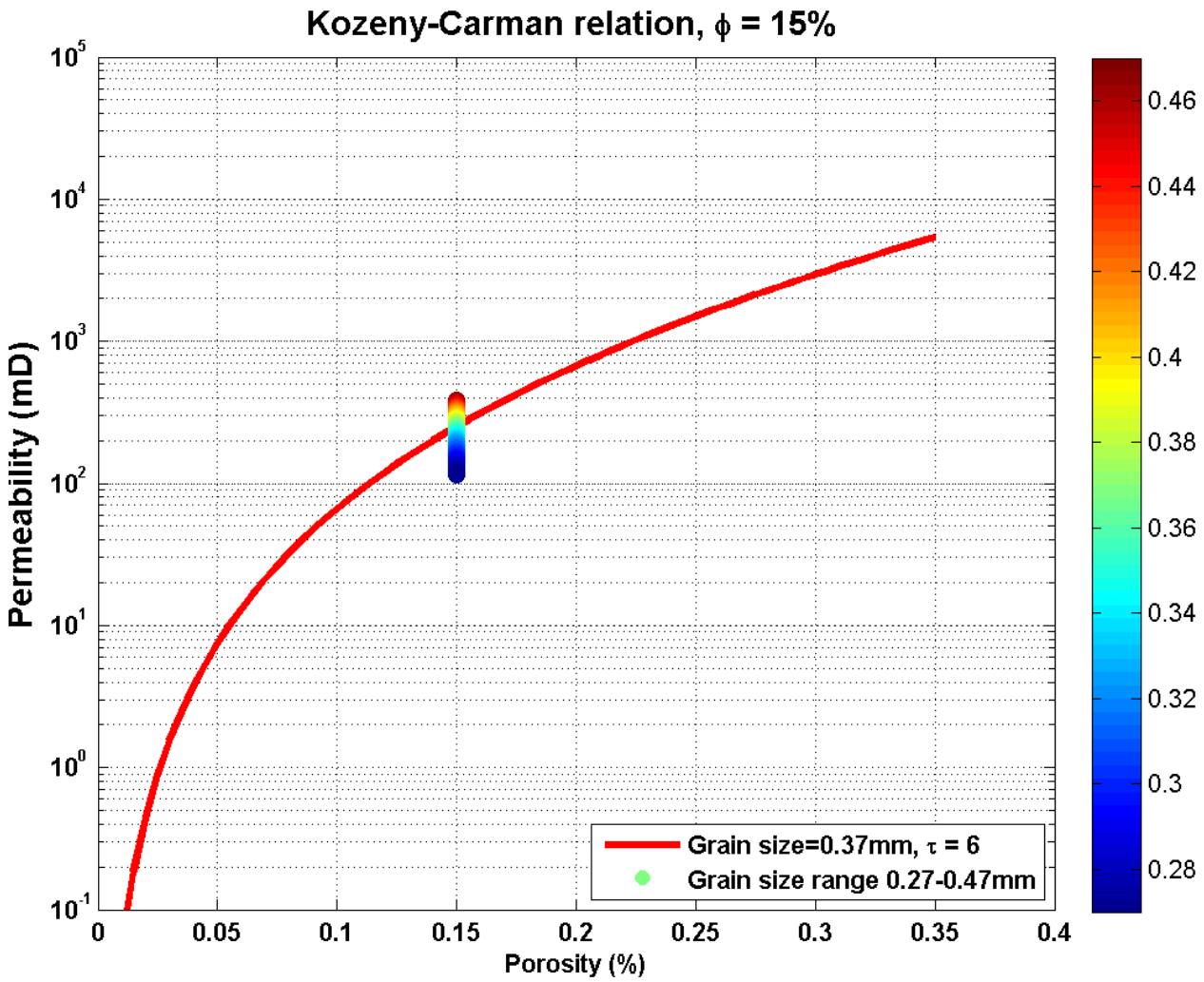

Figure 8-6: Resulting change in permeability when grainsize is varying from 0.27-0.47 mm for a given porosity and tortuosity value.

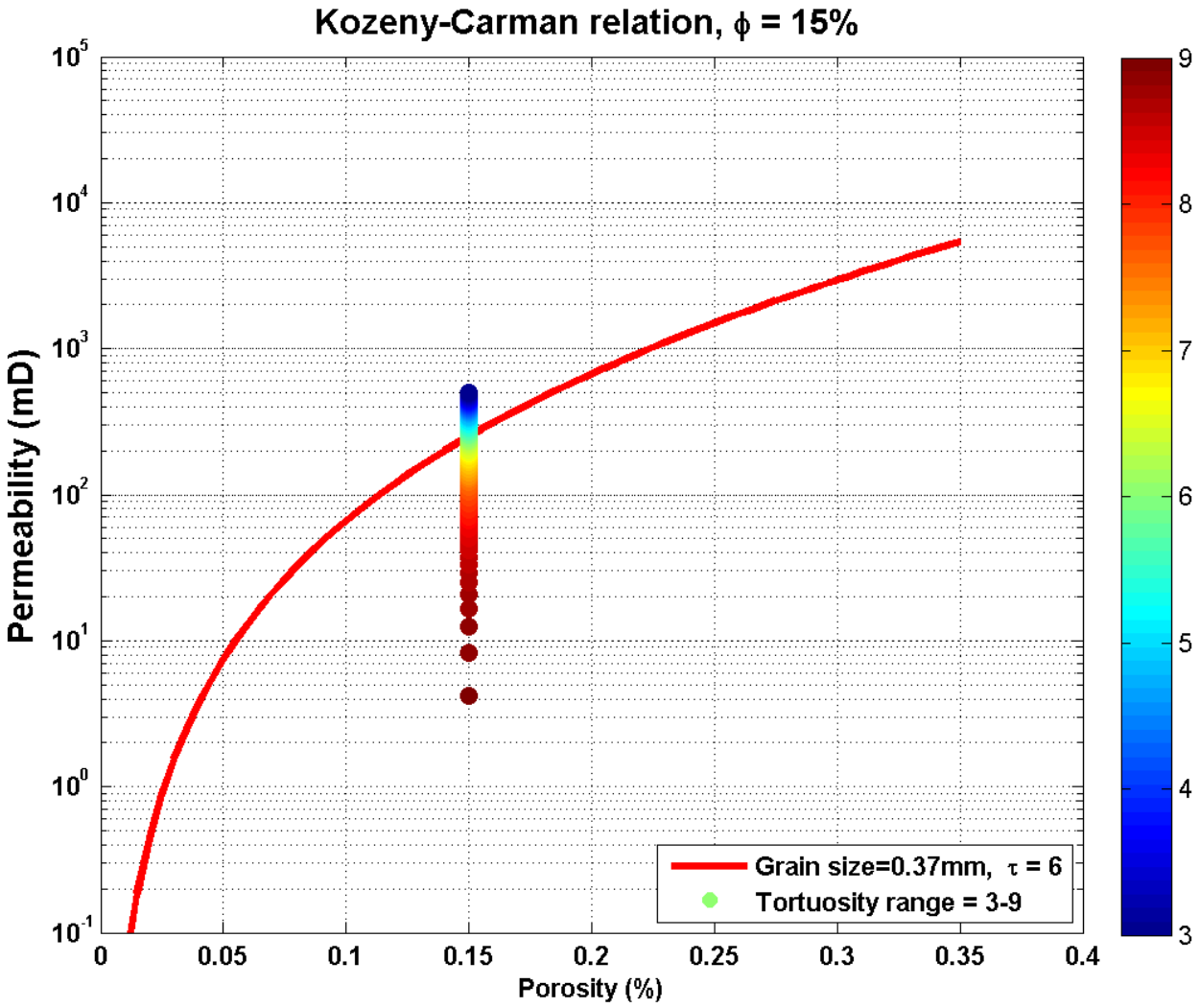

Figure 8-7: Resulting change in permeability when tortuosity is varying from 9-3 for a given porosity and grainsize value.

Figure 8-8 shows the change in permeability because of change in porosity. The red line in this figure gives permeability as a function of tortuosity when porosity and grainsize are 15% and 0.37 mm respectively. The sensitivity of porosity on the resulting permeability is investigated for a tortuosity of 6 and a grainsize of 0.37 mm respectively.

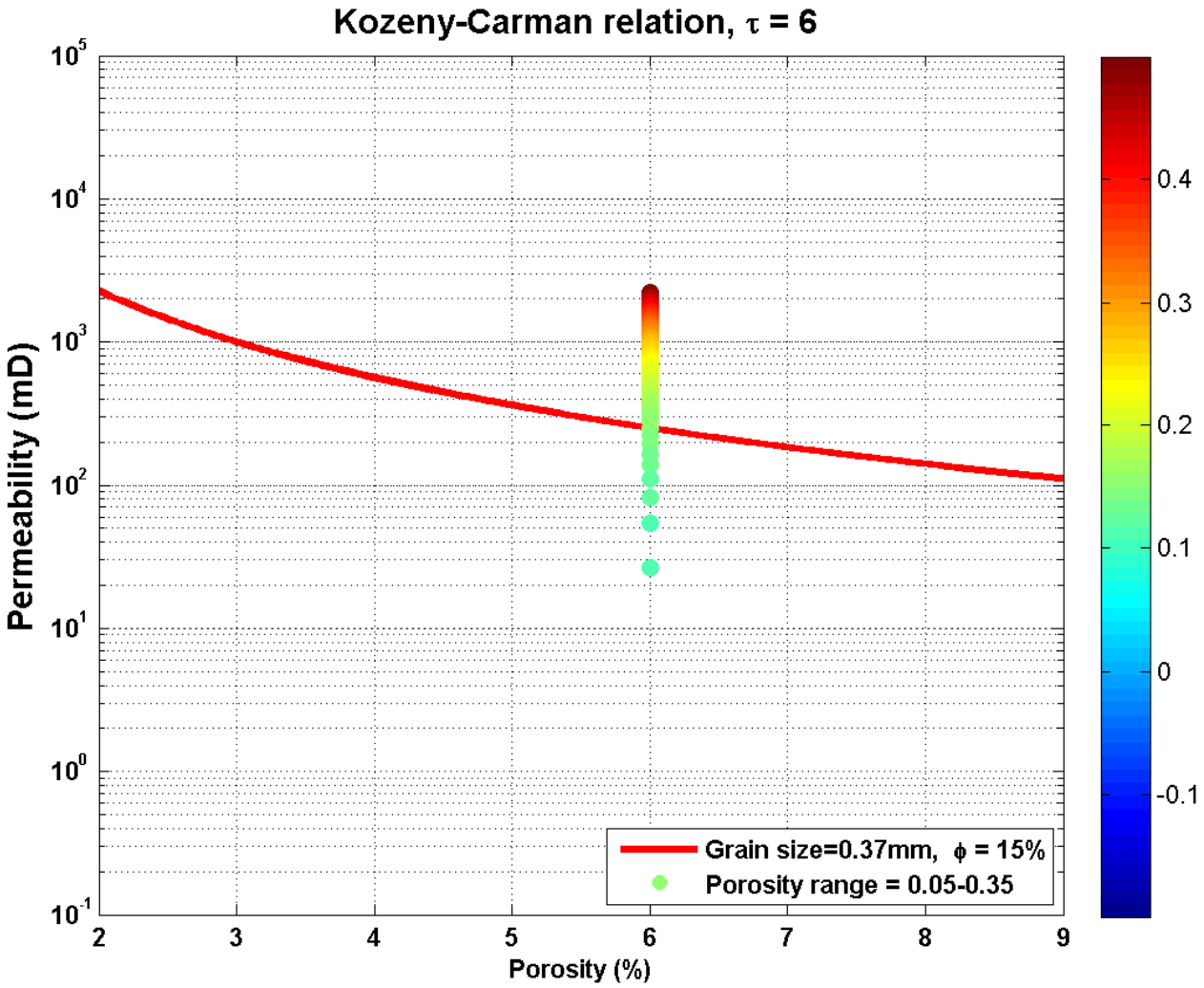

Figure 8-8: Resulting change in permeability when porosity is varying from 5%-35% for a given grainsize and tortuosity.

The assumption behind this simplistic sensitivity analysis is that grainsize, tortuosity and porosity can be investigated individually, and that they are not dependent of each other.

As previously mentioned, it can be argued that porosity is independent of grainsize when the rock is perfectly sorted and have spherical grains, however this is rarely seen in practice. Therefore, the figures above are not strictly true as they treat the parameters independently when they are in fact, to some degree, dependent of each other. Nevertheless, the figures provide a visualization of how the different parameters affect the resulting permeability provided by the Kozeny-Carman relation. The derivatives of the Kozeny-Carman equation with respect to grainsize, tortuosity and porosity are found in Appendix E.

8.3 Porosity and Permeability Estimations in the Test Well and on the Haltenbanken Dataset

The measured velocity and porosity in test well 17 plots below the Raymer line as seen in Figure 7-4. The test well is also a Haltenbanken well, and according to the Norwegian Petroleum Directorate, it is abandoned as a dry well with shows. The test well plots as expected for a Haltenbanken well with low porosity, since the Haltenbanken dataset showed an increasing trend of plotting Garn velocities below the Raymer-line for low porosities. Raymer's relation is not ideal for transforming the measured sonic velocity into porosity in this well, as the estimated porosity will be too high because low velocity values. Figure 7-5 shows that the estimated Raymer-porosity is higher than the measured porosity.

Figure 7-6 shows estimated permeability from the Kozeny-Carman model by using the Raymer porosity. Even though the Raymer-porosity is over-predicted, the porosity is still quite low. This leads to a fairly low permeability estimation that does not plot within Ehrenberg's specific surface area lines. Nevertheless, the modelled permeability is believed to be higher than it really is because the over-estimation in porosity.

Most of the wells in the Haltenbanken dataset have core calibrated permeability logs. These are plotted against the modelled permeability in Figure 7-7 when the fluid corrected sonic log velocity is transformed to porosity by Raymer's model. The plot shows that the modelled permeability is higher than the core-calibrated permeability for low permeabilities and goes towards the core-calibrated permeability values for higher permeabilities. This implies, again, that the Raymer model is less accurate for low porosities¸ resulting in over-estimated porosities. The over-estimated porosity results in too high permeability.

However, when the porosity *is* high, the Raymer model provides good porosity estimates from the measured velocity and Kozeny-Carman gives better permeability estimates. Nevertheless, the modelled permeability generally gives permeabilities that are higher than the core-calibrated permeability, but more so when permeability is low.

8.4 Challenges Regarding the use of Seismic Velocities in the Permeability Prediction

One of the objectives in this analysis is to investigate if seismic interval velocities can be applied to capture relative permeability changes by combining Raymer's model for porosity estimation with Kozeny-Carman's model for permeability estimation.

There are two big challenges when it comes to applying seismic interval velocities in this analysis:

1. The seismic velocities needs to be imaged spatially correct at true depth in order for seismic velocities to be representative for a given depth interval. This demands a correct velocity model.
2. The seismic velocities obtained from either time or depth imaging are inherited low frequent. This means that the seismic velocity will not respond to the rapid lithological changes in the subsurface, but only perceive the slowly varying trends causing the interval velocity model to become erroneous or not representative for certain lithological intervals.

The first challenge applies when the porosity and permeability estimations are performed in depth, which is done for the depth migrated seismic velocity profiles in the well locations of well 5 and 6. The depth migrated seismic profiles at the two locations are used in the Raymer- and Kozeny-Carman models for porosity and permeability estimations. The sonic log and the seismic velocity profile in these locations show large velocity deviations in the Garn interval. This indicates that the seismic velocities mapping in the Garn interval are in fact not representative for this lithology interval.

The problem is that the seismic velocities are too high in the overburden which may be due to velocity anisotropy. Consequently, when the data is depth migrated with this velocity model, the velocities generated from the Garn Fm. are mapped too deep. The apparent seismic velocities in the Garn Fm. is therefore too low. To reduce the seismic interval velocities, velocity in the overburden is reduced by applying Thomson's delta correction factor. The delta factor, applied to different intervals, are found by comparing the resulting time-depth curves of the calibrated seismic velocity profiles with those derived from the check-shots. The delta factor leads to a better correlation with the check-shot time-depth curve, which result in more representable vertical seismic interval velocities for the Garn Fm.

Figure 7-12 and Figure 7-13 show that the calibrated velocity profiles match better with the check-shots than the un-calibrated velocity profile.

It is not only the velocity that changes as a consequence of the delta factor, but the seismic profile is also stretched and squeezed in the different intervals, correcting the velocities to their true depth. The stretching and squeezing are clearly seen in Figure 7-14 and Figure 7-15, where the green seismic velocity profile is stretched and squeezed in different intervals of varying delta factors. This leads the velocity in the Garn interval to increase significantly.

Permeability is estimated from porosity generated by the calibrated and the un-calibrated seismic velocity. The permeability modelled from porosity estimated from calibrated velocity is much closer to the core-calibrated permeability compared to un-calibrated velocities estimating the porosity. This is seen in Figure 7-16 and Figure 7-17 for well 5 and 6 respectively.

The second challenge mentioned in the beginning of this chapter, is addressing the inaccuracy in the way the seismic image is obtained. The image of the subsurface suffers from smoothing and averaging effects as a consequence of the low frequent seismic signal.

From the check-shot data the average interval velocities in the two well locations are estimated, see Table 7-2. These velocities are higher than the interval velocity along the time interpretation of Garn.

The extracted interval velocities 60 milliseconds deeper than the Garn interpretation, is closer to the check-shot velocities. The velocities at the shifted two-way-travel time are applied in the Raymer-Kozeny-Carman model to simulate the model with velocities considered more representable for the Garn interval than the velocities extracted by the un-shifted horizon. The permeability turn out quite close to the average core-calibrated permeability values in the well locations when these shifted velocities are used. Note that this is not a shift of the actual Garn interpretation, this is stressed by the author! It is just a simulation of the permeability when the velocity applied in the model corresponds better with estimated interval velocities from check-shots.

Figure 8-9 show the resulting permeability from using the shifted velocities, and the permeability is much closer to the core-calibrated permeability values.

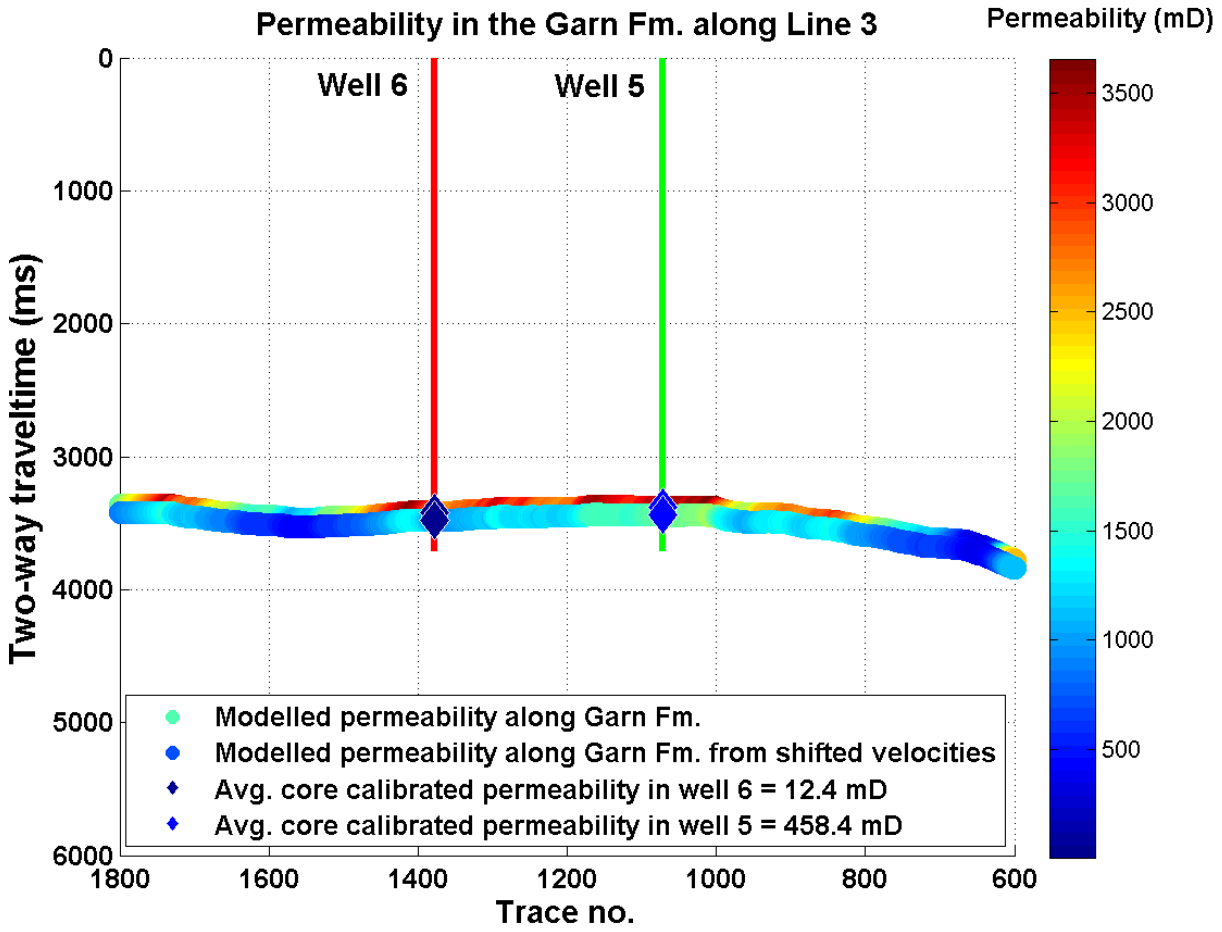

Figure 8-9: Permeability along the time-interpretation of Garn, when the velocities used in the Raymer model corresponds to the interval velocities gained from check-shots.

The figure above show the same results as in Figure 7-16 and Figure 7-17 for well 5 and 6 respectively. All the figures show that estimated permeability is significantly improved compared against core-calibrated permeability when calibrated vertical seismic interval velocities are used in the Raymer-Kozeny-Carman models.

The interesting aspect of Figure 8-9 is that the modelled permeability in well 5 is higher than the permeability in well 6, which is in line with the core calibrated permeability values. It seems that the seismic velocities observe the lateral velocity changes in Garn between well 5 and 6, and that the Raymer-Kozeny-Carman model translate this into relative changes in permeability. Naturally, other factors than relative change in permeability reduce the velocity along Garn. For example, the presence of gas will lower the velocity significantly. In addition, two porous systems can have the same porosity, but different permeability. This method does not take pore geometry into account, as the permeability is estimated directly from porosity.

9 Further Work

To avoid the problem concerning velocities being depth migrated to the wrong depth, the permeability modelling along the Garn-horizon is done in two-way-travel time. In the well locations however, the depth-migration problems are attempted to be reduced by the introduction of the delta factor. The delta factor stretches and squeezes the seismic profile as well as increasing and decreasing the actual velocity value. This is believed to reduce the anisotropy effects in the overburden.

Interpolating the delta factor and apply it to the depth-migrated Garn interpretation may reduce the anisotropy effects affecting the Garn velocities. The permeability estimation can then be performed in depth rather than two-way-travel time, which is much more convenient for obvious reasons.

10 Conclusion

In this analysis, the Kozeny-Carman model estimates the permeability in the Garn Fm. from porosity, when the porosity is estimated from acoustic velocities, measured at different frequencies, by the Raymer model.

- Fluid corrected porosity and velocity field data from 15 Haltenbanken wells confirms that the Raymer model can be applied to estimate porosity and velocity in the clean parts of the middle Jurassic Garn Fm. on Haltenbanken.
- The plotted field data tends to plot more below than above the Raymer-line, and this trend increase for decreasing porosity. Hence, leading to gradual overestimations of the Garn sandstone permeability
- The Kozeny-Carman model seem to be a good model for permeability prediction from porosity. The estimated permeability are in the size range of 1-5 compared with the core-calibrated permeabilities.
- The sensitivity analysis show that the predicted permeability is more sensitive to tortuosity than to grainsize, when the parameters in the Kozeny-Carman equation is considered independently.
- The velocity needs to be precise and high frequent to provide a detailed permeability estimation. Hence, sonic velocity gives better permeability estimates than seismic velocities.
- Seismic velocities are low frequent and do not respond to rapid lithology changes in the subsurface. The seismic velocities need to be imaged spatially correct and at the true depth in order to extract correct velocities and apply them in the model.

11 Nomenclature

ρ_B	Brine density
V_B	Brine velocity
ρ	Bulk density
K	Bulk modulus
K_{dry}	Bulk modulus of dry rock
K_o	Bulk modulus of gas
K_{ma}	Bulk modulus of matrix
K_o	Bulk modulus of oil
K_{sat}	Bulk modulus of saturated rock
K_w	Bulk modulus of water
K_{fl}	Bulk modulus rock saturating fluid
V_{bulk}	Bulk volume of sample
P_c	Capillary pressure
m	Cementation factor
v_{cl}	Clay velocities
V_{cl}	Clay volume
C_d	Coefficient of variation in psd
A	Cross sectional area
l	Curved flow path
σ'	Differential stress
c	Dimensionless shape factor
φ_{eff}	Effective porosity
κ	Factor of proportionality that includes the effect of permeability
ρ_{fl}	Fluid density
γ	Fluid density multiplied by the gravitational acceleration

Q	Fluid flow
v_{fl}	Fluid velocity
F	Formation factor
$GR\ value\ (log)$	Gamma ray log value
ρ_g	Gas density
S_g	Gas saturation
R	Grain and pore radius
d	Grain diameter
$\bar{d}$	Grain size average
g	Gravitational constant
Q_0	Heat conductivity
I	Hydraulic head along the flow path
σ_v	Lithostatic stress
ρ_{ma}	Matrix density
v_{ma}	Matrix velocity
$GR(max)$	Maximum gamma ray log value, also called shale line.
S_b	Mercury saturation as percent of bulk volume
$GR(min)$	Minimum gamma ray log value, also called sand line.
ρ_0	Oil density
S_o	Oil saturation
Psd	Particle size distribution
φ_c	Percolation threshold porosity
k	Permeability
P_f	Pore pressure
φ	Porosity
P	Pressure
ΔP	Pressure head along a pipe

v_p	Pressure wave velocity
R_w	Resistivity of brine
R_0	Resistivity of brine saturated rock
R_t	Resistivity of rock
v_{sand}	Sand velocities
V_{sand}	Sand volume
n	Saturation factor
G	Shear modulus
v_s	Shear wave velocity
γ	Skewness
s	Sodium chloride weight fraction $[ppm/10^6]$
p	Sorting term
S	Specific surface area
L	Straight flow path
T	Temperature
T_0	Temperature at zero datum
K	Thermal conductivity
τ	Tortuosity
a	Tortuosity factor
φ_{tot}	Total porosity
μ	Viscosity
V_{pore}	Volume of pores
ρ_W	Water density
S_w	Water saturation
V_W	Water velocity

12 Bibliography

Ahmed, U., Crary, S. F., & Coates, G. R. (1991). Permeability Estimation: The Various Sources and Their Interrelationships. *Journal of Petroleum Technology, 43*(5), 578-587. doi: 10.2118/19604-PA

Archie, G. E. (1941). The Electrical Resistivity Log as an Aid in Determining Some reservoir Characteristics. *Society of Petroleum Engineers, 146*(1), 54-62. doi: 10.2118/942054-G

Avseth, P., Mukerji, T., Mavko, G., & Dvorkin, J. (2010). Rock-physics diagnostics of depositional texture, diagenetic alterations, and reservoir heterogeneity in high-porosity siliciclastic sediments and rocks — A review of selected models and suggested work flows. *Society of Exploration Geophysicists, 75*(75A31–75A47). doi: 10.1190/1.3483770

Batzle, M., & Wang, Z. (1992). Seismic rock properties of pore fluids. *Society of exploration Geophysics, 57*(11), 1396-1408. doi: 10.1190/1.1443207

Berg, R. R. (1970). Method for Determining Permeability from Reservoir Rock Properties. *Transactions, Gulf Coast Association of Geological Societies, 20*, 303-317.

Carman, P. C. (1937). Fluid flow through granular beds *Institution of Chemical Engineers, 15*, 150-166.

Darcy, H. (1856). *Les fontaines publiques de la ville de Dijon*. Paris: Victor Dalmont.

Dewan, J. T. (1983). *Essentials of Modern Open-hole Log Interpretation*.

Dutta, N. C. (2002). Geopressure prediction using seismic data: Current status and the road ahead. *Soceity of Exploration Geophysicists, 67*(6), 2012-2041.

Dvorkin, J. (2009). Kozeny-Carman equation revisited.

Dvorkin, J., & Nur, A. (1998). Time-average equation revisited. *Geophysics, 63*(2), 460-464.

Ehrenberg, S. N. (1990). Relationship Between Diagenesis and Reservoir quality in Sandstones of the Garn Formation, Haltenbanken , Mid-Norwegian Continental Shelf. *The American Association of Petroleum Geologists Bulletin, 74*(10), 1538-1558.

Fjær, E., Holt, R. M., Horsrud, P., Raaen, A. M., & Risnes, R. (2008). *Petroleum Related Rock Mechanics* (2 ed.). Amsterdam: Elsevier.

Grude, S., Dvorkin, J., & Landrø, M. (2015). Permeability variation with porosity, pore space geometry, and cement type: A case history from the Snøhvit field, the Barents Sea. *Geophysics, 80*(1), D43-D49. doi: 10.1190/geo2014-0064.1

Hubbert, M. K. (1956). Darcy's Law and the Field Equations of the Flow of Underground Fluids: Society of Petroleum Engineers.

Kozeny, J. (1927). Über kapillare Leitung des Wassers im Boden (Aufstieg, Versickerung und Anwendung die Bewässerung) *Akademie der Wissenschaften in Wien, 136*.

Lippard, S. (2014). *Petroleum Geology, Lecture 10: Porosity and Permeability*.

Lundberg, N. H. (2011, 15.06). Haltenbanken: Petroleumsvirksomhet. Retrieved 28.04, 2016, from https://snl.no/Haltenbanken%2Fpetroleumsvirksomhet.

Mavko, G., Mukerji, T., & Dvorkin, J. (2009). *The Rock Physics Handbook*: Cambridge University Press.

Mavko, G., & Nur, A. (1997). The effect of a percolation threshold in the Kozeny-Carman relation. *Geophysics, 62*(5), 1480-1482. doi: 10.1190/1.1444251

Nelson, P. H. (1994). Permeability-porosity Relationships In Sedimentary Rocks. *The Log Analyst, 35*(03), 38-74.

North, F. K. (1985). *Petroleum Geology*: Unwin Hyman Inc., UK.

NPD. (2014). The Fangst Group - Garn Formation. from http://www.npd.no/en/Publications/Reports/Compiled-CO2-atlas/5-The-Norwegian-Sea/51-Geology-of-the-Norwegian-Sea/The-Fangst-Group-Garn-Formation/

Panda, M. N., & Lake, L. W. (1994). Estimation of single-phase permeability from parameters of particle-size distribution. *AAPG Bulletin, 78*(7), 1028-1039.

Poiseuille, J. L. M. (1840). *Recherches exérimentales sur le mouvement des liquides dans les tubes de trés petites diamétres*. Paris: L'Académie des Sciences.

Purcell, W. R. (1949). Capillary Pressures - Their Measurement Using Mercury and the Calculation of Permeability Therefrom. *Journal of Petroleum Technology, 1*(02), 39-48. doi: 10.2118/949039-G

Raymer, L. L. (1981). Elevation And Hydrocarbon Density Correction For Log-derived Permeability Relationships. *The Log Analyst, 22*(03), 1-7.

Raymer, L. L., Hunt, E. R., & Gardner, J. S. (1980). *An Improved Sonic Transit Time-To-Porosity Transform*.

Rider, M. (2000). *The Geological Interpretation of Well Logs* (2 ed.). Scotland: Rider-French Consulting Ltd.

Rubino, J. G., Velis, D. R., & Holliger, K. (2012). Permeability effects on the seismic response of gas reservoirs. *Geophysical Journal International*, 448-468. doi: 10.1111/j.1365-246X.2011.05322.x

Salem, H. S., & Chilingarian, G. V. (1999). The cementation factor of Archie's equation for shaly sandstone reservoirs. *Journal of Petroleum Science and Engineering, 23*(2), 83-93. doi: http://dx.doi.org/10.1016/S0920-4105(99)00009-1

Storvoll, V., Bjørlykke, K., & Mondol, N. H. (2005). Velocity-depth trends in Mesozoic and Cenozoic sediments from the Norwegian Shelf. *AAPG Bulletin, 89*(3), 359-381.

Swanson, B. F. (1981). A Simple Correlation Between Permeabilities and Mercury Capillary Pressures. *Journal of Petroleum Technology, 33*(12), 2498-2504. doi: 10.2118/8234-PA

T. Hantschel, & Kauerauf, A. I. (2009). *Fundamentals of Basin and Petroleum Systems Modeling*. Berlin Heidelberg Springer-Verlag

Walderhaug, O., Eliassen, A., & Aase, N. E. (2012). Prediction of Permeability in Quartz-Rich Sandstones: Examples from the Norwegian Continental Shelf and the Fontainebleau Sandstone. *Journal of sedimentary research, 82*(12), 899-912. doi: 10.2110/jsr.2012.79

Wentworth, C. K. (1922). A Scale of Grade and Class Terms for Clastic Sediments. *The Journal of Geology, 30*(5), 377-392.

Wood, A. W. (1955). *A textbook of sound*: New York : Macmillan.

Wyllie, M. R. J., Gregory, A. R., & Gardner, L. W. (1956). Elastic Wave Velocities in Heterogeneous and Porous Media. *Geophysics, 21*(1), 41-70. doi: 10.1190/1.1438217

Wyllie, M. R. J., & Rose, W. D. (1950). Some Theoretical Considerations Related To The Quantitative Evaluation Of The Physical Characteristics Of Reservoir Rock From Electrical Log Data. *Journal of Petroleum Technology, 2*(4), 105-118. doi: 10.2118/950105-G

Appendix A Empirical Relations for Density and Velocity for Brine and Water

The following relations were used in calculating the density and velocity of water and brine (Batzle & Wang, 1992)

Density of water:

$$p_w[g/cm^3] = 1 + 1 \times 10^{-6}\,(-80T - 3.3T^2 + 0.00175T^3 + 489P - 0.333P^2 - 2TP + 0.016T^2P - 1.3 \times 10^{-5}PT^3 - 0.002TP^2)$$

Density of brine:

$$p_B[g/cm^3] = p_w + s\{0.668 + 0.44s + 1 \times 10^{-6}[300P - 2400Ps + T(80 + 3T - 3300s - 13P + 47Ps)]\}$$

Velocity of water:

$$V_w = \sum_{i=0}^{4}\sum_{j=0}^{3} w_{ij}T^iP^j$$

For the constant w_{ij} refer to Table 1 in (Batzle & Wang, 1992)

Velocity of brine:

$$V_B = V_w + s(1170 - 9.6T + 0.055T^2 - 8.5 \times 10^{-5}T^3 + 2.6P - 0.0029TP - 0.0476P^2) + s^{1.5}(780 - 10P + 0.16P^2) - 820s^2$$

Appendix B Fluid Substitution

Appendix B.1 Gassmann's equations

Appendix B.1.1 Dry rock bulk modulus

$$K_{dry} = \frac{K_{sat}\left(\frac{\varphi\, K_{ma}}{K_{fl} + 1 - \varphi}\right) - K_{ma}}{\frac{\varphi\, K_{ma}}{K_{fl}} + \frac{K_{sat}}{K_{ma} - 1 - \varphi}}$$

Appendix B.1.2 Saturated rock bulk modulus

$$K_{sat} = K_{dry} + \frac{\left(1 - \frac{K_{dry}}{K_{ma}}\right)^2}{\frac{\varphi}{K_{fl}} + \frac{(1-\varphi)}{K_{ma}} - \frac{K_{dry}}{{K_{ma}}^2}}$$

Appendix B.2 Pressure and Stress Eestimation

A subsurface formation has to carry the weight of the overlying formation, and the lithostatic stress at the bottom of a column of height z where the density varies with depth is (Fjær, Holt, Horsrud, Raaen, & Risnes, 2008).

$$\sigma_v = g \int_0^D \rho(z) dz$$

g is the gravitational acceleration and the density, ρ, is the property measured by the density log in the well.

The pore pressure at a depth D is given by the weight of the fluid column above the given depth

$$P_f = g \int_0^D \rho_{fl}(z) dz$$

The stress at a given depth is generated by the overlying formation, carried partly by the pore pressure and the framework of the formation at the given depth. The part carried out by the framework of the rock is termed differential stress and is equal to pore pressure subtracted from the lithostatic pressure (Dutta, 2002).

$$\sigma' = \sigma_v - P_f$$

The figure below show the stress versus depth for well 15.

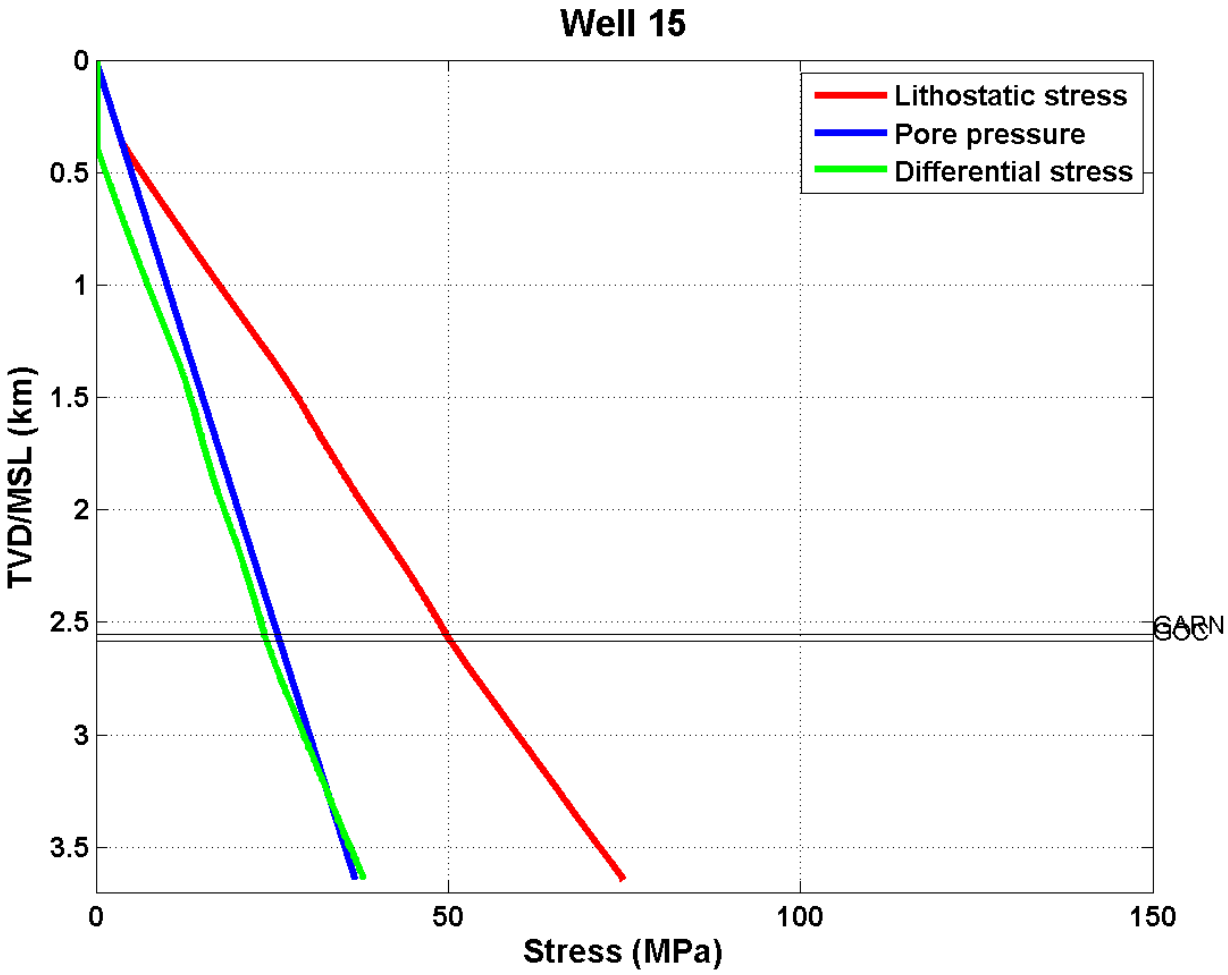

Figure Apx 1: Lithostatic stress, pore pressure and differential stress.

Appendix B.3 Temperature Estimation

The temperature at a given depth is given by (T. Hantschel & Kauerauf, 2009):

$$T = T_0 + z\frac{Q_0}{\mathrm{K}}$$

Where T_0 is the temperature at zero datum (in this case the temperature at the seafloor, that is the temperature of the sea water, assumed to be 3°C), Q_0 is the heat flow, K is the thermal conductivity and z is the depth. Rewriting this equation gives

$$\frac{Q_0}{\mathrm{K}} = \frac{T - T_0}{z}$$

T is the temperature measured at the bottom of the well.

This is a simple way for calculating the gradient and the method assumes that the temperature increase linearly with depth.

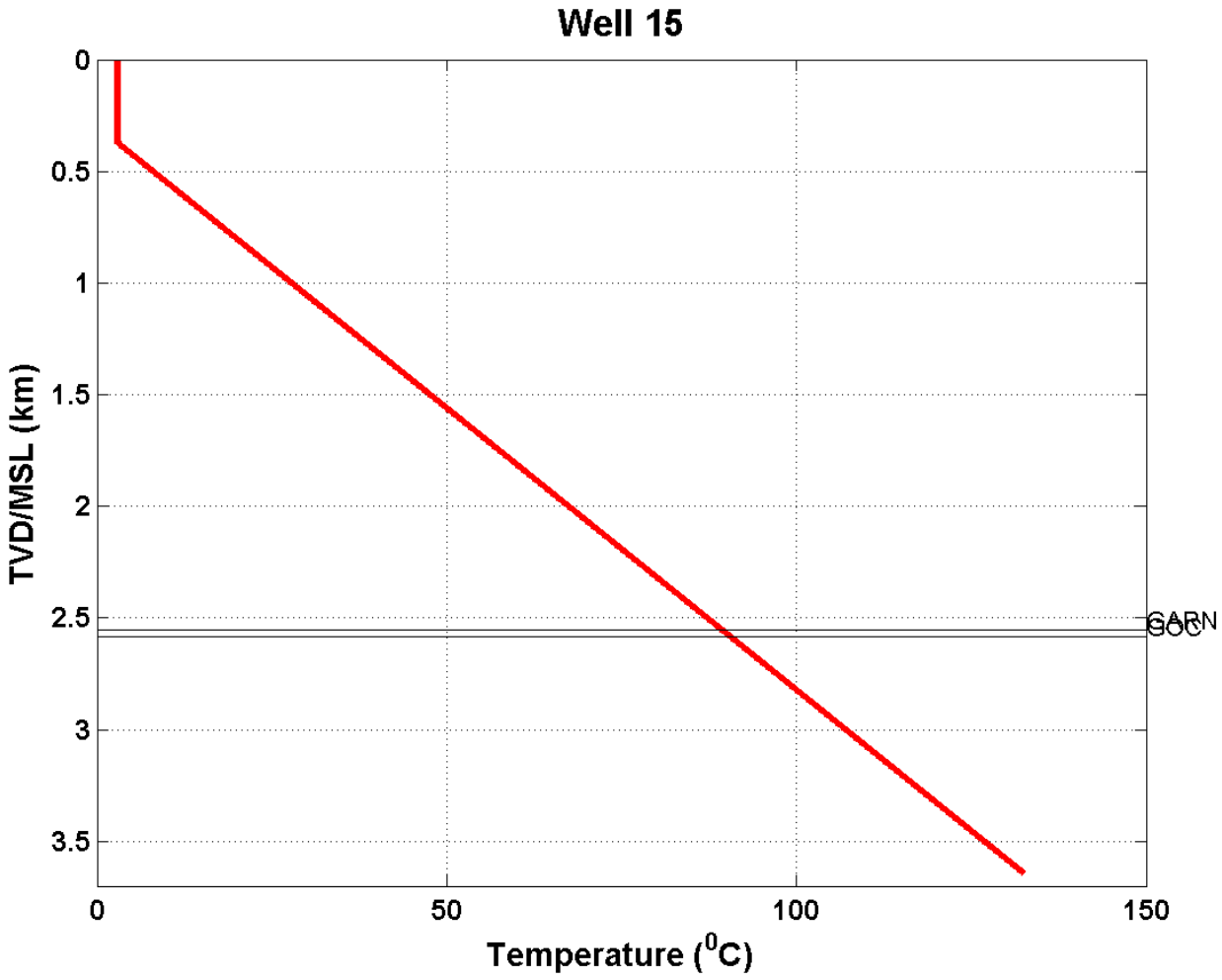

Figure Apx 2: Estimated temperature gradient well 15.

Appendix B.4 Fluid Corrected Density

$$\rho = (1 - \varphi)\rho_{ma} + \varphi\rho_b$$

Appendix B.5 Estimation of Bulk modulus for In-situ Fluid Mixture

The dry rock bulk modulus is necessary to calculate the effective bulk modulus of the rock saturated with the new fluid. To calculate K_{dry}, the bulk modulus of the in-situ fluid mixture is needed.

K_{fl} can be found from Wood's formula (Wood, 1955).

$$\frac{1}{K_{fl}} = \frac{S_w}{K_w} + \frac{S_0}{K_o} + \frac{S_g}{K_g}$$

The fluid mixture bulk modulus, K_{fl}, is dependent on the bulk modulus of each fluid in the fluid mix and the saturation of each fluid.

Appendix B.6 Estimation of Fluid Saturations

The saturations are found by using Archie's equation (Archie, 1941). Archie found the following simple relation between a brine-filled rock and the resistivity of the brine

$$R_0 = FR_w$$

Where R_0 is the resistivity of a brine-saturated rock, R_w is the resistivity of the brine filling the pores and F is the formation factor found by Archie in 1945 to be (when the tortuosity factor is set to 1)

$$F = \varphi^{-m}$$

Combining these equations gives

$$R_0 = R_w \varphi^{-m}$$

In his paper, Archie shows a relation acquired by a variety of investigators obtained between the water saturation and the resulting resistivity of the rock, termed R_t (Archie, 1941)

$$S_w = \left(\frac{R_0}{R_t}\right)^{\frac{1}{n}}$$

Where n is the saturation factor.

Inserting the expression for R_0 gives

$$S_w = \left[\frac{R_w}{\varphi^m R_t}\right]^{\frac{1}{n}}$$

m and n is put to 2, and the water saturation becomes

$$S_w = \sqrt{\frac{R_w}{\varphi^2 R_t}}$$

The resistivity of the brine is needed before calculating the water saturation. The brine resistivity can be calculated from a relationship with temperature given by (Dewan, 1983):

$$R_w = [6.8(1 + 0.0545T - 1.127 \times 10^{-4}T^2)]^{-1}$$

Where T is the average temperature in the Garn Fm.

Appendix B.7 Estimation of Bulk Modulus for Fluids

The bulk modulus of a fluid can be calculated from velocity and density for each fluid

$$K_{fl} = \rho_{fl} V_{p,fl}{}^2$$

Appendix B.8 Estimation of In-situ Bulk Modulus for Rock

The bulk modulus of the rock with in-situ saturation is calculated by using the relationship between velocity, bulk density and shear modulus.

$$V_p = \sqrt{\frac{K_{sat} + \frac{4}{3} G_{sat}}{\rho}}$$

$$V_s = \sqrt{\frac{G_{sat}}{\rho}}$$

The bulk density is

$$\rho = (1 - \varphi)\rho_{ma} + \varphi\rho_{fl}$$

Where density of the fluid mixture is a weighted average of the density of each fluid and the fraction of the total saturation they occupy

$$\rho_{fl} = (1 - S_w)\rho_0 + S_w\rho_w$$

Where S_w is the mean water saturation in the Garn Fm.

From Han et al. a relation for the S-wave velocity are obtained.

$$\mathrm{V_s[km/s]} = 3.52 - 4.91\varphi - 1.89V_{cl}$$

From this relation the shear modulus can be expressed as

$$K_{sat} = \rho_b \left({V_p}^2 - \frac{4}{3} {V_{s,Han}}^2 \right)$$

This expression are inserted into the P-wave velocity-equation above. V_p comes from the velocity log.

All the necessary parameters for calculating K_{dry} are now obtained.

With K_{dry} available K_{sat} can be calculated for the desired fluid mixture, which in this analyses are 100% brine.

Appendix B.9 Fluid Corrected Velocity

$$V_p = \sqrt{\frac{K_{sat} + \frac{4}{3} G_{sat}}{\rho_b}}$$

Appendix C Porosity and Permeability Relations

There exists several predictive models for permeability, and they can be sorted into four classes:

1. Models based on grainsize and mineralogy
2. Models based on surface area and water saturation
3. Well log models
4. Models based on pore dimension

In the following chapters each class are described by using models fitting into each class as examples. The reader should have in mind that these models are all based at some level to the Kozeny-Carman relation.

Appendix C.1 Models Based on Grainsize and Mineralogy

Berg (1970) presented a petrographical model linking variables such as grain size, shape and sorting to permeability (Berg, 1970).

$$k = 5.1 \times 10^{-6} \varphi^{5.1} d^2 e^{-1.385\, p}$$

Where d is the median grain diameter in millimetres and p is a sorting term.

As Nelson (1994) summarizes Berg's model:

"Berg's model appears to be a usable means of estimating permeability in unconsolidated sands and in relatively clean consolidated quatzose rocks."

Appendix C.2 Models Based on Surface area and Water Saturation

Several relationships for estimating the permeability from in-situ measurements or porosity and residual water saturation have been suggested.

Timur (1968) evaluated several possible relations to obtain the permeability from porosity and residual water saturation by analysing 155 sandstone samples originating from three North-American oilfields with varying degrees of sorting, consolidation and ranges of porosity. He arrived at the following expression:

$$k = \frac{a\, \varphi^b}{S_{wi}^2}$$

Where the coefficients a and b are determined statistically, S_{wi} is the residual water saturation and φ is the porosity.

His experiments suggests that porosity is a better predictor for permeability than is the residual water saturation, but that specific relations between permeability, porosity and residual water saturation, established empirically for the specific field, give better permeability predictions than a general relation, such as the Kozeny-Carman relation.

It is not easy to apply this equation since it is based entirely on core data. Also, the core data used to obtain the residual water saturation, S_{wi}, is obtained for a fixed value of capillary pressure. In a reservoir the capillary pressure will vary with height, so since the residual water

saturation varies with the capillary pressure it is necessary to assume a functional dependence between these parameters (Raymer, 1981).

There are no theoretical basis for the substitution of specific surface area and residual water saturation, so even though the two models are quite similar, this equation is a strictly empirical relation.

Timur's (1968) permeability model offer a viable method for permeability estimation where porosity and irreducible water saturation can be estimated. Difficulties arises when there are uncertainties in the residual water saturation, as within an extensive transition zone (Nelson, 1994).

Appendix C.3 Well Log Models

In fields where log- and core-data are at hand, approaches for permeability estimation are based on grainsize and water saturation.

According to Nelson (1994):

"Linear regression techniques have become very popular for establishing predictors for geologic variables because the methods are effective at predicting mean values, are fast computationally, are available in statistical software packages, and provide a means of assessing errors."

In the simplest regression model, porosity is the only independent variable:

$$\log(k) = a + b\varphi$$

Where a and b are regression coefficients. By dividing the field into parts, individual regression coefficients can be established for each part of the field for increasing accuracy.

More variables can be added, for example, gamma ray values or shale volume can be included as independent variables for adding petrographical information in the predictive relationship. If too many variables are added, the prediction might cause instability in the permeability estimation.

Appendix C.4 Models Based on Pore Dimension

It is the connectivity of pores that determines the permeability, not grainsize and sorting, nor porosity. Thus, all the relations above are indirect relationships.

Pore dimension is measured by mercury injection and methods are developed to measure the capillary pressure. An equation indicating a theoretical relationship between the capillary pressure and permeability can then be used to estimate the permeability from the capillary pressure (Purcell, 1949).

Swanson's equation from 1981 is an example of a model expressing the permeability from pore dimension through use of mercury injection and capillary pressure curves. The model provides air or brine permeability from a single point on the capillary curve. The regression relationship are based on permeabilities and capillary pressure data on 203 sandstone samples from 41 formations and 116 carbonates from 33 formations.

The method picks the maximum ratio between mercury saturation to pressure, $\left(\frac{S_b}{P_c}\right)_{max}$ from the capillary pressure curve, arguing that at this point all the connected pores are filled with mercury. At this point, the capillary pressure "corresponds to pore sizes effectively interconnecting the total major pore system and, thus, those that dominate fluid flow " (Swanson, 1981).

From linear regression, Swanson obtained the following simple equation.

$$k = a\left(\frac{S_b}{P_c}\right)^c_{max}$$

Where the constants a and c depend on the rock type (sandstone or carbonate) and the fluid type (air or brine). S_b is defined as the mercury saturation as percent of bulk volume.

Appendix D Seismic Velocities

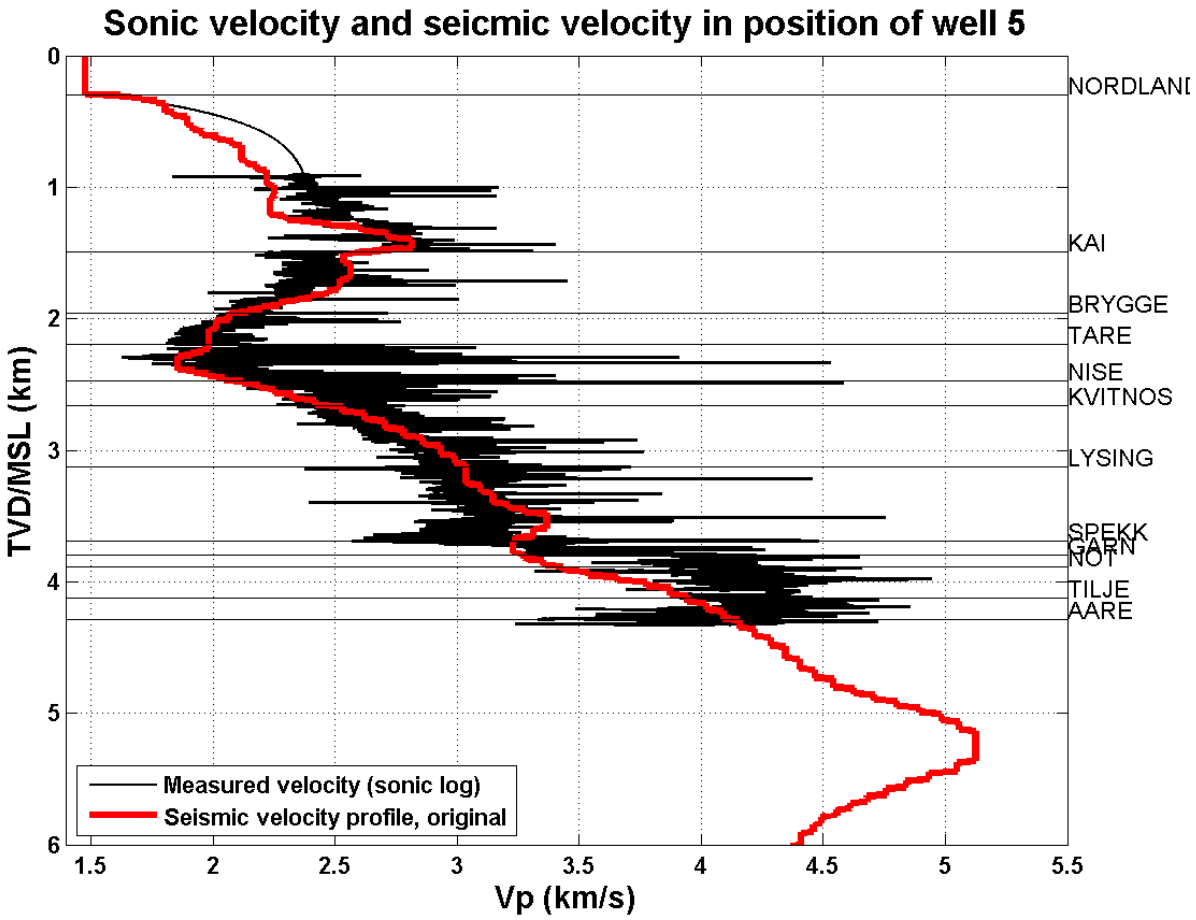

Figure Apx 3: Sonic log and seismic velocity profile in the well location of well 6.

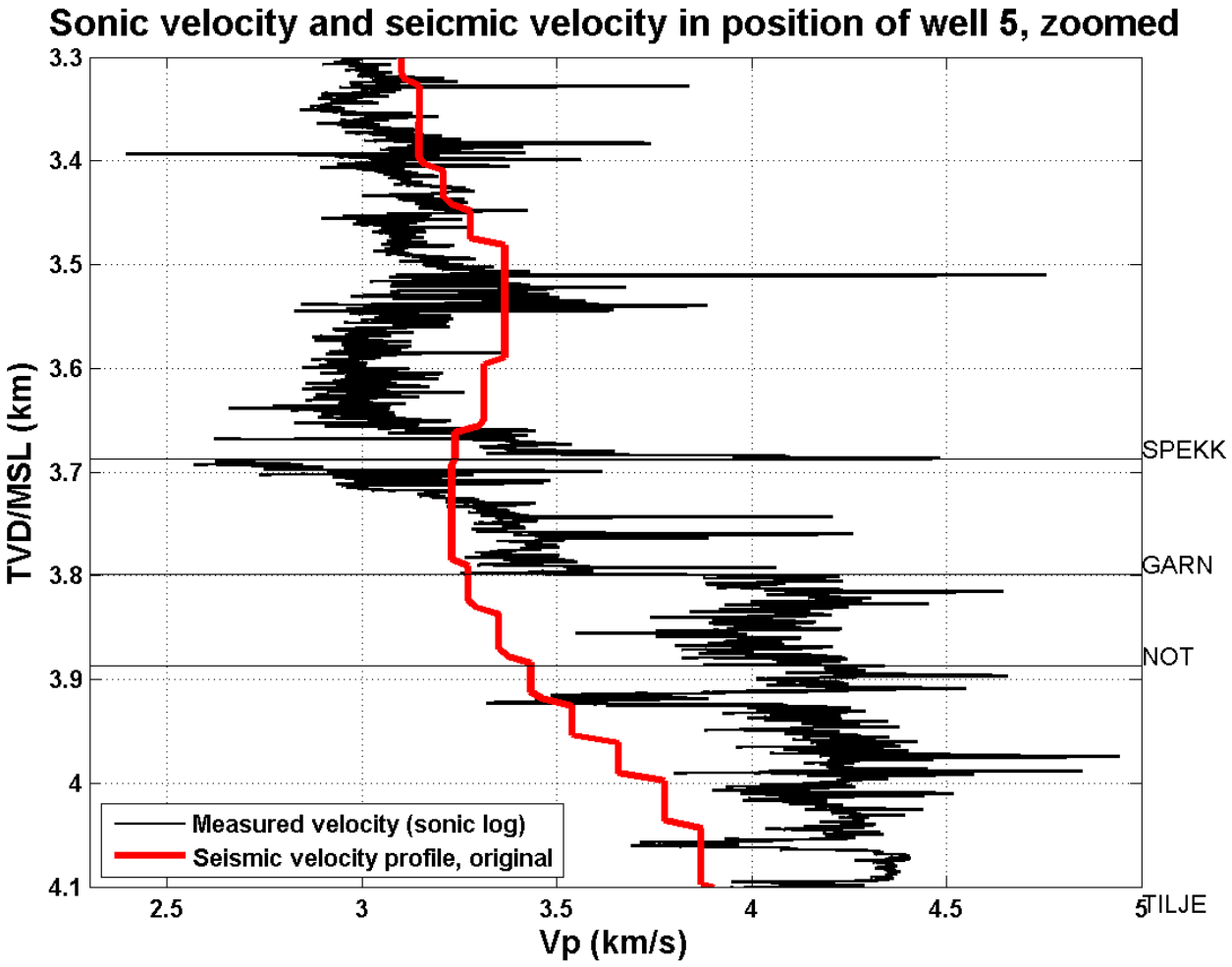

Figure Apx 4: Sonic log and seismic velocity profile in the well location of well 5, zoomed in to the Garn interval.

Appendix D.1 Permeability Modelling along Line 1

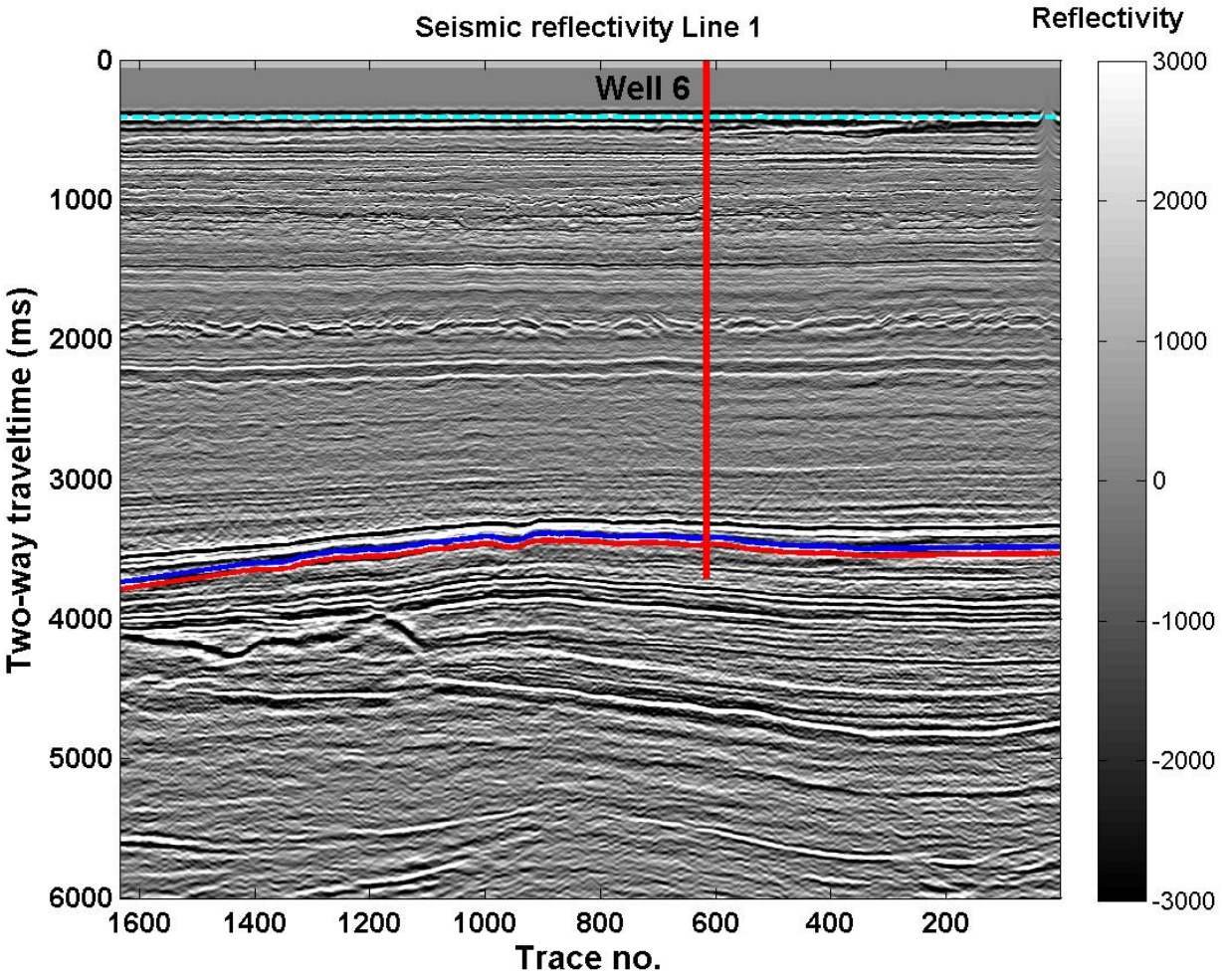

Figure Apx 5: Reflectivity seismic along Line 1 in time, together with the well location of well 6 and the Garn interpretation.

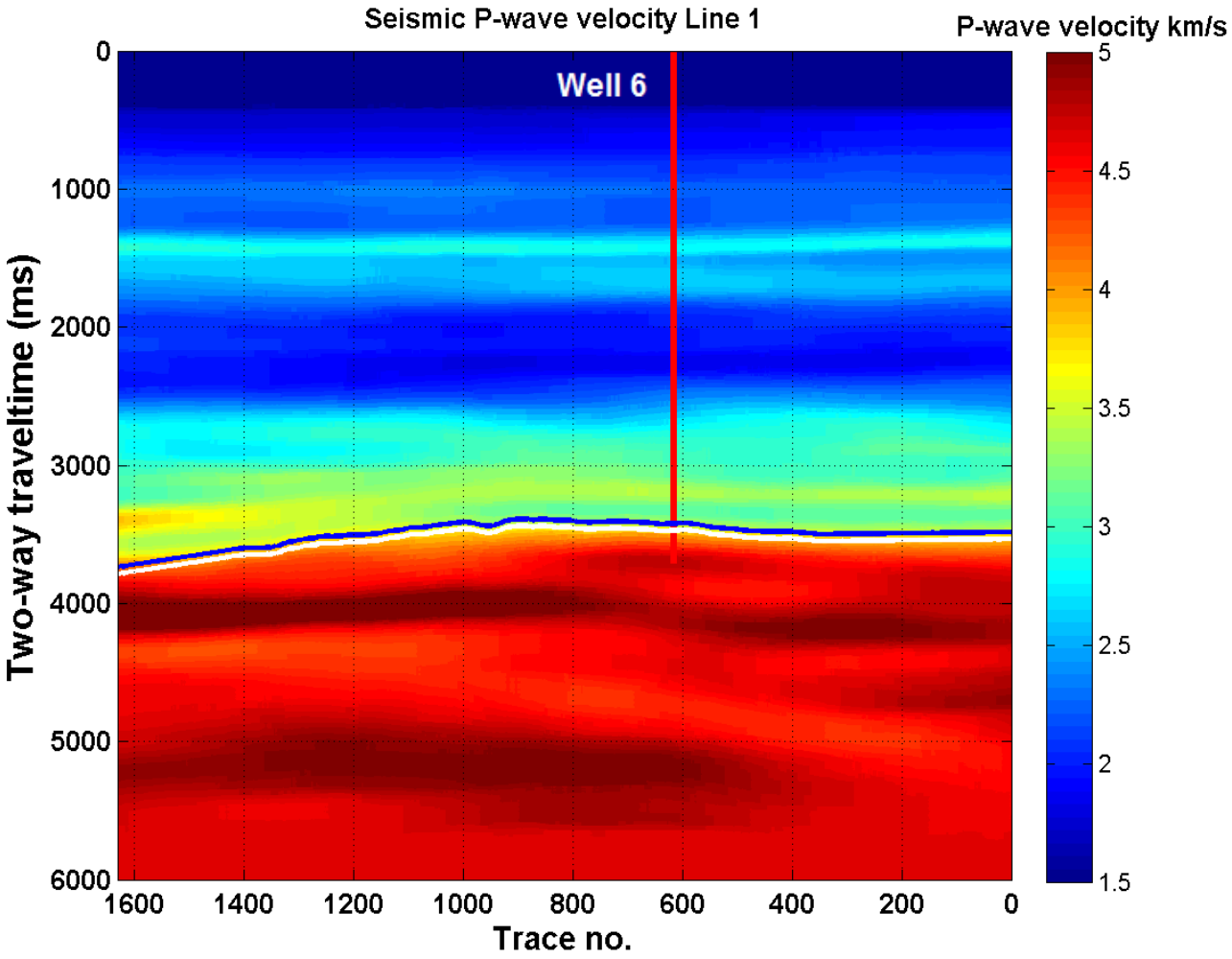

Figure Apx 6: Velocity model for Line 1, together with the well location of well 6 and the Garn interpretation.

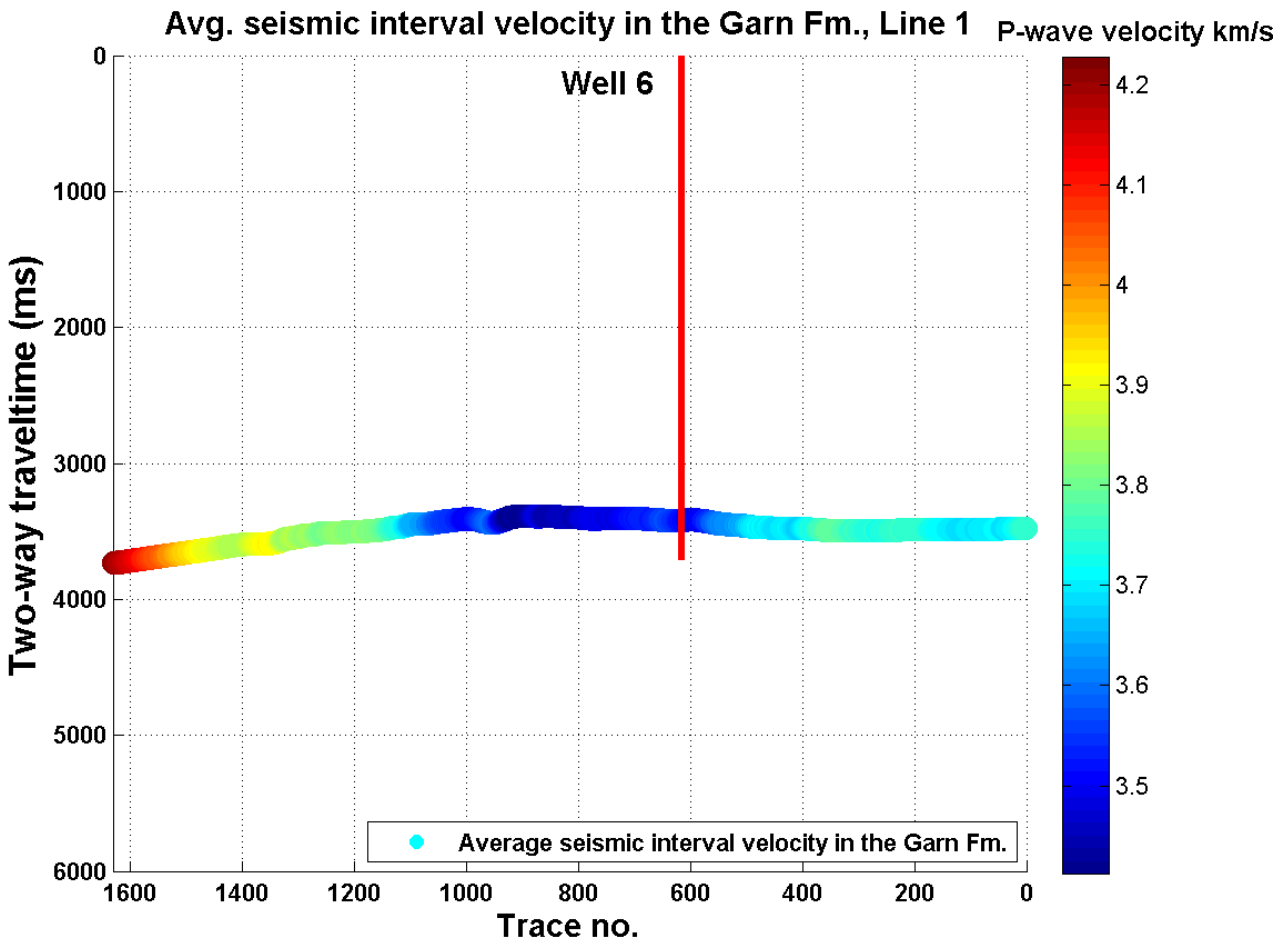

Figure Apx 7: Extracted P-wave velocity from the velocity model along the Garn interpretation in time.

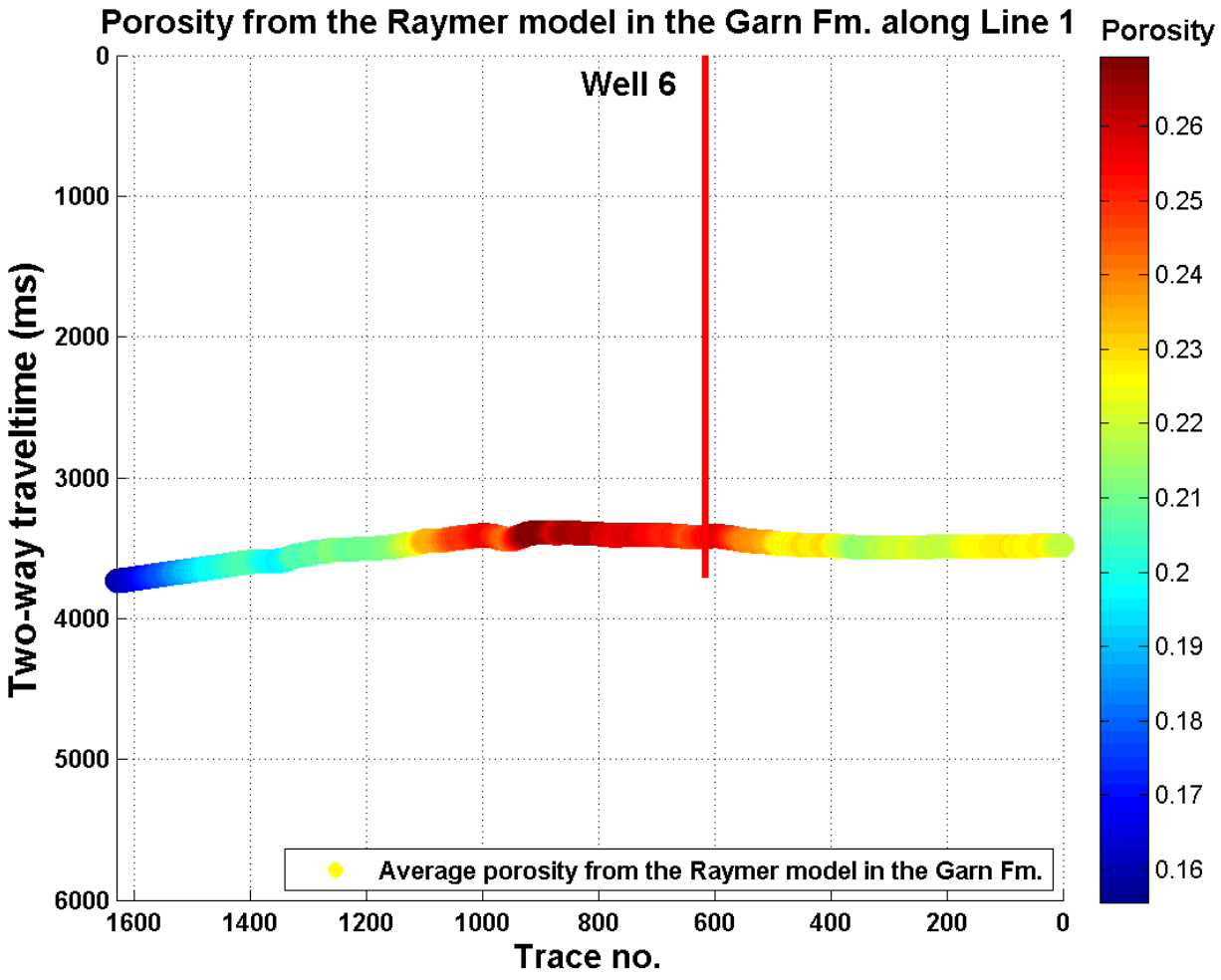

Figure Apx 8: Porosity modelled along the Garn interpretation in time by transforming extracted seismic velocities from the velocity model into porosity by Raymer's model.

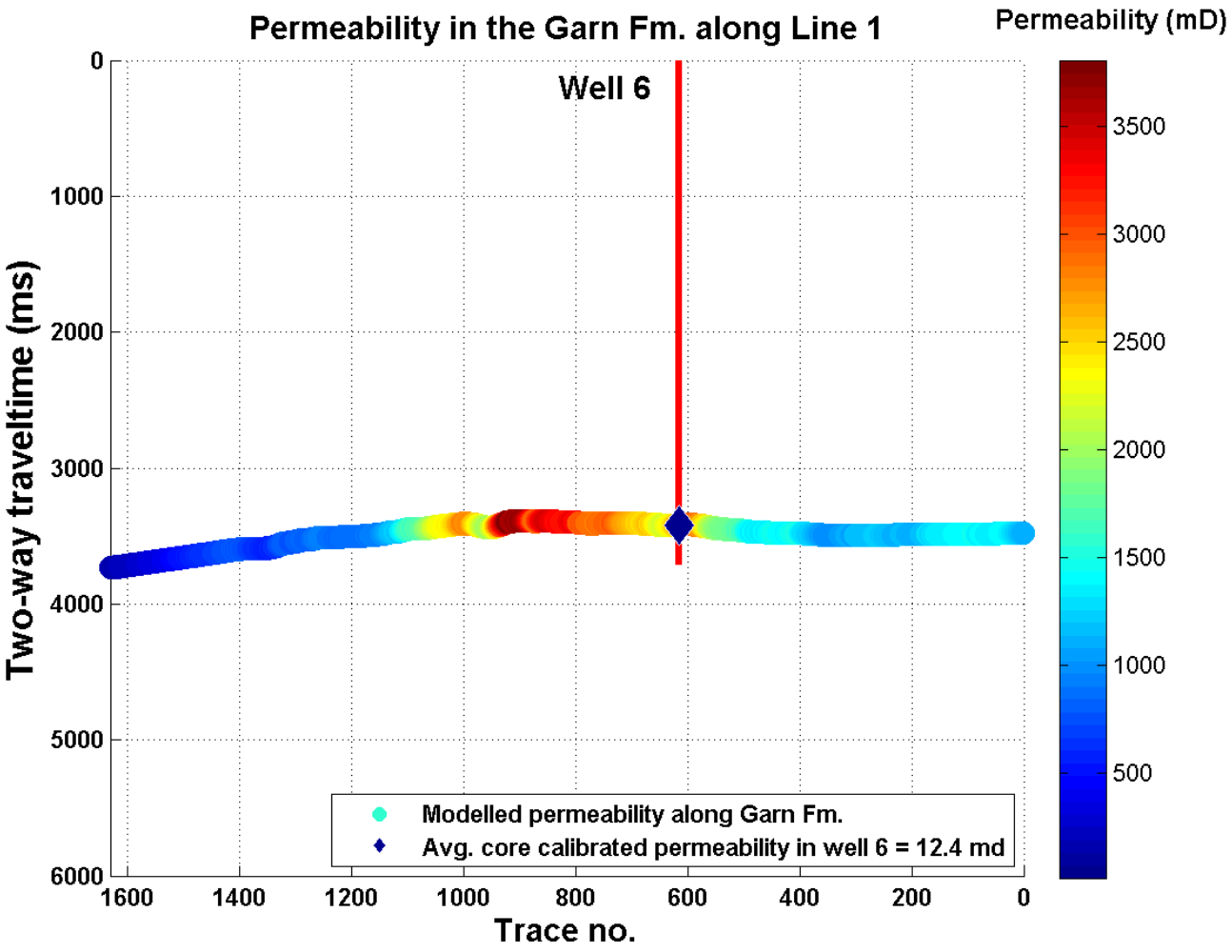

Figure Apx 9: The modelled permeability from the Raymer-Kozeny-Carman model along the time-interpretation of the Garn Fm.

Appendix D.2 Permeability Modelling along Line 2

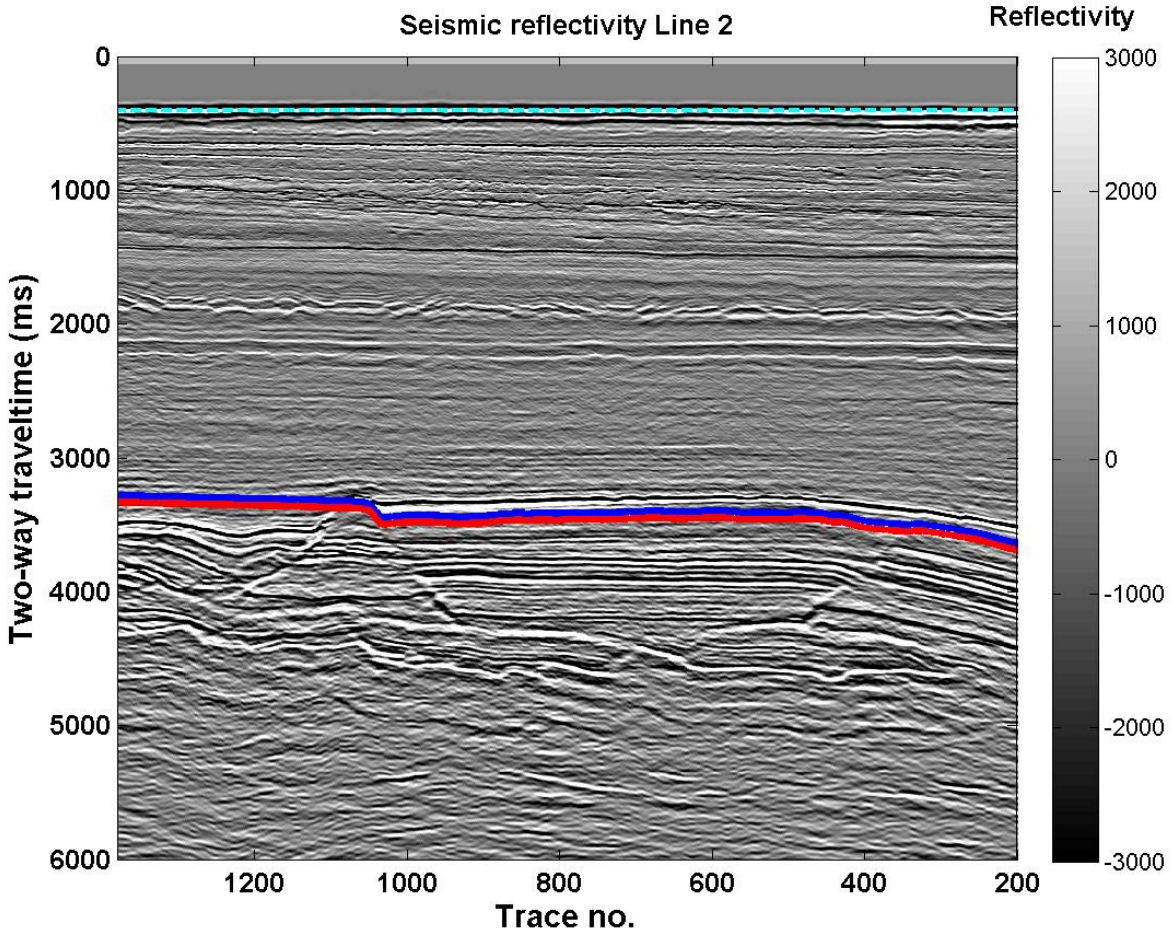

Figure Apx 10: Reflectivity seismic along Line 2 in time, together with the Garn interpretation.

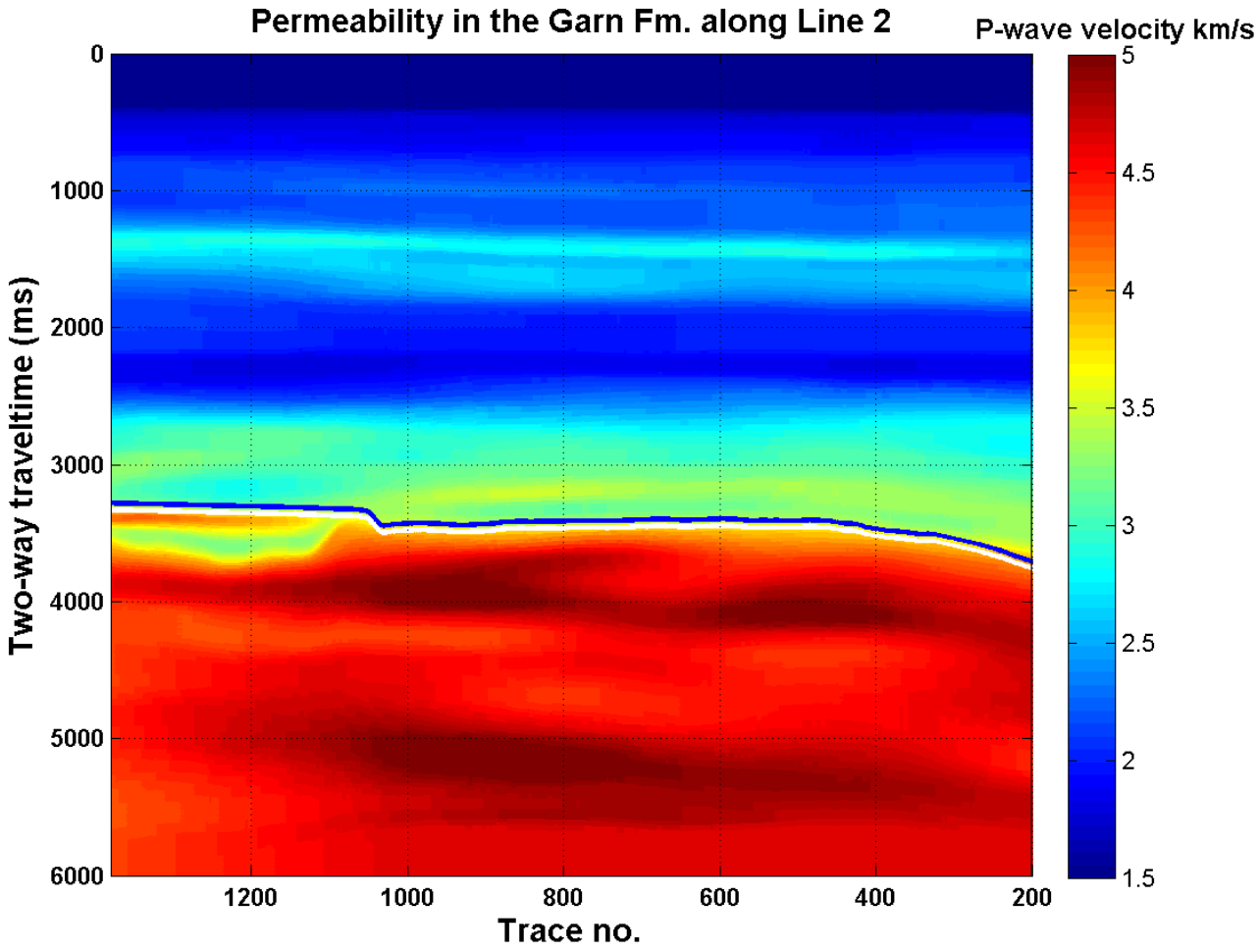

Figure Apx 11: Velocity model for Line 2, together with the Garn interpretation.

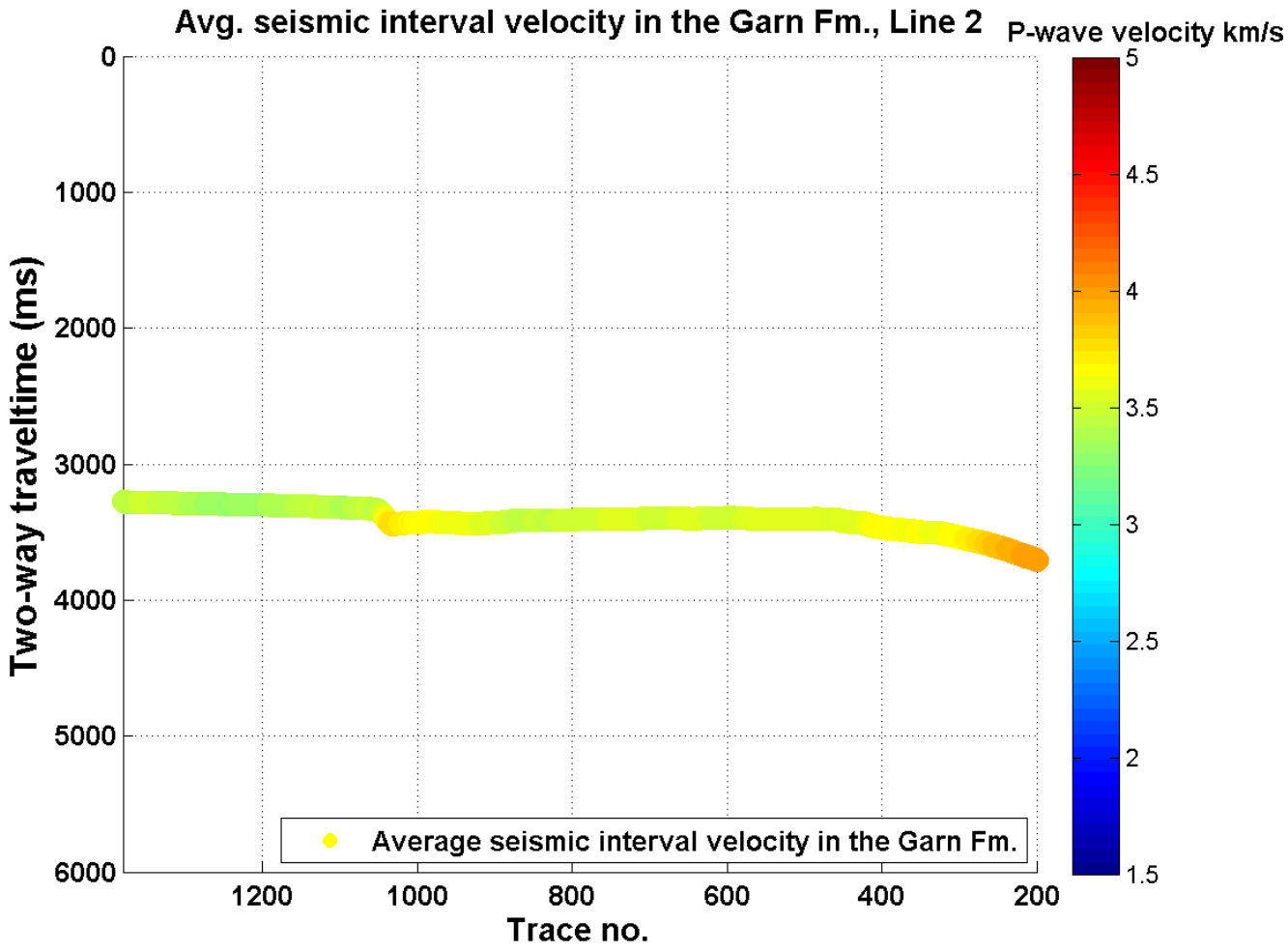

Figure Apx 12: Extracted P-wave velocity from the velocity model along the Garn interpretation in time.

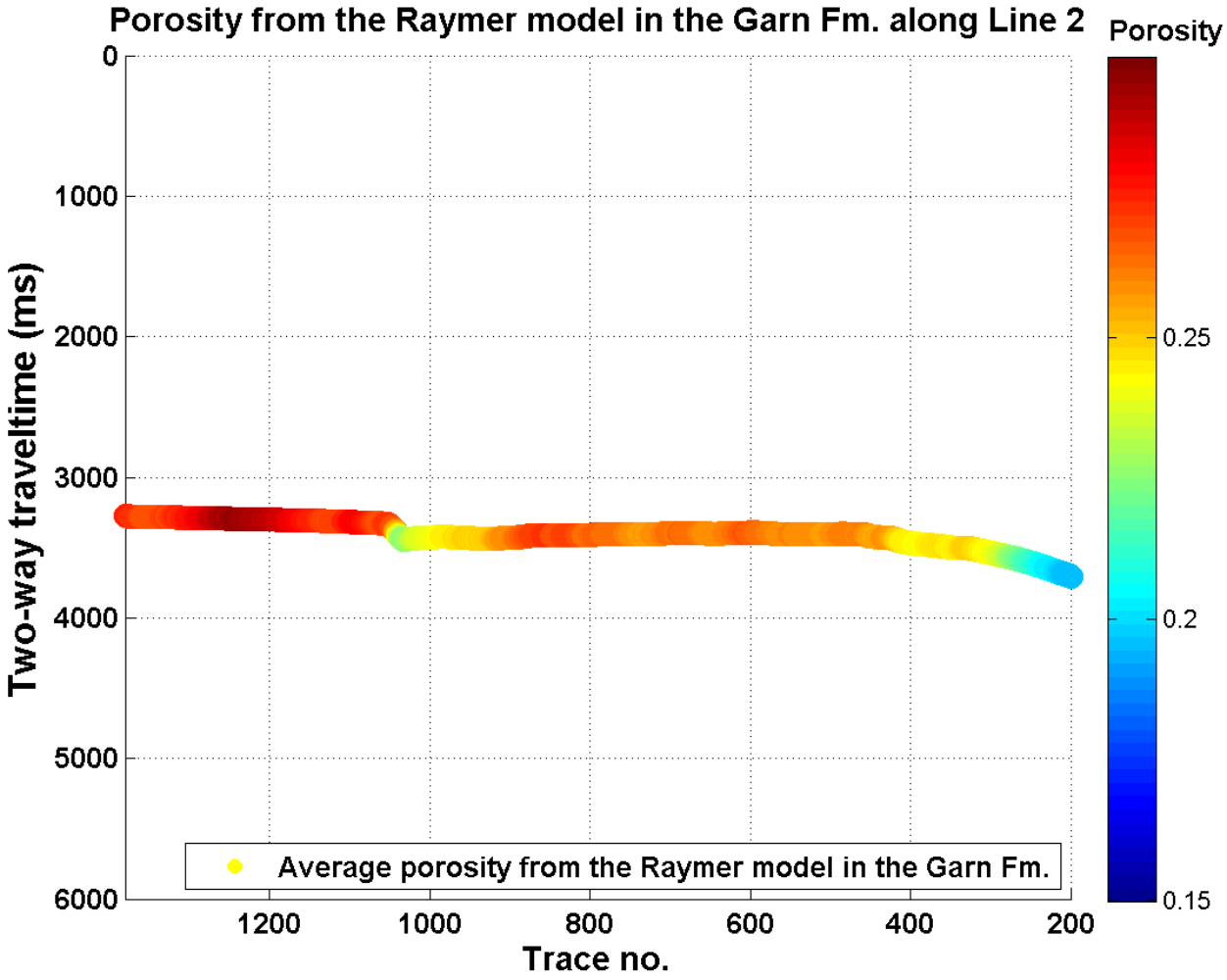

Figure Apx 13: Porosity modelled along the Garn interpretation in time by transforming extracted seismic velocities from the velocity model into porosity by Raymer's model.

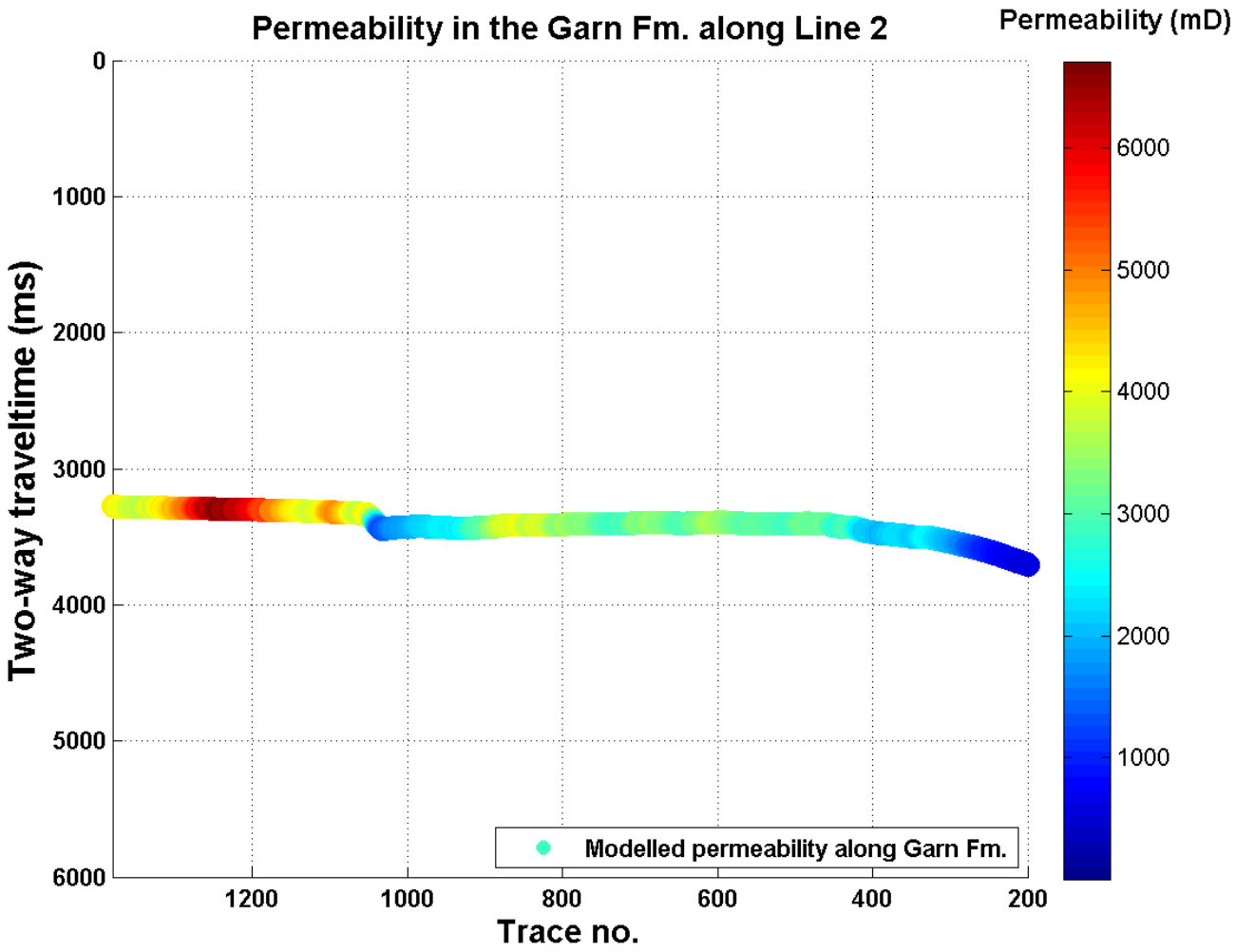

Figure Apx 14: The modelled permeability from the Raymer-Kozeny-Carman model along the time-interpretation of the Garn Fm.

Appendix E Derivative of the Kozeny-Carman Equation

The derivative of the Kozeny-Carman equation with respect to grainsize:

$$\frac{\partial k}{\partial d} = \frac{2d\varphi^3}{72(1-\varphi)^2\tau^2}$$

The derivative of the Kozeny-Carman equation with respect to tortuosity:

$$\frac{\partial k}{\partial \tau} = -\frac{d^2\varphi^3}{36(1-\varphi)^2\tau^3}$$

The derivative of the Kozeny-Carman equation with respect to porosity:

$$\frac{\partial k}{\partial \varphi} = \frac{d^2}{72\tau^2}\left(\frac{3\varphi^3}{(1-\varphi)^2} + \frac{2\varphi^3}{(1-\varphi)^3}\right)$$